UNIVERSITY OF CALIFORNIA SAN DIEGO

Two Dimensional Infrared (2D IR) Spectroscopy of Molecular Vibrational Polaritons (MVPs)

A dissertation submitted in partial satisfaction of the
requirements for the degree
Doctor of Philosophy

in

Materials Science and Engineering

by

Bo Xiang

Committee in charge:

Professor Wei Xiong, Chair
Professor Richard Averitt
Professor Zhaowei Liu
Professor Yizhuang You
Professor Joel Yuen-Zhou

2020

The dissertation of Bo Xiang is approved, and it is acceptable in quality and form for publication on microfilm and electronically:

_____

_____

_____

_____

_____

Chair

University of California San Diego

2020

TABLE OF CONTENTS

LIST OF FIGURES

LIST OF TABLES

ACKNOWLEDGEMENTS

I would like to acknowledge Professor Wei Xiong for his support as my advisor and the chair of my committee. He has mentored and prepared me for a future member of the field of academia. I would like to acknowledge all my former and current labmates for their help and accompany on both the research and other aspects of my life. I would also like to acknowledge all my collaborators for providing many great opportunities to work on interdisciplinary projects.

Chapter 1, in full, is currently being prepared for submission for publication of the material. Bo Xiang; Wei Xiong., The dissertation author was the primary investigator and author of this paper.

Chapter 4, in full, is a reprint of the material as it appears in Proceedings of the National Academy of Sciences, 2018. Bo Xiang; Raphael F. Ribeiro; Adam D. Dunkelberger; Jiaxi Wang; Yingmin Li; Blake S. Simpkins; Jeffrey C. Owrutsky; Joel Yuen-Zhou; Wei Xiong., National Academy of Sciences, 2018. The dissertation author was the primary investigator and author of this paper.

Chapter 5, in full, is a reprint of the material as it appears in Science Advances, 2019. Bo Xiang; Raphael F. Ribeiro; Yingmin Li; Adam D. Dunkelberger; Blake S. Simpkins; Joel Yuen-Zhou; Wei Xiong., American Association for the Advancement of Science, 2019. The dissertation author was the primary investigator and author of this paper.

Chapter 6, in full, is a reprint of the material as it appears in the Journal of Physical Chemistry A, 2019. Bo Xiang; Raphael F. Ribeiro; Liying Chen; Jiaxi Wang; Matthew Du; Joel Yuen-Zhou; Wei Xiong., American Chemical Society, 2019. The dissertation author was the primary investigator and author of this paper.

Chapter 7, in full, is currently being prepared for submission for publication of the material. Bo Xiang; Jiaxi Wang; Zimo Yang; Wei Xiong. The dissertation author was the primary investigator and author of this paper.

Chapter 8, in full, is a reprint of the material as it appears in the Science, 2020. Bo Xiang;

Raphael F. Ribeiro; Matthew Du; Liying Chen; Zimo Yang; Jiaxi Wang; Joel Yuen-Zhou; Wei Xiong., American Association for the Advancement of Science, 2020. The dissertation author was the primary investigator and author of this paper.

VITA

2014	B. S. in Materials Science and Engineering, Zhejiang University, Hangzhou, China
2015	M. S. in Materials Science and Engineering, University of California San Diego
2015-2016	Teaching Assistant, University of California San Diego
2016-2020	Research Assistant, University of California San Diego
2020	Ph. D. in Materials Science and Engineering, University of California San Diego

ABSTRACT OF THE DISSERTATION

Two Dimensional Infrared (2D IR) Spectroscopy of Molecular Vibrational Polaritons (MVPs)

by

Bo Xiang

Doctor of Philosophy in Materials Science and Engineering

University of California San Diego, 2020

Professor Wei Xiong, Chair

In this dissertation, the application of advanced spectroscopy, such as two-dimensional infrared (2D IR) spectroscopy to vibrational-polaritons challenges and advances our understanding in both fields, as mentioned detailly in the introduction. In the fourth chapter, 2D IR uniquely resolves excitation of hybrid light-matter polaritons and unexpected dark states in a state-selective manner, revealing otherwise hidden interactions between them. Moreover, 2D IR signals highlight the impact of molecular anharmonicities which are applicable to virtually all molecular systems.

Besides revealing the polariton-dark modes interactions, the spectroscopy tools has also been employed to study the optical nonlinearities of the molecular vibrational polaritons. In the fifth chapter, the control of vibrational polariton coherent nonlinearities has been fulfilled

by manipulation of macroscopic parameters such as cavity longitudinal length or molecular concentration. In chapter six, we studied the long-lived dynamics of vibrational polaritons in various solvent environments. While the relaxation from upper polariton (UP) to dark modes is always fast (<5 ps) regardless of the medium, lower polariton (LP) in low polarity solvents shows much slower transfer (10-30 ps) into dark modes in highly nonpolar solvents, despite the fact that the LP lifetime remains within 5 ps, suggesting the hidden intermediate states in the LP to dark mode pathway.

Based on the knowledge of the molecular vibrational polaritons, two novel applications have been shown in chapter seven and eight. In chapter seven, a dual-cavity system has been employed to explore the intercavity polaritonic interactions enabled by molecular vibrations. The combination of 2D IR and imaging system has offered an extra dimension (spatial) to view the possible propagation of polaritonic nonlinear responses in space. In chapter eight, the polariton-enabled intermolecular vibrational energy transfer has been studied in chapter five, providing a new transfer pathway to the molecular systems with naturally weak dipole-dipole coupling strength.

The research mentioned in this dissertation has reviewed the current challenge and invoked new questions raised by exciting results in the hope of stimulating more fundamental studies. The novel chemical physics properties of MVPs grant a bright future of applications in new chemistry/biochemistry, energy devices, novel optics, and quantum computation.

Chapter 1

Introduction

Under strong light-matter coupling conditions, cavity vacuum photons and molecular vibration modes hybridize to form molecular vibrational polaritons (MVP).[1–14] The hybridization leads two bright eigenstates with new characteristic transition frequencies. The eigenstate at lower and higher frequencies are known as the lower polariton (LP) and the upper polariton (UP), respectively. The spatial overlap between cavity modes and an ensemble of molecular vibrational modes gives rise to strong coupling (SC). It provides polaritons unique properties adapted from both photons and molecules, including alternations in potential energy surface, hybrid properties of photon and molecules, and delocalized collective molecular motions. Thus, both molecular and photon behaviors under SC condition should differ from themselves along.

Modification of molecular properties, such as potential energy surface and cooperative motions of molecules under SC conditions, could result in changes in chemical reactions. Recent reports from the Ebbesen group[4, 5, 15, 16] in Strasbourg, France, have shown several fascinating examples of how SC can modify reaction pathways. They have reported altering reaction branching ratios and enhancing or suppressing chemical reaction rates under SC conditions, making SC a promising ground for manipulating chemical reactions. On the other front, photonic properties can be changed by strong coupling to molecules, which enables new frontiers in

photonics and quantum information research.[17–22] A few pioneered research has demonstrated that SC allows macroscopic dependent optical nonlinearity, intercavity nonlinear interactions, and transient optical transparency.[9, 20, 23, 24]

The fast advancements of MVP in the past few years have shown its great potential in areas of chemistry, materials science, photonics, and even quantum information science. The ability to leverage light-molecule SC to tackle long-standing chemical reaction challenges hinges on the fundamental understanding of molecular physics and chemical reactions in cavities. Also, the nonlinear optical phenomenon warrants further developments towards quantum photonic behaviors and potential applications in photonic circuitry and quantum simulations. Other future advances of molecular vibrational polaritons include room-temperature realizations of superfluids, polariton lasing, and polariton condensates. In this perspective, we highlight recent developments in the emerging molecular vibrational polariton fields from our and other groups in the hope of invoking more research activities in this field in both fundamental and applied aspects.

1.1 The Basic Theory of Polariton

Here we briefly describe the delocalized and hybridized nature of MVPs and the modification of energy levels from a theoretical perspective. For complete theoretical treatment, we refer to recent reviews. The Hamiltonian of the polaritons can be written as[1, 13, 25]

$$\begin{aligned} \widehat{H}_{polariton} &= \widehat{H}_{cav} + \widehat{H}_{vib} + \widehat{H}_{int} \\ &= E_{cav}\hat{a}^{\dagger}\hat{a} + \sum E_{vib}\hat{b}_i^{\dagger}\hat{b}_i + \sum g_i(\hat{a}^{\dagger}\hat{b}_i + \hat{b}_i^{\dagger}\hat{a}) \end{aligned} \tag{1.1}$$

$\widehat{H}_{cav}$ and $\widehat{H}_{vib}$ are the Hamiltonians of the cavity and vibrational modes, respectively, and $\widehat{H}_{int}$ is the Hamiltonian for the interactions between them. On the second line of 6.1, E_{cav} and E_{vib}

are the energy of cavity and vibrational modes, $\hat{a}_i^\dagger$ and $\hat{a}_i$ are the photon (cavity mode) creation and annihilation operators, $\hat{b}_i^\dagger$ and $\hat{b}_i$ are the dipole (vibrational mode) creation and annihilation operators, and g_i is the individual dipole-photon interaction strength.

In the simplest scenario, when a single dipole couples to a single photon cavity mode, the Hamiltonian can be written in a 2 by 2 matrix form 6.2,

$$\begin{pmatrix} E_{cav} & g_0 \\ g_0 & E_{vib} \end{pmatrix} \begin{pmatrix} \alpha_{cav} \\ \alpha_{vib} \end{pmatrix} = E \begin{pmatrix} \alpha_{cav} \\ \alpha_{vib} \end{pmatrix} \tag{1.2}$$

the amplitudes squared of α_{cav} and α_{vib} are the Hopfield coefficients of photon and vibrational dipole modes, whose squared magnitude represents the fractions of either photon or molecular modes in the polaritons. By diagonalization, two new eigenstates (LP and UP) are formed. The polariton wavefunction is[1]

$$\begin{aligned} |UP\rangle &= c_{1,1}|e\rangle|0\rangle_c + c_{1,2}|g\rangle|1\rangle_c \\ |LP\rangle &= c_{2,1}|e\rangle|0\rangle_c + c_{2,2}|g\rangle|1\rangle_c \end{aligned} \tag{1.3}$$

If expanding to N molecules all couple to the same single cavity modes, there are two bright polariton states, whose wavefunctions are [1]

$$\begin{aligned} |UP\rangle &= \sum_1^N c_{1,m}|e\rangle_m|0\rangle_c + c_{1,N+1}|g\rangle|1\rangle_c \\ |LP\rangle &= \sum_1^N c_{2,m}|e\rangle_m|0\rangle_c + c_{2,N+1}|g\rangle|1\rangle_c \end{aligned} \tag{1.4}$$

In both scenarios, the polariton wavefunctions are composed of molecular wavefunctions and a cavity wavefunction. Thus, it reveals the hybrid nature of polaritons. For the case of N>1, more than one molecular wavefunction participates in the polariton wavefunction, in phase with each other. Therefore eq. 1.4 represents the delocalized nature of polaritons. In both the single and ensemble molecule cases, the two bright polariton states have their characteristic eigenenergy:[1, 25]

$$E_{LP,UP} = \frac{1}{2}\left[E_{cav} + E_{vib} \mp \sqrt{4Ng_0^2 + (E_{cav} - E_{vib})^2}\right] \tag{1.5}$$

Thus, the energy of polariton shifts away from the pure molecular states, and the shift depends on the number of molecules, N, individual molecular coupling strength g_0, and cavity detuning $\Delta = E_{cav} - E_{vib}$. The energy separation between LP and UP are the Rabi splitting, 2Ω, We note when N>1, there are also N-1 dark states and the collective coupling strength (Rabi splitting) becomes $\sqrt{N}g_0$ at zero detunings. A representative energy diagram of the light-matter SC phenomenon is shown in Figure 1.1.

The criterion for SC is that the energy exchange rate between the dipole and the cavity mode has to be faster than the decay rates of the constituent states. In the frequency domain, it manifests as the separation of the LP and UP peaks must exceed the full width of half maximum (FWHM) of both the vibrational and the cavity mode.

$$\Omega > \Gamma_{vib} \quad or \quad \Gamma_{cav} \tag{1.6}$$

Because g_0 depend on the strength of electric fields $E = \sqrt{\frac{\hbar\omega}{2\varepsilon_0 V}}$ and the transition dipole

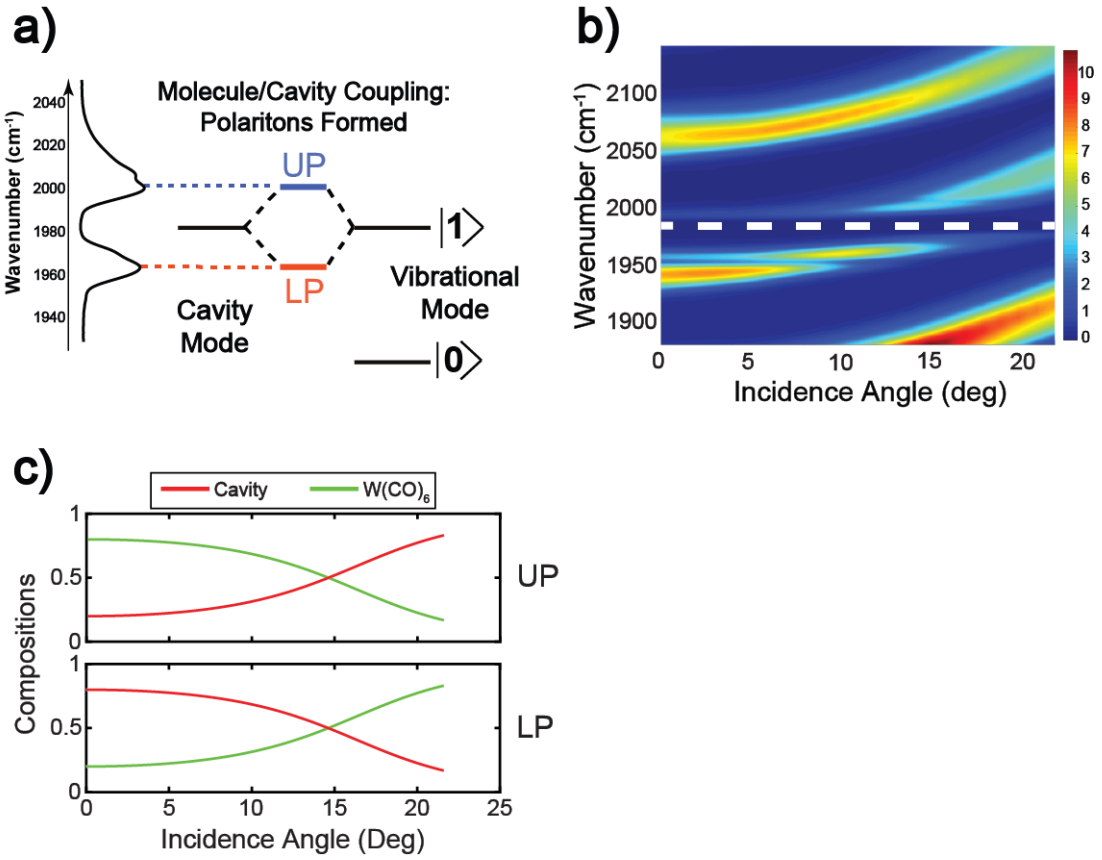

Figure 1.1: (a) Formation of vibrational polaritons by strongly coupled molecular vibration and cavity modes. (Left) vibrational polariton FTIR spectrum of $W(CO)_6$. (b) Dispersion of IR transmission. (c) Hopfield coefficients of UP and LP states.

moments,[26] this leads to

$$\Omega \propto \sqrt{N/V} = \sqrt{C} \tag{1.7}$$

Thus, a sufficient concentration of the molecules inside the cavity is necessary for strong coupling. Also, a large dipole moment would increase g_0, which makes vibrational SC favors molecules with big absorption cross-sections. Lastly, coupling strength also depends on the cavity electric field. For example, several pioneering works have been published in the exciton-polariton

regime, where the intense electromagnetic fields of plasmon modes enabled single-particle strong coupling. Such a development has yet been reported for MVP because of the relatively smaller vibrational transition dipole moments than their electronic counterparts. However, the precedence in exciton-polaritons warrants new designs of the microcavity with enhanced field strengths for vibrational SC.

A unique point of polaritons is that polaritons' composition can be tuned by in-plane momentum wave-vector, $k_{\|}$, which relies on the photon incident angle, θ, in the following manner [25]

$$k_{\|} = n_c \frac{2\pi}{\lambda_c} \tan[\sin^{-1}(\frac{\sin\theta}{n_c})] \tag{1.8}$$

λ_C is the wavelength of cavity resonance, and n_c is the cavity refractive index. By tuning wave-vector, it directly controls the detuning (Δ). Thus, detuning is related to the composition of LP and UP, as shown in equation 1.9. the Hopfield coefficients of molecular vibrational mode and cavity mode ($|\alpha_{vib}|^2$ and $|\alpha_{cav}|^2$, respectively) are:[25]

$$\begin{aligned} |\alpha_{vib}|^2 &= \frac{1}{2}(1 + \frac{\Delta(k_{\|})}{\sqrt{\Delta(k_{\|})^2 + 4g_0^2}}), \\ |\alpha_{cav}|^2 &= \frac{1}{2}(1 - \frac{\Delta(k_{\|})}{\sqrt{\Delta(k_{\|})^2 + 4g_0^2}}) \end{aligned} \tag{1.9}$$

Figure 1.1b (2) demonstrates the dispersive feature of a polariton system. The minimized Rabi splitting position corresponds to the zero-detuning point. With increasing detuning, the UP branch becomes more photon-like while the LP branch shows more molecular fraction, as

indicated from the Hopfield coefficient plot (Figure1.1c).

Correspondingly, the decay dynamics of LP/UP polaritons are also tuned, because they also depend on Hopfield coefficients.[25]

$$\begin{aligned}\gamma_{LP} &= |\alpha_{vib}|^2\gamma_{vib} + |\alpha_{cav}|^2\gamma_{cav} = \gamma_{vib} + |\alpha_{cav}|^2(\gamma_{cav} - \gamma_{vib}),\\ \gamma_{UP} &= |\alpha_{cav}|^2\gamma_{vib} + |\alpha_{vib}|^2\gamma_{cav} = \gamma_{vib} + |\alpha_{vib}|^2(\gamma_{cav} - \gamma_{vib})\end{aligned} \tag{1.10}$$

In a typical solution-phase system, γ_{vib}, the dephasing lifetime of a dipole, is ~ 1 ps^{-1}, while similarly γ_{cav}, the cavity lifetime, is $10^{-1} \sim 1$ ps^{-1}.[25] As a result, detuning can manipulate the decay rate of polariton based on the application purpose. For specific applications that need a long lifetime, both high Q cavities and long lifetime vibrational modes are necessary.

1.2 Polariton Fabrications

The molecular vibrational polariton systems can be prepared by filling a Febry-Perot cavity composed of two mirrors with high reflectivity (e.g., metal coated or distributed Bragg reflector (DBR)) with molecular solutions at sufficient concentration. In more advanced settings, a microfluidic cavity cell [4, 5, 15] or cavity with patterned structures [22] can be deployed. A recent example of new cavity development is photonic crystal cavities.[27] Silicon-based cavities can be made by partially etching the SiN layer on a SiO_2-capped Si substrate, to form the 1D array of photonic structures. Such cavities can host transition metal dichalcogenides (TMDs), in which photons are confined in a small volume, enhancing photon-TMD coupling.

1.3 Cavity-catalytic Reactionns

Polariton, an active research topic in physics for decades, gains attention in the chemistry community for its potential to modify chemical reactions. Thermodynamically, by hybridizing molecules with the cavity mode, the polariton energy level is shifted from the bare molecular energy, which has been predicted to impact the chemical processes, e.g., chemical reactivity can be changed and new energy transfer pathways would be enabled. Recently, Ebbesen's group has reported several cavity-catalyzed/inhibited reactions[4, 5, 15, 28, 29], one of which showed modified selectivity.[4]

The first report[15] of cavity modified reactions was in the exciton-polariton regime, on a photoisomerization reaction between spiropyran (SPI) and merocyanine (MC). Photoexcited SPI goes through a ring cleavage process and forms MC, through a photoexcited intermediate state (I) (Figure 1.2a, top panel). The cavity mode with the electronic transition of conjugated MC strongly couple to form two polariton states (UP and LP). Subsequently, the isomerization from SPI to MC became favorable over the reverse reaction (MC to SPI). The author explained this change of reactions by the mechanism that in the cavity, only the optical bright UP and LP can be optically excited, and because LP has a fast-photonic decay channel back to the ground electronic state of MC, it depletes the pathway to I and isomerization to SPI (Figure 1.2a, bottom panel). On the contrary, the isomerization from uncoupled SPI to MC remains not altered.

More fascinating and peculiar findings[4, 28] lie in that vibrational strong coupled reactions under thermal conditions. Recently, the reactivity and selectivity of two parallel reaction pathways were modified via the vibrational SC. In this work, the silane derivative, tert-butyldimethyl{[4 (trimethylsilyl)but-3-yn-1-yl]oxy}silane (R in Figure 1.2b, top panel), as the reactant, could lead to two products: product 1 with breaking Si-O stretching band and product 2 with breaking Si-C stretching band. Without SC, the yield of product 1 was higher than product 2 (Figure 1.2b, outside cavity). However, via SC to all the Si-based vibrational modes, the yields of

both products were flipped, leading to more product 2 (Figure 1.2b). The change of selectivity also depended on detuning, as it was only modified when specific modes were strongly-coupled, which remains a topic of further studies.

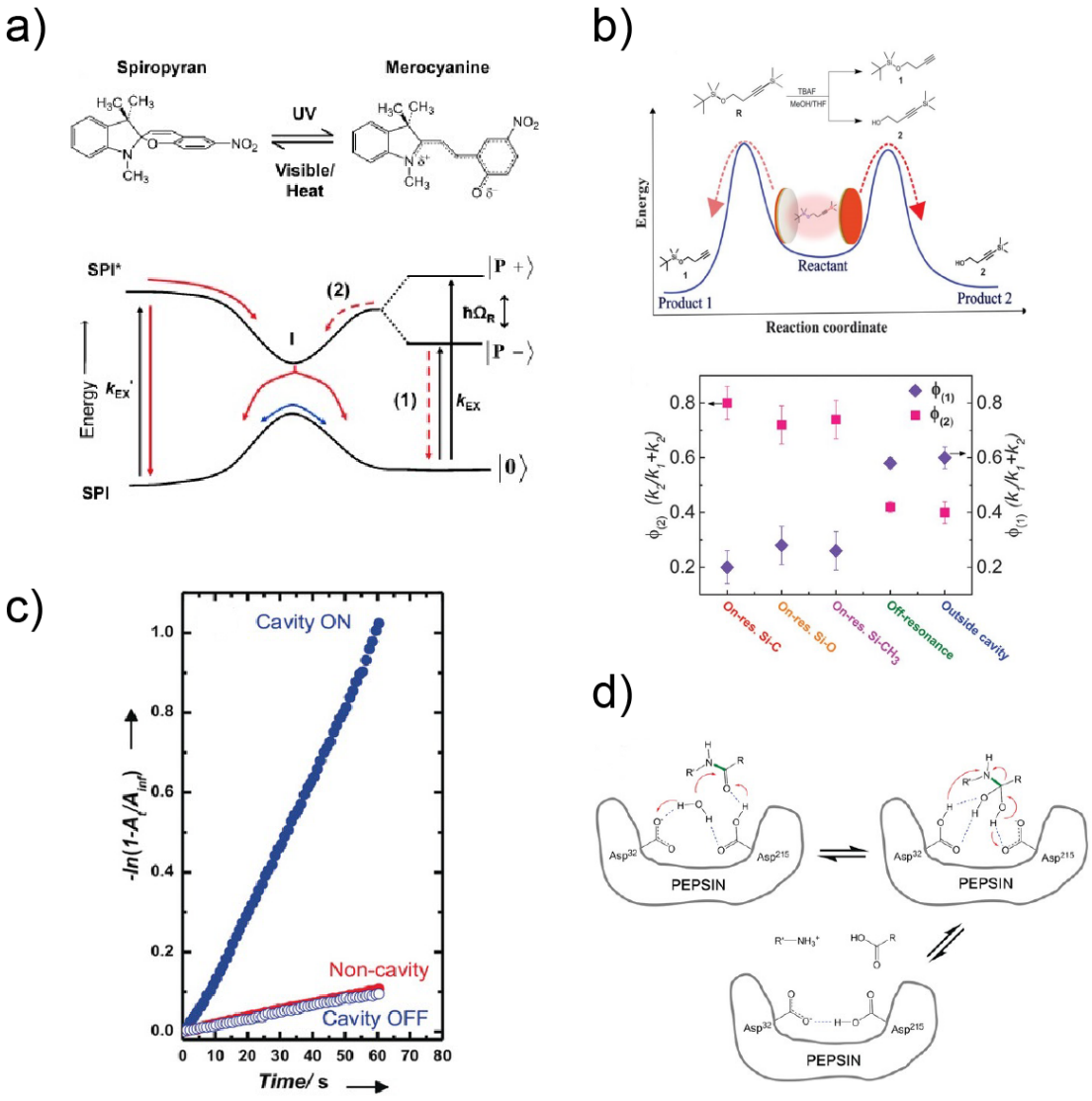

Figure 1.2: (a) Top: The molecular structure of SPI and MC; Bottom: Energy diagram of the two isomers. (b) Top: Silyl cleavage pathways; Bottom: The yields of product. (c) Kinetic traces measured at 407 nm. (d) A mechanistic model of peptide bond cleavage.

While most of the reactions in cavities showed suppressed reaction rates, there was one report[28] showing a reaction being accelerated. In this work, both para-nitrophenyl acetate

(PNPA) and ethyl acetate (EtOAc) were strongly coupled to the cavity modes of the microcavity, in which PNPA could hydrolyze with EtOAc. Because both PNPA and EtOAc have carbonyl modes absorbing at a similar frequency, the reactants PNPA can reach to strong coupling without the need of high molecular concentrations. The reaction rate under SC was roughly one order of magnitude larger ($1.6\times10^{-2}s^{-1}$) than either the rate when cavity mode was off-resonance ($0.16\times10^{-2}s^{-1}$) or the one without SC ($0.18\times10^{-2}s^{-1}$) (Figure 1.2c). The authors proposed that the increasing rate was related to an enhanced cooperative effect between PNPA and EtOAc. Using ultrafast spectroscopy, our group recently demonstrated that cooperative effects and intermolecular vibrational energy transfer indeed exist under SC conditions (see section 'Strong Coupling Enabled New Vibrational Energy Transfer Pathways' for details), shedding light to the mechanism of this cavity-catalysis observation.

Similar cavity-modified reactions were also demonstrated on an enzymatic reaction:[29] a pair of aspartic acid on the enzymes activated water nucleophile attack to an amino acid, which leads it to dissociate. (Figure 1.2d). OH-stretching modes of water, as the reactant and media, were strongly coupled to cavities. The SC to water decelerated enzymatic reaction by 4.5-fold. The authors proposed that SC of water vibrational modes affect the balance of intermolecular forces, leading to changes in folding and substrate binding/product release. However, a recent theoretical study of water under SC condition showed that only rotational dynamics of water were affected.[30] A deeper understanding of the effects of strongly coupled water is necessary by a combined effort of ultrafast spectroscopy, such as 2D IR spectroscopy,[2, 31–33] and new theoretical modeling.[1, 10, 13]

Theoreticians have started their efforts in understanding these unique reaction events, by simulating the potential under SC. The Yuen-Zhou group[34] has demonstrated the effect of catalytic vibrational SC using a Marcus-Levich-Jortner electron transfer model. In their model, although entropy favors the direct transition from reactant to product dark modes, the kinetic processes through polaritonic channels (LP) can still dominate the whole process, especially

under Marcus inversed regime, where SC shifts the activation energy to zero. However, other recent theoretical works have concluded that molecular dynamics under the classical mechanic framework cannot explain the observed experimental results.[35, 36] Thus, a unified theoretical understanding of the SC-modified reactions is still an open field that deserves more effort soon.

So far, SC has made specific reaction pathways favored, acting as catalysts or inhibitors. These initial works[4–6, 15, 26, 28, 29] are just the beginning of a fascinating endeavor. There are many research opportunities in both preparation and characterization of cavity catalyzed reactions, as well as understanding the detailed mechanisms of cavity-catalyzed chemical reactions. On the preparation and characterization front, more advanced cavities, beyond the Fabry-Perot cavity could bring stronger local E-field with smaller cavity volume and high-quality factors, which could compensate for the low concentration of reactants, and advance the frontier of cavity-catalytic reactions. Furthermore, the primary characterization method of reactions[4–6, 15, 26, 28, 29] currently is optical, e.g., FTIR or UV-Vis spectroscopy. It will become essential to use other analytical methods such as cryotomography and mass spectrometry to characterize and quantify the reaction rates.

On the mechanism front, there remain many unanswered questions, such as why most reactions under SC conditions are all suppressed? What is the origin of cavity detuning dependence? What is the role of dark reservoir modes? Performing ultrafast time-resolved spectroscopy could gain the mechanistic insights of polaritons, as the polaritonic kinetics, e.g., energy transfer between polaritonic and molecular states or inter-polaritonic states, occur on the ultrafast time scales. A couple of groups, including us, have applied a suite of ultrafast spectroscopy[1, 2, 14] to this emerging field of MVPs. In the next several sections, we will briefly introduce some critical ultrafast dynamic studies on MVPs.

1.4 Ultrafast Dynamics of Polariton Systems

Femtosecond pump-probe spectroscopy, which sends a pump pulse to excite polariton and a follow-up probe pulse to interrogate the transient polaritonic or molecular states, is a powerful way to reveal ultrafast dynamics of polaritons. It has been widely used in exciton-polaritons. The team of Owrutsky, Dunkelberger, and Simpkins at Naval Research Laboratory[3] have reported the first ultrafast spectroscopy of MVPs, in which they found detuning dependent polariton and dark state dynamics, and provided a general framework to explain the nonlinear spectral features. Our group with the NRL team further revealed polariton state-resolved ultrafast dynamics using time-resolved two-dimensional IR spectroscopy (2D IR).[7, 37]

In the 2D IR technique[2, 31–33] (Figure 1.3a), two pump pulses, and a probe pulse interact with samples at delayed time incidences (t_1, t_2, and t_3). After the first IR pulse, a vibrational coherence is generated, which is converted into a subsequent population (or coherence) state by the second IR pulse. The coherence after the first IR pulse is characterized by scanning t_1 using the mid-IR pulse shaper. After waiting for t_2, the third IR pulse (probe) impinges on the sample, and the resulting macroscopic polarization emits an IR signal. After numerical or instrumental Fourier transform, the pump and probe frequencies are resolved in 2D IR spectra. 2D IR is pump-probe spectroscopy with the excitation states resolved in the frequency domain, which distinguish the dynamics of different states better. For example, a key feature shown in 2D IR of polaritons[2] was the unexpected peak in the middle of UP and LP peaks along the ω_1 axis, which came from the dark reservoir modes. This result showed that the dark modes are not entirely optically invisible due to the photonic and molecular inhomogeneity.

Currently, most studies in our group have been focused on a model polariton system, $W(CO)_6$ coupled with the FP cavity. In these studies,[2, 7, 9, 22] we have learned that hybridizing molecular modes and optical modes can modify the intrinsic molecular dynamic feature through the energy exchange between the two. We summarize the main dynamic features of MVPs below.

1.5 Coherent Rabi Oscillations and Transient Optical Modulation in Polaritons

The pump-probe dynamics focused on MVPs with Rabi splitting about 40 cm^{-1}. At early time delay, the pump-probe spectra show two prominent absorptive transient features (Figure 1.3b), which oscillate strongly in the time domain.[14] The oscillation period is 0.8 ps, corresponding to a frequency of 42 cm^{-1}, matching with the Rabi splitting of the systems. Thus, the oscillation is a Rabi oscillation between LP and UP, or the coherent energy exchange between cavity modes and molecular states. Similar behaviors were also observed in quantum-well based exciton-polaritons.[38]

The Rabi oscillation was further studied using 2D IR.[9, 39] By taking a spectral cut at specific frequencies (e.g., cut at UP (Figure 1.3f)), we observed that the Rabi oscillation occurred for both UP and LP states. By applying Fourier transform along with the Rabi oscillation time t_2, we can resolve and separate the spectral components that oscillate (AC) and do not oscillate (DC) over t_2. The AC spectrum shows pure absorptive lineshape, resembling the pump-probe lineshape at early time delay (Figure 1.3b), suggesting that at early-time, the coherent dynamics dominate the nonlinear responses of polariton systems. In contrast, the DC spectral component has very different lineshape, and we will discuss it later (Figure 1.3g, blue trace, similar to Figure 1.3c). The mechanism of nonlinear AC signal (Figure 1.3h) is related to nonlinear dephasing, as the experimental signal can be simulated by modulating the dephasing lifetime (or linewidth) of each mode in a transfer matrix model. Such ultrafast optical modulations laid the foundation for transient all-optical blocks and switches. Furthermore, the polariton Rabi oscillations show potentials in quantum information processing and photonic circuitry. To further manipulate individual quantum pathways, we developed a shaper-based approach to selectively exciting only specific quantum states of the system, which could be useful in quantum information technology.

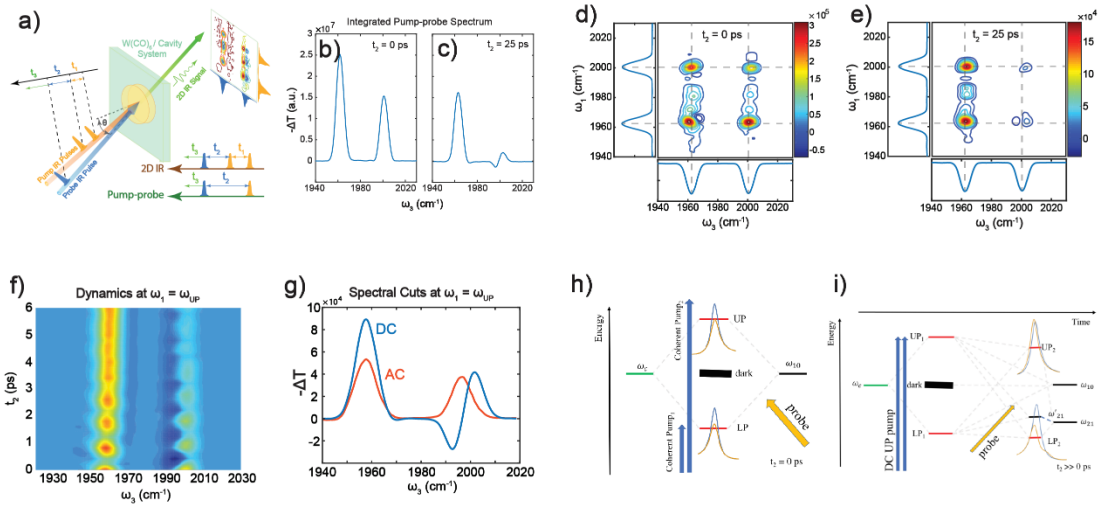

Figure 1.3: (a) 2D IR setup. Pump-probe spectra at (b) early and (c) late time delays. 2D IR spectra at (d) early and (e) late time delays. (f) Time-dependent nonlinear response. (g) AC and DC spectra of UP cut. (h) Energy diagrams of (h) the AC signal and (i) the DC signal.

Interestingly, Dunkelberger et al.[37] reported that optical modulation also occurred in the intermediate regime (Rabi splitting $\sim$10 cm^{-1}), but differently. In the intermediate-coupling regime, upon optical excitation, Rabi splitting contracts upon removal of the ground states. As pump power increases to a limit, the doublet polariton features disappeared, leaving a Gaussian profile transmission peak. This phenomenon is transient transparency due to the ground state population inversion. The lifetime of the central dip and the LP peaks were close to bare molecule lifetimes, suggesting under intermediate coupling conditions, molecular modes dominate the dynamics. Nevertheless, under intermediate coupling conditions, unusual ultrafast optical modulation could occur for novel optical devices and applications.

1.6 Polariton-to-Dark State Relaxation Dynamics

When the pump-probe time delay (t_2 of 2D IR) exceeds the lifetime of polaritons, polaritons relax into the dark reservoir modes, which manifests as the slow dynamics.[7] The characteristic pump-probe spectra at a long-time delay are shown in Figure 1.3c. After being

pumped, the Rabi splitting decreases because of the ground-state population depletion. As a result, the UP (LP) resonance undergoes a shift towards a lower (higher) frequency, which results in a derivative lineshape in the UP side of the pump-probe spectrum (Figure 1.3c) and of 2D IR (Figure 1.3e). In addition to the derivative feature, a substantial absorption appears at the LP side. This feature appears because the dark mode overtone ν_{12} transition (from first excited to second excited states, the schematic illustration shown in Figure 1.3i) is near-resonant with LP transition. As a result, ν_{12} becomes visible through the LP transmission window. We note the spectral lineshape at a long-time delay resembles the DC component after Fourier analysis[9] (Figure 1.3b). This similarity makes sense because the spectra at a long-time delay represent the incoherent dynamics in the microcavity. Nevertheless, the absorptive feature near LP can be used as a signature to follow polariton transfer to dark modes as well as dark mode relaxation.

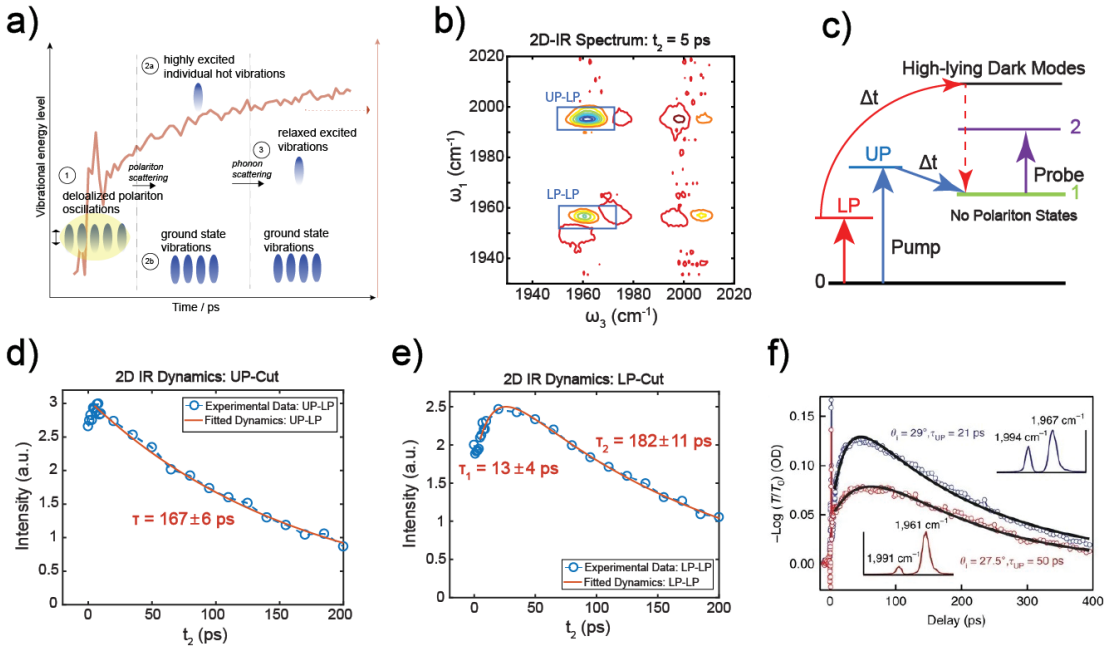

Figure 1.4: (a) Polariton hot vibration dynamics. (b) 2D IR spectrum of strongly coupled system. (c) Energy diagram of the population transfer process of the polariton system in equilibriu. 2D IR dynamics of (d) LP and (e) UP states for the SC system. (f) Angle-dependent dynamics.

Following this ν_{12} spectral signature, the dark state dynamics manifest as a multi-exponential rise and decay in pump-probe dynamics. The rising time, appearing after a sharp relaxation of polariton, represents the dynamics of populating the first excited dark states. The lagging time between the polariton decay and dark states excitation, suggests, when polariton decay, it does not directly transfer to the first excited states of dark modes, but instead, going through a hidden intermediate state. Using 2D IR, we found that the lagging time only exists when pumping LP (Figure 1.4d), while upon pumping UP, the polariton systems decay into dark mode directly (Figure 1.4e). Previous frequency-resolved pump-probe study on $W(CO)_6$ showed that when pumping at 1960 cm^{-1} (near LP), the second and third excited vibrational states are preferentially excited. In our experiment, because LP is near 1960 cm^{-1}, we hypothesized that LP relaxed directly into the high-lying excited dark states as the intermediates, and then relaxes down back to the first excited dark modes, causing the delayed rising dynamics. We refer to it as polaritonic hot vibrational dynamics. The hot vibrational dynamics only occurred in nonpolar solvent environments (hexane and pentane), due to that molecular relaxation lifetime is sufficiently long enough in nonpolar solvents, for the excited state to be populated higher.

The dark state relaxation dynamics also showed cavity dependence. The Naval Research Laboratory team[14, 37] determined that the lifetime of dark state would be $\sim$20% longer than the bare molecular system, and highly detuning dependence (Figure 1.4f). The polariton lifetime of exciton-polariton systems also showed similar detuning dependence, which could be explained by the polariton compositions change. The detuning dependence of dark states in MVP is more complicated, as it could be due to net-dynamics from polariton lifetime changes, warrant more studies in the future.

Though the generality of polariton hot vibrational dynamics remains to be examined, there are similarities between this mechanism and the well-known plasmonic hot-electron dynamics. In MVP, the polariton excitation creates a delocalized macroscopic vibrational polarization, which can coherently interact with each other and generate coherent nonlinear signals with quantum

Rabi oscillations. The delocalized macroscopic polarization resembles the plasmon excitation. Then, these collective coherent polariton states quickly lose their characters and relax the energy into individual incoherent dark modes. Depending on the dielectric environments, MVPs can relax to high-lying (hot) vibrational states (Figure 4a), similar to the hot electron dynamics in plasmons. The possibility of reaching hot vibrational modes could open a new regime of mode elective chemistry using polaritons in the future.

1.7 Quantitative Scaling of Nonlinear Responses

We found a peculiar effect[9] of the nonlinear responses of MVPs - unlike normal nonlinearity, the nonlinearity of MVPs is not an intensive property of the systems. In molecular systems, when the systems are scaled in concentration and sample length, both the linear and nonlinear responses scale equally, indicating that the nonlinear susceptibility is an intensive property. However, in MVPs, when either the cavity thickness or molecular concentration decreases, the nonlinear signal increases relative to linear responses (referred to as polariton bleach) (Figure 1.5). This macroscopic dependence indicated that under SC, macroscopic collective molecular vibrational polarization formed, making polariton to be sensitive to macroscopic cavity thickness. Such sensitivity to macroscopic parameters lacks in molecular systems because each molecule behaves independently. This effect is related to the polariton blockade effects – when excitation reaches to saturation limits, higher-level polariton transition shifts out of the polariton transmission window, because of polariton-polariton interactions (mechanism shown in Figure 1.5a). As a result, the remaining polariton interacts less with incoming photons. When the thinner cavity or less molecular concentration is used (Figure 1.5b and c), it is easier to saturate the systems, and therefore evoke more significant nonlinearity. Small volume cavities such as photonic crystal cavities could further enlarge this effect.

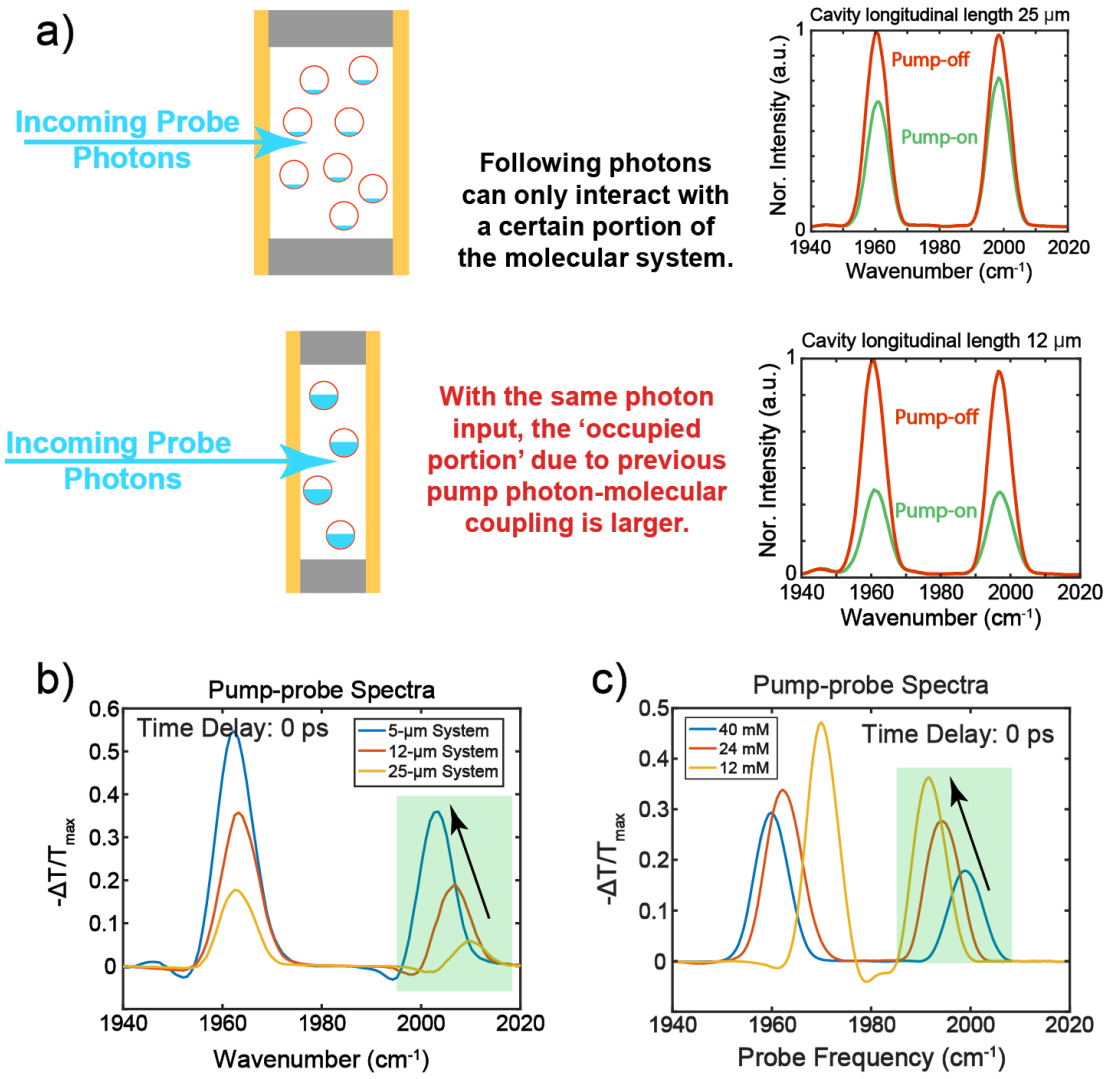

Figure 1.5: (a) The 'polariton bleach' mechanism. (b) Pump-probe spectra with various cavity longitudinal lengths (5, 12.5, and 25 microns). (c) Pump-probe spectra showing the polariton bleach with various molecular concentrations (40, 24, and 12 mM).

1.8 Strong Coupling Enabled New Vibrational Energy Transfer Pathways

While the study above builds the foundation of MVP dynamics, in real chemical reaction systems, different molecules and their vibrational modes are involved. In this case, more exotic molecular dynamics could occur. For example, the delocalized natures of polaritons allow

new vibrational energy transfer between molecules. There have been theoretical studies in this direction. For example, the Yuen-Zhou group proposed a few novel energy transfer schemes from theoretical aspects.[10–13, 34, 40, 41] They showed that energy transfer could differ drastically based on coupling schemes.[11] When bare donor modes are close in energy to acceptor-UP (Figure 1.6a), the reversal of donor and acceptor roles by SC results in the new 'FRET' scenario, allowing the energy transfer from acceptor mode to donor mode. This work sheds light on how to harness SC to enhance the molecular energy transfer processes.

To realize exotic energy transfer, one needs to make microcavity coupled to more than one molecular modes. Such work (Figure 1.6b) was first done in the hybrid of PMMA and DMF in the microcavities.[42] After introduced into the cavity, the two vibrational modes of PMMA and DMF, which were uncoupled originally, were both strongly coupled to the cavity mode and form three new polariton states, LP, MP, and UP. The three states all had the components of vibrational modes of PMMA and DMF (α_{PMMA} and α_{DMF}) as well as the cavity mode (α_{cav}). UP was most PMMA-like, while LP was most similar to DMF mode. MP was simultaneously composed by photon, PMMA, and DMF modes, as indicated by the Hopfield coefficient calculation (Figure 1.6b). Recently, another example of coupling 4 vibrational modes to one cavity modes, and thereby generating five polariton bands, has been reported. To keep multiple vibrational modes all strongly coupled to the same cavity mode, the detuning between modes need to be controlled within the coupling strength. For example, the energy gap between two vibrational modes should be comparable or less than $(g_1 + g_2)$, the sum of the individual coupling strengths. The preparation of multiple polariton systems reaches the first step for enabling intermolecular energy transfer in cavities. However, it does not guarantee that intermolecular energy transfer occurs.

To examine the energy transfer dynamics, we conducted ultrafast time-dependent spectroscopy to show the existence of intermolecular energy transfer under SC conditions.[8] We prepared SC between two originally uncoupled molecular modes (asymmetric CO stretching modes of $W(CO)_6$, donor, and $W^{13}(CO)_6$, acceptor), and the FP cavity modes. Without cavity,

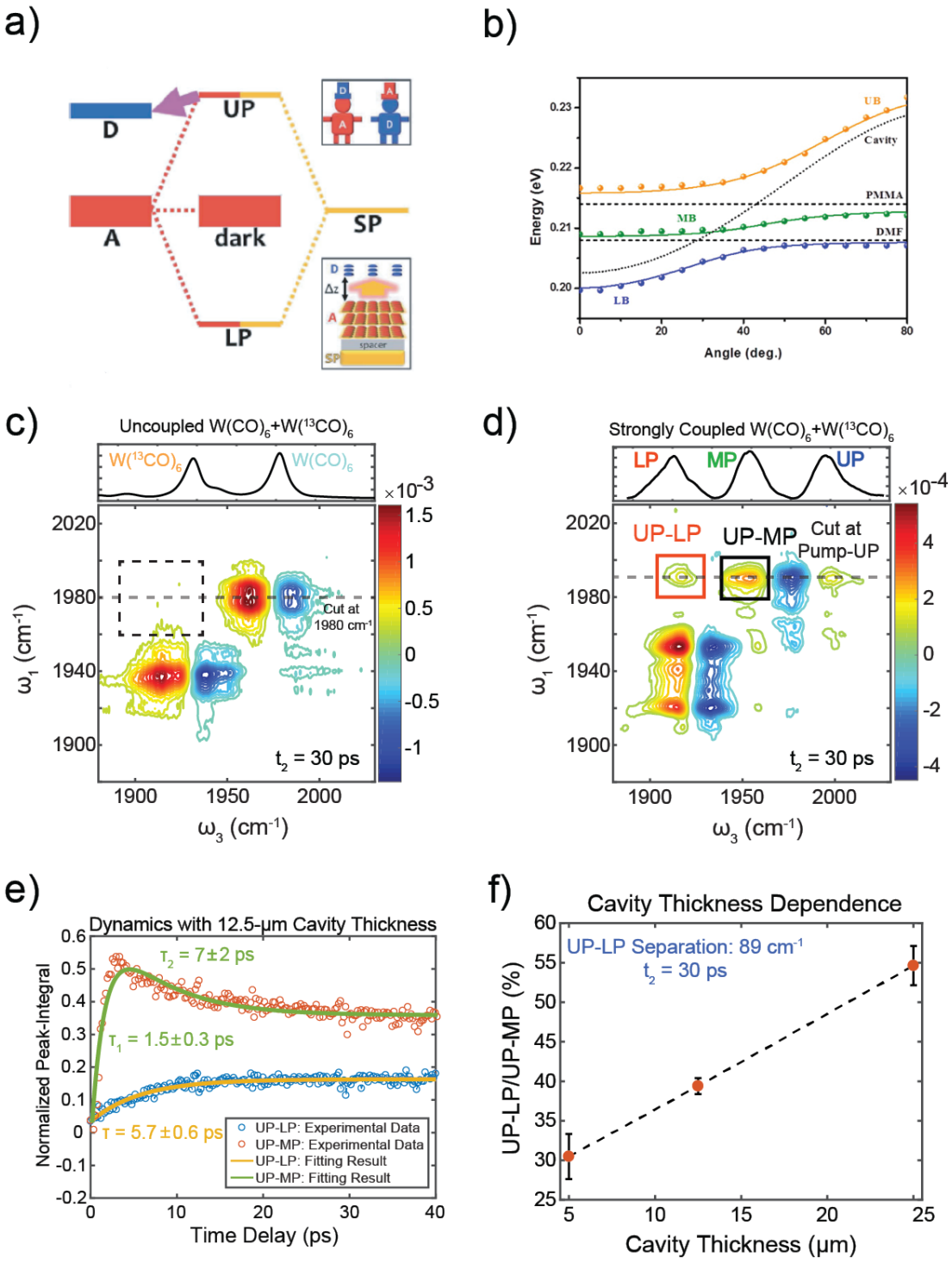

Figure 1.6: (a) The reversal FRET scenario. (b) Dispersive curves. 2D IR spectra of (c) uncoupled and (d) strongly coupled $W(CO)_6/W^{13}(CO)_6$. (e) Dynamic traces of UP-MP and UP-LP peak integrals. (f) UP-LP/UP-MP peak ratio with various cavity thicknesses.

the intermolecular FRET efficiency was insignificant (Figure 1.6c), as indicated by the lack of cross-peaks in 2D IR. In the SC regime, however, when the two molecular modes and cavity mode hybridized and form UP/MP/LP states (Figure 1.6d), the excitation of UP (mostly composed of donor and cavity modes) led to significant energy transfer to acceptor mode, shown as the cross peak (red square) of Figure 1.6d. The composition of donor and acceptor modes ratio in UP state was $\sim$14:1 (obtained from Hopfield coefficients of UP) while pumping UP state led the energy redistribution between donor and acceptor, which was 2.5:1 (Peak ratio obtained from Figure 1.6d). This result indicated extraordinary energy redistribution when the two molecular modes share the same cavity mode. Time-dependent features (Figure 1.6e) showed upon pumping UP, the donor population rises within around 1.5 ps through UP relaxation, while the acceptor population rises in $\sim$5 ps. Lastly, we controlled the energy redistribution ratio by changing the cavity longitudinal length (Figure 1.6f). We found that a thicker length cavity gave more efficient energy transfer, e.g., by increasing cavity from 5 to 25 μm the energy transfer efficiency increased from 30% to 55%. The thicker cavity led to longer polariton lifetime, which ensured more time for energy transfer under strong coupling.

By coupling the cavity mode with other molecular modes, molecular modes can benefit from the delocalization nature of the cavity. The evidence of intermolecular vibrational energy transfer supports the explanation that cooperativity and energy transfer between vibrational modes of reactants and solvents exist under strong-coupling conditions, which can lead to a change of chemical reactivities.

1.9 Nonlinear Polariton-Polariton Couplings for Quantum Information Science

Besides enabling interactions between molecules through photon cavity modes, cavity modes can also be coupled through molecular vibrational modes. Such a nonlinear coupling

among different cavity modes has applications[43, 44] in photonic circuitry, quantum computation, optical sensors. Thus, polariton-polariton interaction is an active research field.[17–22] Mainly, much research has been carried out in the exciton-polariton field. For example, recently, the Nelson group used a laser annular trap to trap polaritons, and by taking advantage of the mobility difference between polaritons and excitons, they disentangled the polariton-polariton and polariton-exciton interactions and carried out accurate measurements on the interaction strength.

For MVPs, because vibrational dipole interactions are short distance and weak, it has less effect to influence to polariton-polariton interaction measurements. However, the polariton-polariton interactions in MVPs remain unknown. The early-time polariton dynamics[9, 14, 39] shed light on polariton-polariton interactions in MVPs, which triggered our recent attempt to enable nonlinear interactions between spatially adjacent MVPs. The key idea is to take advantage of the photon-molecule duality of polaritons, where the photon is spatially delocalized, and the molecular modes have nonlinearity, the combination of which enables a delocalized nonlinear interaction among cavities.

We achieved this idea by employing a dual-cavity system.[22] The two adjacent cavities had different thicknesses, forming two cavity modes with their own frequency (Figure 1.7a). Because of photon mode delocalization, there was a mode volume overlap at the boundary between two cavity modes. We prepared the polariton systems by encapsulating a saturated $W(CO)_6$/hexane solution in the coupled-cavity matrix. The linear transmission spectrum shows four polaritonic peaks (UP1, UP2, LP1, LP2), suggesting two subsets of molecular vibrational mode coupled to two cavity modes, respectively, forming two sets of LP/UP polaritons (Figure 1.7b). However, we found only when a photon-hopping (delocalization) component existed between the two cavities (model 2, Figure 1.7c, bottom panel), the linear spectral is fully simulated, whereas uncoupled two-cavity model could not reproduce the experimental results (model 1, top three panels, Figure 1.7c). This agreement suggests that delocalization at the boundary made molecules strongly coupled to the cavity mode it resides in and weakly couple to

the adjacent cavity.

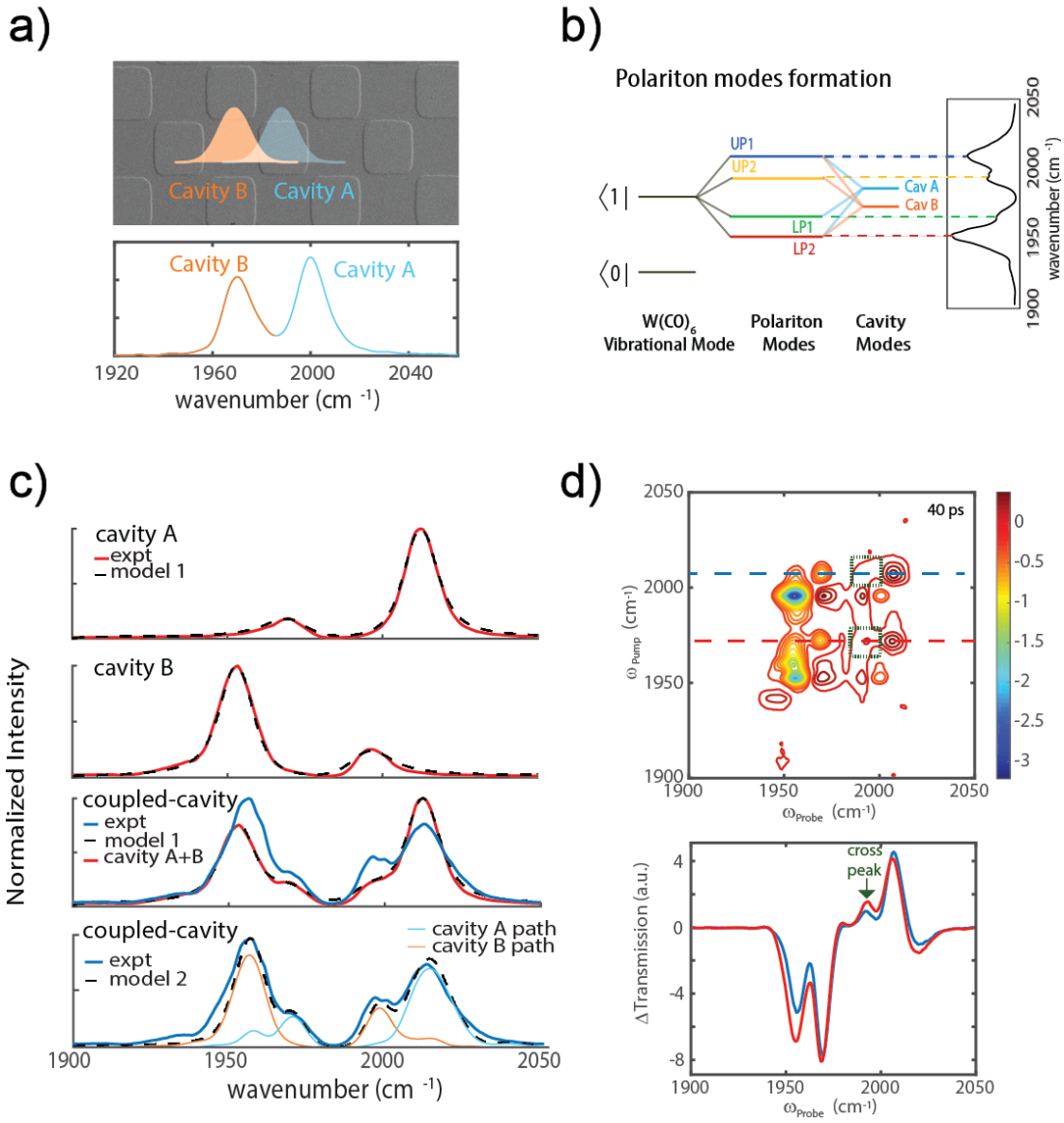

Figure 1.7: (a) Top: SEM of the patterned cavity mirror; bottom: FTIR of the dual-cavity. (b) Energy diagram of polaritons. (c) Experimental and simulated linear spectra. (d) Top: 2D IR of $W(CO)_6$/hexane in the dual cavity. Bottom: 2D IR cuts at UP1 (blue) and LP1 (red).

This delocalization enabled the nonlinear interaction between polaritons at adjacent cavities, evidenced from 2D IR experiments. The dual-cavity polariton system showed two sets of 2D IR peaks (diagonal and cross-peaks) as labeled by the two solid squares. Because the

spectra were taken at 40 ps, the spectral signature is due to excited dark mode absorption and Rabi splitting contractions. A few unexpected cross-peaks are evidence of intercavity polariton interactions. For example, the spectral cut at $\omega_1 = \omega_{UP1}$ and ω_{LP1} (Figure 1.7d, bottom panel) showed cross-peaks at $\omega_3 = \omega_{UP2}$ (dashed box in the top panel and green arrows in the bottom panel of Figure 1.7d). Both represented the interactions between polaritons from cavity A to the UP of cavity B. Simulations indicated that such cross-peaks only exist when both molecular anharmonicity and photon hopping are enabled. Thus, this phenomenon could be explained as: when polaritons in cavity A were exited, they quickly relax to dark modes. Because part of the excited dark modes resides in the overlapped volume between cavity A and B, it causes Rabi splitting contraction of the polariton in cavity B. Thus, it is the incoherent excited dark mode population shared across two cavities lead to the intercavity polariton interactions.

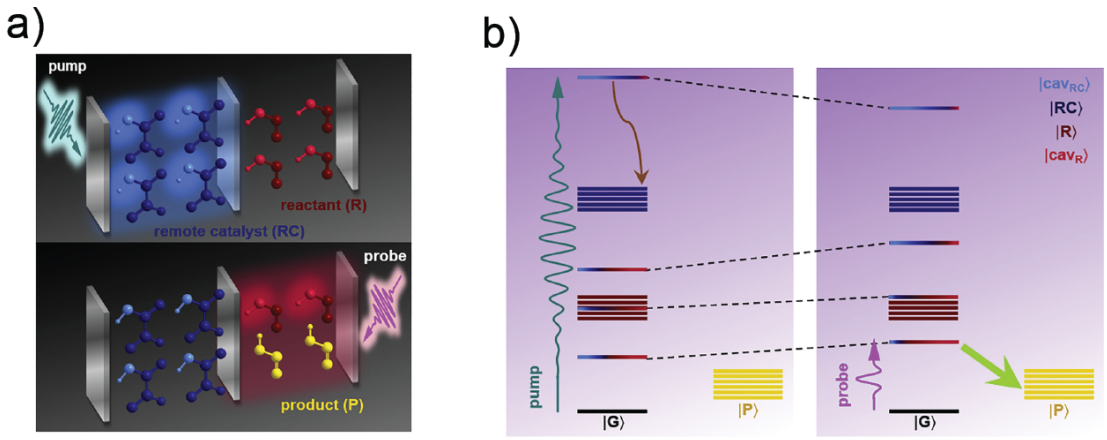

Figure 1.8: (a) Simplified visualization of remote catalysis. (b) Energetic representation. Left: upon pumping, the highest polariton relaxes to RC dark states. Right: efficient transfer into the product-yielding state occurs.

The idea of cross-cavity interactions between polaritons can be applied to control chemical reactions. For example, the Yuen-Zhou group recently proposed a cavity-induced remote catalytic reaction of **Cis** $\rightarrow$ **trans** isomerization of nitrous acid[12] (shown in Figure 1.8a). The remote catalyst (RC) is spatially separated from the reactant (R), but R and RC are connected by forming the same polaritons with the two connected cavity modes. Without optical exciting RC, the probe

pulse cannot trigger the reaction because it is off-resonance with LP, which is composed mostly by R. Sufficient optical pumping RC can shift LP into resonance with the probe pulse (Figure 1.8b), which enables reaction toward product state (P). The simulation results showed that increasing pump power could enhance product yield. The experimental and theoretical works discussed here could guide the rational design of SC devices to alter reactions and energy transportations.

1.10 Conclusion and Outlook

In this perspective, by giving an overview of the current status of MVPs, we hope to stimulate more interest in this emerging field. The field is still at the infancy stage in both chemical reaction and its corresponding chemical physics and mechanism aspects. From the reaction perspective, the generality of cavity-modified reactions is worth to explore. From chemical physics and mechanism perspective, the proposed mechanism, in particular, energy dynamics in the strong-coupled systems, remain to be validated. Current chemical physics studies have been limited to model systems, and relevant research in more complex systems is necessary. Lastly, early studies have shown molecular vibrational polariton's potential for ultrafast photonics and quantum information research. Thus, it is a fertile ground for physical chemistry and material chemistry research.

Chapter 1, in full, is currently being prepared for submission for publication of the material. Bo Xiang; Wei Xiong., The dissertation author was the primary investigator and author of this paper.

Chapter 2

Multidimensional Vibrational Spectroscopy in Theory

2.1 Linear Macroscopic Polarization

Macroscopic polarization is the signal emitted by a system in interaction with an external electric field. In general, the polarization (P(ω)) of a sample induced by light of frequency ω is expanded in powers of the incident electric fields ($E_i(\omega)$): [45]

$$\begin{aligned} P(\omega) &= \varepsilon_0[\chi^{(1)}E_1(\omega) + \chi^{(2)}E_1(\omega)E_2(\omega) + \chi^{(3)}E_1(\omega)E_2(\omega)E_3(\omega) \\ &\quad + \chi^{(4)}E_1(\omega)E_2(\omega)E_3(\omega)E_4(\omega) + \cdots] \\ &\equiv P^{(1)}(\omega) + P^{(2)}(\omega) + P^{(3)}(\omega) + P^{(4)}(\omega) + \cdots \end{aligned} \tag{2.1}$$

In linear optics, the polarization depends linearly on the electric field E:

$$P(\omega) = P^{(1)}(\omega) = \varepsilon_0\chi^{(1)} \cdot E(\omega) \tag{2.2}$$

with $\chi^{(1)}$ the linear susceptibility. This susceptibility is related to IR absorption spectroscopy.

For linear spectroscopy such as FTIR, macroscopic polarization relies on the linear response as described in time-domain representation in the following function:[33]

$$P(t) = P^{(1)}(t) = \frac{i}{\hbar}\int_0^\infty dt_1 \mu_1 E_0(t-t_1)\cdot R^{(1)}(t_1) \tag{2.3}$$

where μ_1 is the transition dipole moment of the sample, and $R^{(1)}(t_1)$ is the first order response function. The emitted signal field $E^{(1)}(t)$ is given by:

$$E^{(1)}(t) \propto iP^{(1)}(t) \tag{2.4}$$

which is called the free induction decay.

2.2 Nonlinear Macroscopic Polarization

However, when the external electric fields are intense enough, the above linear relation between macroscopic polarization and electric field does not hold anymore because the nonlinear terms in the expansion (Eq. 2.1) become non-negligible.

2D IR is a third order spectroscopic technique and as such, the macroscopic response ($P^{(3)}(t)$) is associated with $\chi^{(3)}$ and a function of three input pulses. In ultrafast spectroscopy,

it is more convenient to use a time-domain representation instead of the frequency-domain representation of Eq. 2.1. In a 2D IR pulse sequence each pulse interacts with the sample at time intervals t_1, t_2, and t_3. Therefore, an expression for the macroscopic polarizability can be written as:[46]

$$P^{(3)}(t) \propto (\frac{i}{\hbar})^3 \int_0^\infty dt_3 \int_0^\infty dt_2 \int_0^\infty dt_1 \mu_3 E_3(t-t_3) \mu_2 E_2(t-t_3-t_2) \\ \mu_1 E_1(t-t_3-t_2-t_1) \cdot R^{(3)}(t_3, t_2, t_1) \tag{2.5}$$

where $P^{(3)}(t)$ results from the convolution of the three external IR fields with the response function $R^{(3)}(t)$ generated by samples. The emitted signal field $E^{(3)}(t)$ is given by:

$$E^{(3)}(t) \propto iP^{(3)}(t) \tag{2.6}$$

The variables t_i are time intervals between the successive ultrashort IR pulses. These time delays can be controlled in experiments and are scanned to acquire 2D spectra, as well as dynamics of systems under study. The response function $R^{(3)}(t)$ constitutes all possible pathways for the electric fields to act on the sample and emit signal. For the simple case of a single vibrational mode that is not coupled to any other mode, three pathways known as ground state bleach (GSB), stimulated emission (SE), and excited state absorption (ESA) are represented in the energy-level diagram (Figure 2.1, reproduced from [46]) introduced by Albrecht et al.[47, 48]

For a standard 2D IR signal, the three lowest vibrational levels, i.e. v = 0, 1, 2 are often in consideration. The 0 -1 transition (GSB/SE) and 1-2 transition (ESA) result in opposite signs of the signal: 0 -1 transition reduce absorption of the probe IR pulse, while 1-2 transition introduce

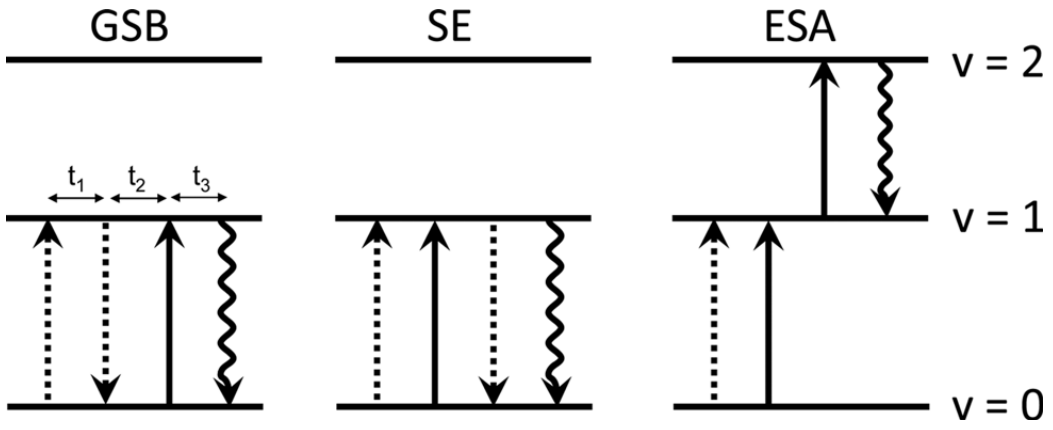

Figure 2.1: Energy level diagrams for third-order IR spectroscopy. Only rephasing diagrams are shown for clarity. Vibrational states (v = 0, 1, 2) are represented by horizontal lines. Signal emission is indicated with a wavy arrow.

new absorption (Figure 2.2, reproduced from[49]). Therefore, for a vibrational mode to be observable in 2D IR, the mode cannot be a ideal harmonic mode — 0 -1 and 1-2 transition will have same frequency yet opposite sign and cancel out each other.

In general, the three pulses involved in Two-dimensional IR are two pump pulses and a probe pulse. The first and third interaction with IR pulse to produce vibrational coherences, which oscillate as functions of t_1 and t_3, respectively. Thus, t_1 and t_3 are referred to as "coherence time". The second pump pulse interacts with the system and converts the coherence state produced by first pump pulse to a population state, which makes t_2 the "population time". 2D IR spectra for a fixed population time t_2 are obtained after a 2D Fourier transformation of the emitted field as a function of coherence times t_1 and t_3,[33] which correspond to the two spectral axes in 2D IR spectra. often called "pump" (ω_1) and "probe" (ω_3) The shape of the resulting 2D IR spectra will depend on t_2.

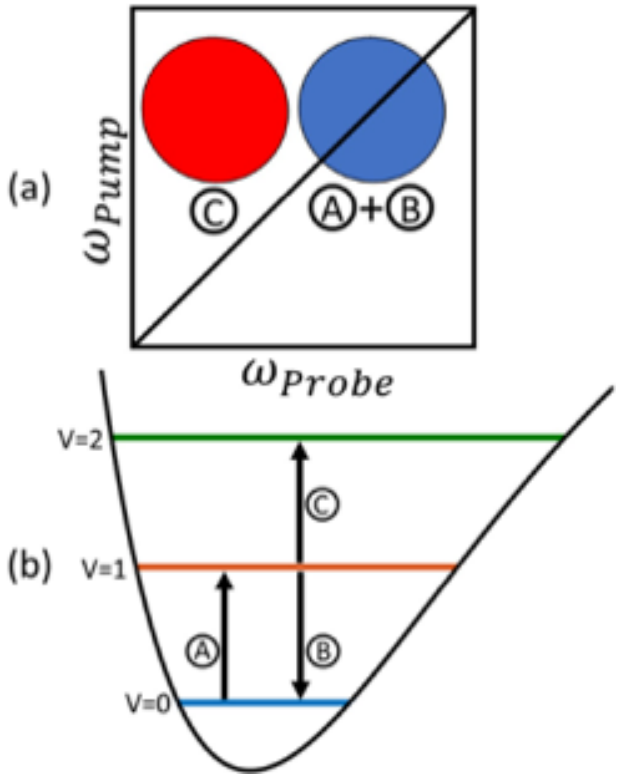

Figure 2.2: a) Cartoon representation of a 2D IR spectrum. b) corresponding enerfy level diagram in an anharmonic vibrational mode. Transitions are labeled as a, b, and c.

Chapter 3

Multidimensional Vibrational Spectroscopy in Practice

3.1 Experimental Setup for 2D IR Spectroscopy

2D IR spectra were collected in pump-probe geometry, as shown in the schemetic layout in Figure 3.1.[50, 51] The pulse sequence is described in Figure 3.2. Two pump pulses and a probe pulse (pulse duration of 100-150 fs) interact with samples at delayed times (t_1, t_2 and t_3).

To generate the pulse sequence, 800 nm laser pulses ($\approx$35 fs, $\approx$6 W, 1 kHz) were generated by ultrafast Ti:Sapphire regenerative amplifier (Astrella, Coherent) . The 800 nm was converted into mid-IR pulses by optical parametric amplifier (TOPAS, LightConversion) followed by a different frequency generation process on a Type II $AgGaS_2$ crystal (Eksma). The mid-IR pulse (30 μJ) was split into two beams by a CaF_2 wedge beam-splitter. The majority (95%) was sent into a Ge-AOM based pulse shaper (QuickShape Kit, PhaseTech) to prepare the two pump pulse in the pulse sequences, whereas 5% mid-IR served as the probe. The pump pulse pair (2 μJ at the sample), the probe ($<$0.5 μJ) were all focused and spatially overlapped on the sample by a f = 10 cm parabolic mirror and collimated by another parabolic mirror in a symmetric geometry. To

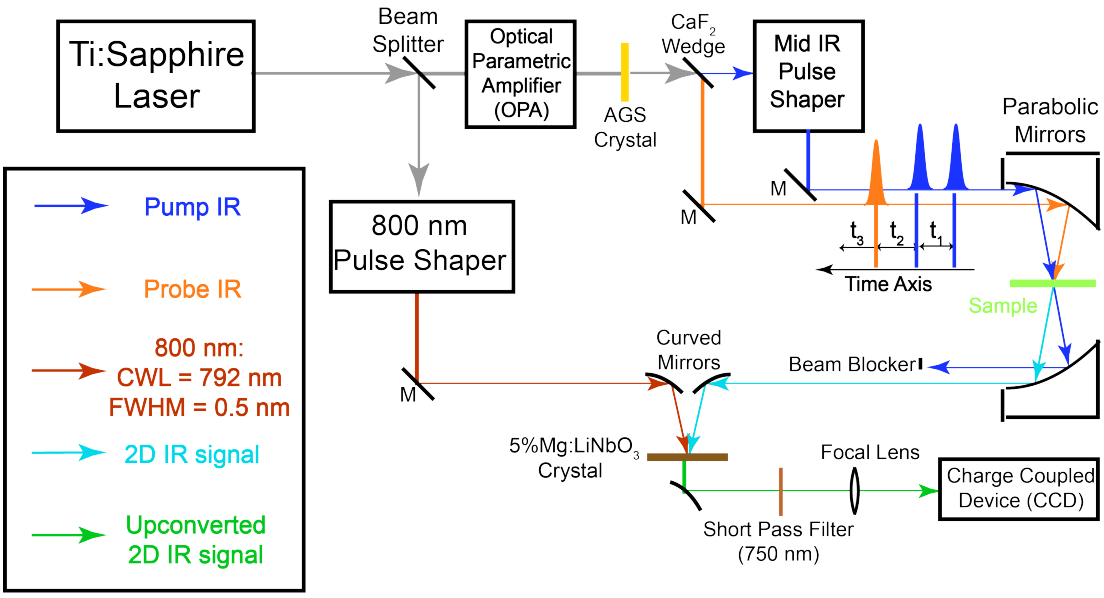

Figure 3.1: Scheme of 2D IR experimental setup.

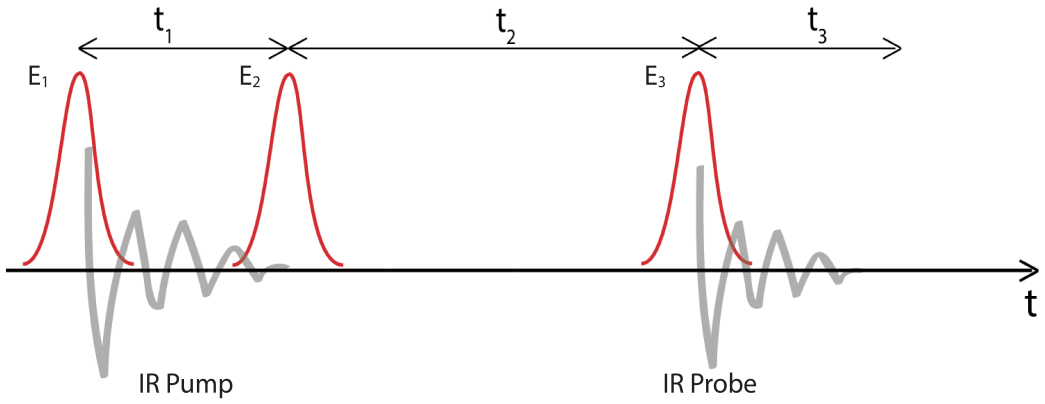

Figure 3.2: Pulse sequence in 2D IR experiment.E_1, E_2 and E_3 are the mid IR pulses interacting with the molecules.

study the molecular vibrational polariton systems, a rotational stage has been employed to mount the polariton samples so that the incidence angle of IR can be tuned. In order to detect the output IR signal by the CCD camera (256 $\times$ 1,024, Andor), the collimated signal and the probe beam were then upconverted by a residue 800 nm beam on a 5%Mg: $LiNbO_3$ crystal. [52, 53] The 800 nm beam that comes out of the OPA passes through an 800 nm pulse shaper which narrows its spectrum in the frequency domain (center wavelength of 791 nm and a FWHM of 0.5 nm or 9.5

cm^{-1}).

3.2 2D IR Data Collection and Analysis

In the 2D IR experiments, two vibrational coherences were generated during t_1 and t_3 periods, respectively. The first coherence was measured by scanning t_1 time from 0 to 2000 fs (could vary depending on the free induction decay time of the vibrational mode) in steps of 20 fs using the pulse shaper, where a rotating frame at f_0=1583 cm^{-1} was used to shift the oscillation period to 80 fs, so that the scanning step can meet with the Nyquist frequency requirement. After waiting for t_2, the third IR pulse (probe) interacts the sample, and generate the second coherence. The resulting macroscopic polarization emits an IR signal. This IR signal is upconverted by a narrow-band 800 nm beam. The upconversion process covers the t_3 time delay and the 800 nm pulse duration determines the scanning length of t_3.[54, 55] The up-converted IR signals (second vibrational coherence) were experimentally Fourier transformed by a spectrograph and detected by a CCD camera. To get full absorptive 2D IR spectra, the first vibrational coherence was numerical Fourier transformed along t_1 axis. The pump and probe pulses had the same polarization in 2D IR measurements. For the time dependent 2D IR measurements, t_2 was scanned by a computerized delay stage.

Chapter 4

Molecular vibrational polaritons and their interactions with dark reservoir modes

4.1 Introduction

Molecular vibrational-polaritons can be described as delocalized quantum superpositions of molecular vibrations and electromagnetic modes resulting from strong coupling between them,[56, 57] which extend across a macroscopic number of molecules in the entire photonic mode (Figure 4.1a and b). Following the impressive developments in the field of exciton-polaritons, including room-temperature tabletop realizations of superfluids,[58] polariton lasing,[59] and Bose-Einstein condensates,[60] it is anticipated that vibrational-polaritons will open opportunities for new photonic and molecular phenomena. While some have been recently explored, such as chemical reactivity control through modified vibrational dynamics, and tailored potential energy landscapes,[3, 42, 56] other promising applications are still waiting for experimental demonstrations, e.g., long-range mesoscopic vibrational energy transfer, novel optical switches and lasing in mid-IR regime. Vibrational-polaritons have been probed in polymers, neat liquids, and solutions[3, 42] using steady-state optical responses, including linear IR and Raman spectroscopy.

This research revealed enhanced Raman scattering[61] and modified kinetics of chemical reactions, even in the absence of external pumping.[15, 57] The first time-resolved spectroscopic study of these systems showed vibrational-polariton dynamics that were significantly faster than that of the uncoupled molecule and highly sensitive to the light-matter composition of the polaritons (i.e., the Hopfield coefficients).[14]

However, important aspects of vibrational-polaritons are still not understood because molecular vibrations behave qualitatively different from the well-studied excitons (excitons consist of an electron-hole pair while the vibrational degree of freedom is a weakly-perturbed harmonic oscillator), and the polariton-polariton interactions, as well as the couplings between polaritons and other degrees of freedom cannot be accessed through steady-state spectroscopy. For instance, it is known that the hybrid cavity has many dark states in comparison to the few bright modes:[57, 62, 63] One type of dark states share molecular components and some small photonic character with polaritons as a result of disorder.[62] Another type of dark states, termed "uncoupled" molecules, consist of molecular vibrations which are not coupled to the cavity electric field (e.g., because they may be outside the photonic-mode volume, or because their transition dipole moment is orthogonal to the external field polarization), which should not contribute to polariton transmission spectra. Further development of molecular vibrational-polariton photonic devices hinges on detailed understanding the role of dark states in microcavities and how they interact with the bright polariton states. However, since darks states are invisible in linear spectroscopy, we know little about them.

In the following, we report the first ultrafast 2D IR spectroscopy[64] investigation of vibrational-polaritons, to resolve state-selective excitation and population transfer, and thereby reveal hidden dark states and their influences on polaritons. The combined effort in utilizing 2D IR spectroscopy to study novel vibrational-polariton states advances our understanding of both fields. 2D IR spectroscopy can explicitly excite and detect transitions in a state-selective manner, which reveals unexpected interactions between dark states and vibrational-polaritons as well as

direct excitation of dark states. These vibrational-polaritons bring 2D IR into a new regime that has never been explored before and presents new theoretical challenges. The mere existence of vibrational-polariton pump-probe[14] and 2D IR signals is direct evidence of deviations from the harmonic polariton model and motivates our development of a theoretical treatment of nonlinear polariton response incorporating vibrational anharmonicities. We find that in contrast to the well-studied exciton-polariton, whose main source of nonlinearities is the so-called "phase space filling" effect which arises due to Pauli exclusion,[65, 66] vibrational polaritons feature new sources of nonlinearity - nuclear and electrical anharmonicities, which enable and determine optical features in the 2D IR spectra of vibrational-polaritons. These new findings represent a major step forward in the critical development of a comprehensive understanding of how to achieve novel mid-IR photonic behavior with molecular vibrational-polaritons.

4.2 Results

The $W(CO)_6$ (Sigma-Aldrich) /cavity system is prepared in IR spectral cell (Harrick) containing two dielectric CaF_2 mirrors separated by a 25 μm spacer and filled with nearly saturated $W(CO)_6$/hexane solution. The dielectric mirror has a $\sim$96 % reflectivity. Because the Rabi splitting (37 cm^{-1}) is larger than the full-width-at-half-max of both cavity ($\sim$10 cm^{-1}) and $W(CO)_6$ vibrational ($\sim$3 cm^{-1}) modes, the strong coupling criteria is satisfied. . In the strong coupling regime, upper and lower polariton branches (termed UP and LP) are formed upon hybridization of vibrational and cavity modes (Figure 4.1c). By adjusting the tilt angle, θ(Figure 4.1a), the cavity resonance can be tuned across the vibrational transition, thus revealing a dispersive anti-crossing and allowing control of the polariton light-matter composition (Figure 4.1d).[3, 57, 60] When the cavity-vibration detuning is zero (i.e., frequency of both is 1983 cm^{-1}), LP and UP have equal photonic and delocalized-vibration characters (Figure 4.1c). The energy difference between the polariton branches at this condition ($\sim$37 cm^{-1}) corresponds to the

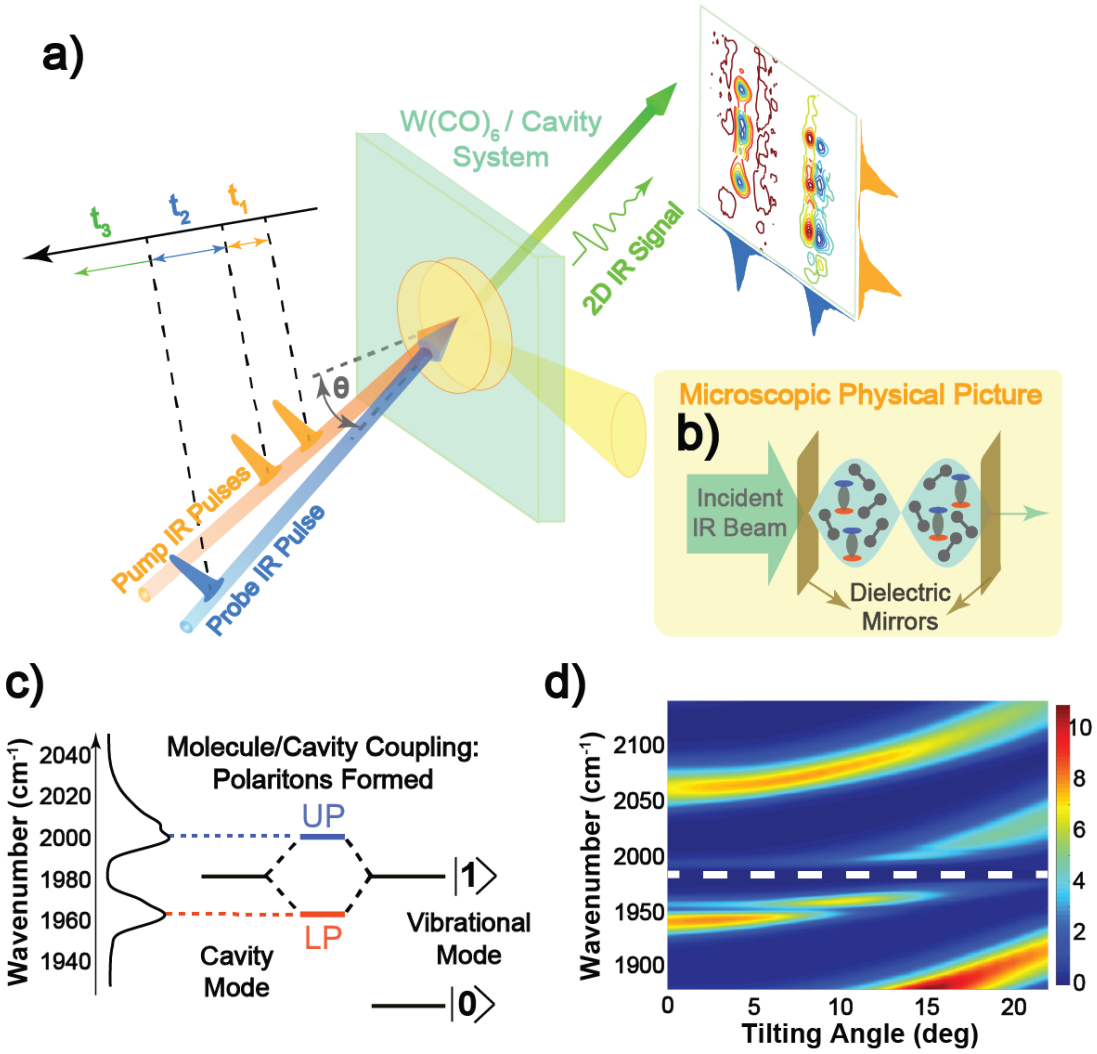

Figure 4.1: (a) 2D IR setup. (b) Microscopic physics of molecules inside of a microcavity. (c) Formation of vibrational polaritons by strongly coupled molecular vibration and cavity modes. (d) Dispersion of IR transmission of strongly coupled $W(CO)_6$ system.

vacuum Rabi splitting. Blue-tuning the cavity probes an LP transition with stronger vibrational character while the UP has a higher photonic component. Red-tuning has the opposite effect.

4.2.1 Pump-probe and Free Induction Decay

We first confirm that the pump-probe response of molecules both inside and outside the cavity agree with published results.[14, 67, 68] The transient spectrum for uncoupled $W(CO)_6$

(Figure 4.2a) is well-understood. The negative feature at 1983 cm^{-1} corresponds to ground state bleach and stimulated emission while positive features indicate absorption in newly populated excited states. Importantly, for this uncoupled system, only the peak amplitudes vary with excited-state population, i.e., the spectral position of each transient feature remains fixed at the frequency corresponding to the excited or bleached state irrespective of the pump-induced transient population. Notable qualitative differences are observed between the bare molecule pump-probe response (Figure 4.2a) and that of the strongly-coupled system (Figure 4.2b). As further explained below, the distinctive features in the polaritonic spectra do not necessarily correspond to transient population changes of states. Instead, they are due to the interaction of cavity photons with the matter polarization originating from excited-state absorption, ground-state bleach, and stimulated emission of reservoir modes.

To obtain 2D IR spectra, t_1 is scanned to measure the free induction decay (FID) of vibrational coherences. A comparison of FID of ω_{01} peak of $W(CO)_6$ in free space and the peak at 1968 cm^{-1} in microcavity shows that dephasing time of vibrational-polariton is shorter than that of free molecular vibrations for all k values. This is due to the hybrid nature of the polaritons, whose dephasing times will have a contribution from the cavity, which has shorter dephasing time than the molecule in our system. If a cavity with a narrow resonance linewidth and a long dephasing time is used, and the polariton has a large fractional photon character, we expect that dephasing times could become longer than the natural dephasing time of the vibrations of the free molecules, which has the potential to manipulate coherence transfer in long lived coherences. Aside from the modified FID, we also observe "quantum beating". This is expected for polariton spectroscopy, since we coherently excite both UP and LP and the beating period $\sim$0.75 ps matches the Rabi splitting frequency. However, as we show later, an unexpected "dark mode" transition also contributes to the beating in FID traces.

4.2.2 2D IR Spectra of Vibrational Polaritons

A 2D IR spectrum is generated by numerical Fourier transforming the t_1 FID traces at individual ω_3 frequency. 2D IR spectroscopy reveals coherences between states using a three IR pulse sequence (Figure 4.1a). We focus on results obtained at t_2 = 25 ps, where spectral oscillations have ceased, and after which only incoherent polariton-polariton and polariton-dark state interactions are significant. There are sharp contrasts between the 2D IR spectra of uncoupled $W(CO)_6$ (Figure 4.2c shows ground state bleach/stimulated emission and excited-state absorption at the frequencies of those transitions) and cavity-coupled $W(CO)_6$ (Figure 4.2d shows strong excited-state absorption features extending along the ω_1 axis and weaker features near the UP region). We have eliminated the possibility of a cavity-induced spectral filtering effect contributing to the 2D IR spectra.

Details of the cavity-coupled response are more clearly seen in Figure 4.3 where we have rescaled each region for visibility. Figure 4.3 shows many features along the diagonal, where the system is pumped and probed at the same frequency, as well as cross peaks, indicating coupling or energy transfer between modes. Along the diagonal, we observe a large absorptive feature in the LP region (ω_1=ω_3=ω_{LP}) (Figure 4.3c), and a derivative-like modulation in the UP region (ω_1=ω_3=ω_{UP}) (Figure 4.3d). Additionally, "cross peaks" appear when exciting either polariton mode.[69] Specifically, when the UP is excited, a strong feature (Figure 4.3a) identical to that of Figure 4.3c is observed when the system is probed at the LP frequency (ω_1=ω_{UP}, ω_3=ω_{LP}), and the derivative lineshape observed in Figure 4.3d also appears when the LP is excited (ω_1=ω_{LP}, ω_3=ω_{UP}) (Figure 4.3f). Calculations based on Fresnel expressions[14] associate the large, absorptive feature located at the LP region ($\sim$1960 cm^{-1}) with the coupling of the cavity mode to v = 1 to 2 polarization (due to transient v = 1 dark population). The derivative lineshape in the UP region and weak negative responses at the edges of the LP region are essentially manifestations of a redshift of the UP transition and a blueshift of the LP, ascribed mainly to an effective Rabi splitting contraction induced by reduction of ground state (v = 0) population. The motion of the

LP is somewhat obscured because of the large absorptive feature at LP region.

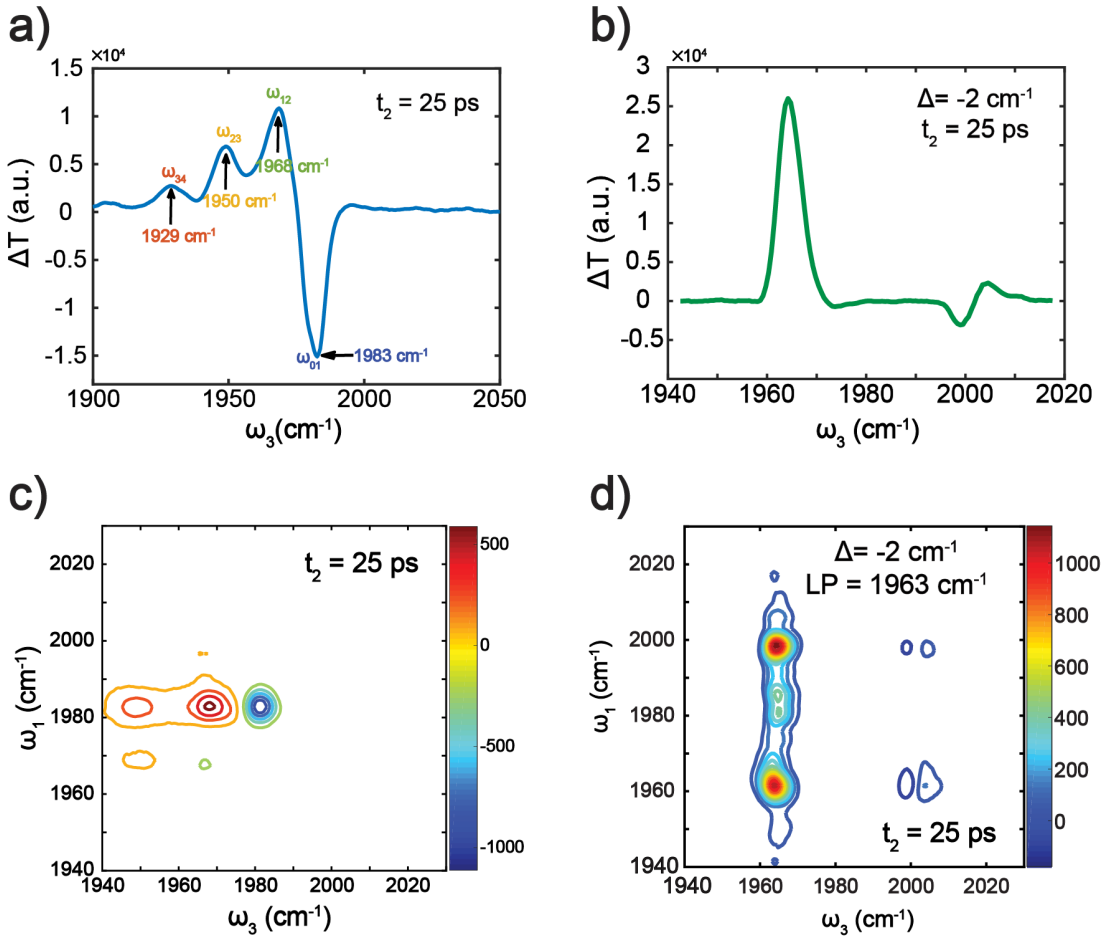

Figure 4.2: Pump-probe spectra of (a) uncoupled $W(CO)_6$ and (b) strongly coupled $W(CO)_6$ system. 2D IR spectra of (c) uncoupled $W(CO)_6$ and (d) strongly coupled $W(CO)_6$ system.

4.2.3 Unexpected 2D IR peaks reveal dark state populations

A third set of features requires discussion. When the system is excited at the ω_{01} frequency, and probed at the LP and UP frequencies, (Figure 4.3b and e), peaks are observed, consistent with the presence of v = 1 dark state population. While these features are similar to those discussed above, their presence when exciting at the ω_{01} frequency indicates direct excitation of dark states of $W(CO)_6$ despite their "dark" nature. This direct excitation of dark modes is comparatively weak

(see unscaled data of Figure 4.2d). We believe it occurs by way of non-unity cavity reflections and disorder in the molecular system[62] (the phenomenon is analogous to the observed direct excitation of bare excitons in systems with exciton-polaritons)[65]. The former is necessary for excitation of molecular vibrations which are not coupled to the cavity mode, and the latter is needed for exciting dark states which share molecular component with polaritons. Given that the uncoupled molecules are not expected to have influence on polariton optical response (since they provide no contribution to the polariton formations, e.g. Rabi splitting), the correlations between vibrational-polaritons and dark-states (Figure 4.2d, 4.3b and 4.3e) indicate that many of the dark-modes excited at 1983 cm^{-1} are formed from molecules which contribute significantly to polariton transitions. These dark-states define a coupled reservoir. Notably, disorder of the molecular system is expected to substantially localize these modes.[70] Thus, we expect them to behave very similarly to pure molecule excitations - their optical transitions and lifetimes are similar to those of uncoupled molecules.[14]

The features in Figure 4.3b and 4.3e have not been observed in any polariton coherent 2D spectroscopy and indicate significant interaction between the so-called dark modes and bright polaritons - when one mode (dark) is excited, it influences the optical response of the others (polaritons)[66]. A similar interaction, but in the opposite order (exciting polaritons and influencing dark modes), is also evident in the 2D IR spectra. The large absorptive features in Figure 4.3a and 4.3c are due to dark excited state population and occur after selective excitation of either polariton. The fact that response is qualitatively similar when exciting at the LP, UP, or even the dark state frequency, indicates that there are polariton-dark state interactions that lead polaritonic excitations (either LP or UP) to transfer into dark states possibly via phonon scattering.[71]

The existence of dark state peaks imposes difficulty in disentangling certain spectral signatures. In principle, the large positive signals observed near the LP (Figs.3a, b and c) are a mixture of two principle, the large positive signals observed near the LP (Figs.3a, b and c) are a

mixture of two contributions: nonlinear polariton optical response and excited-state absorption from the coupled reservoir state hot bands.[14] In contrast, the 2D spectra that probe UP states are easier to understand (Figs.3d, e and f), and reveal interactions between various states. For example, the derivative-like feature in Figure 4.3e and 4.3f indicates that by populating either the LP or dark modes, the UP frequency is modulated. Such insights are obfuscated when probing near the LP due to its near-resonance with the coupled reservoir excited-state absorption.

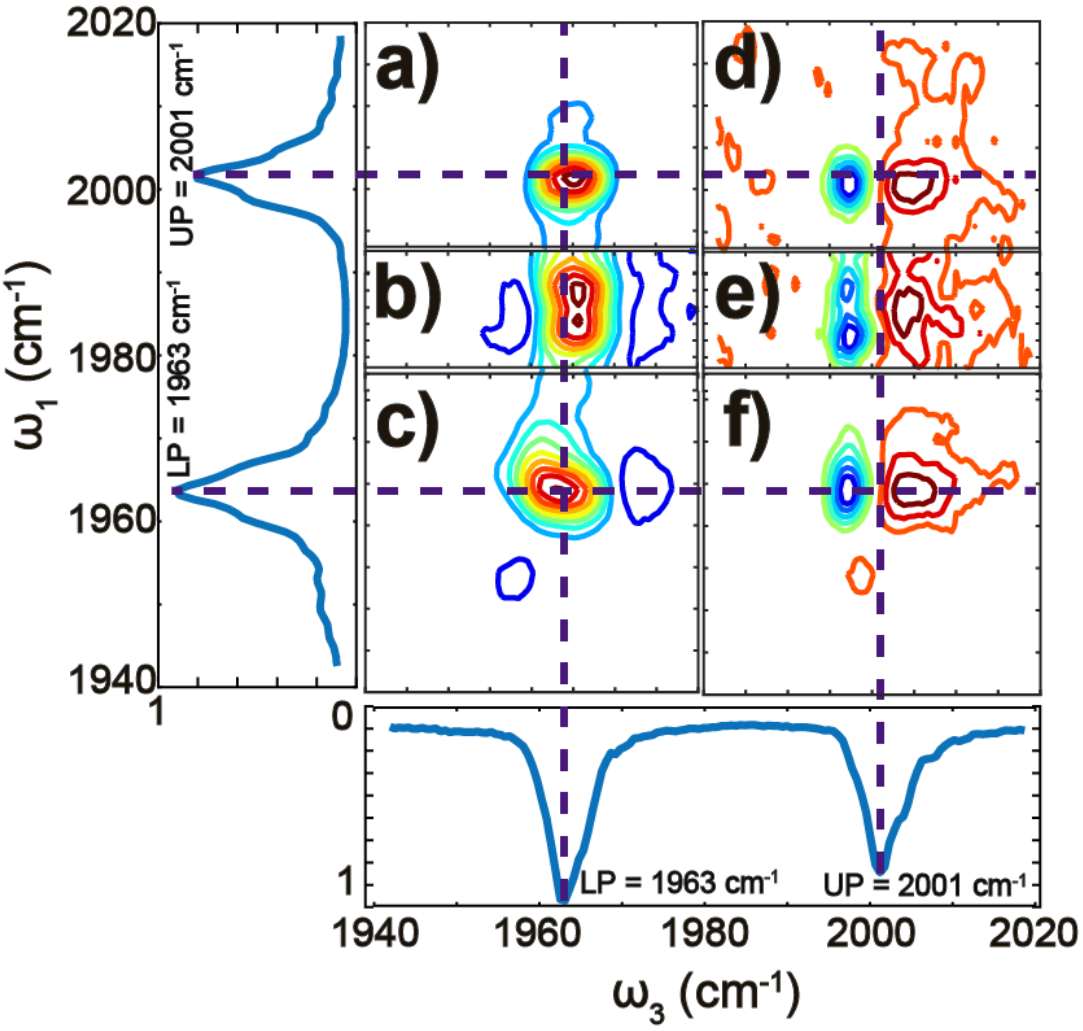

Figure 4.3: 2D IR spectrum of $W(CO)_6$/cavity polariton system at 25 ps delay. Each spectral region is scaled to its own intensity maximum and minimum. Spectra of the pump and probe pulses are shown on their respective axes.

4.2.4 Cavity-Detuning-Dependent Response

Important insights arise from examining the system response as a function of cavity detuning. The data in Figure 4.4 correspond to spectral cuts along the probe frequency axis (ω_3) with the pump frequency (ω_1) fixed at the reservoir mode (ω_{01}), LP, and UP frequencies (ω_{LP} and ω_{LP}) (Figure 4.4a, b, and c, respectively). The cavity is detuned by rotating the sample as described in Figure 4.1a. When exciting at ω_1 = 1983 cm^{-1} (dark state, Figure 4.4a), a large positive feature is seen near the LP region; it is maximal when the cavity is tuned such that the LP frequency is 1968 cm^{-1}. On the other hand, while the spectral cuts at LP and UP frequencies (Figure 4.4b and c) show a similar feature, it is maximized when LP is tuned to 1963 cm^{-1}.

As discussed above, the large feature in the LP region can be attributed to the existence of an excited-state population in the v1 coupled reservoir states. Therefore, the detuning-dependent intensity of this peak indicates either (i) a varying sensitivity to reservoir state population or (ii) a detuning-dependent efficiency in generating coupled reservoir population. First, we examine Figure 4.4a where reservoir states are excited directly. In this case, the signal is maximized when the LP resonance is tuned to the ω_{12} band ($\sim$1968 cm^{-1}). This behavior is analogous to a cavity-enhanced optical response where the excited-state population of reservoir states is most sensitively probed when the polariton resonance is coincident with the transition being probed.[72] In other words, the reservoir population may not be influenced much by tuning but our ability to see it is. However, when exciting the polaritons (Figure 4.4b and c), this feature is maximized when the LP frequency is 1963 cm^{-1}. This frequency does not align with the reservoir ω_{12} transition, but it is near the condition of zero detuning between the cavity and the vibration. Under these excitation conditions, polaritons are first excited and then decay into the coupled reservoir states causing the nonlinear optical response near the LP. We propose that the generation of polariton excitations, which subsequently decay into reservoir population, is maximized when the initial polariton absorption is maximized (i.e., at zero detuning). We note that the calculation of cavity detuning is highly sensitive to the calibration of the spectrograph and the current values

are determined based on both frequencies and intensities of the LP and UP. Nevertheless, these results indicate that even after a relatively long delay time of 25 ps (relative to the cavity lifetime, which is < 5 ps), the resultant excited-state population can be manipulated via the excitation frequency (polariton vs dark state excitation) or angle (the relative photon-vibration character of the polariton), which may prove useful in future implementation of cavity-modified molecular excitations.

4.2.5 Origin of 2D IR spectra of vibrational-polaritons: deviations from the free harmonic boson

Even though we have shown that 2D IR spectra reveal dark states and their interactions with polaritons, the origin of the 2D IR spectra of vibrational-polaritons is an interesting topic in its own right. Given previous emphasis on their linear response, polaritons have been primarily described within the free boson picture, featuring harmonic oscillator dynamics.[73] However, it is well-known that harmonic systems exhibit vanishing nonlinear optical response.[74] Thus, the observation of vibrational-polariton pump-probe[14] and 2D IR signals necessarily indicates that this free bosonic picture does not generally hold, and that anharmonicities in the system must exist to give rise to nonlinear spectra. In inorganic semiconductor exciton-polaritons, effective anharmonicities are induced by Coulomb scattering and the so-called "phase space filling" mechanism due to Pauli exclusion of electrons and holes.[75] For vibrations, nuclear and electrical (or dipolar) anharmonicity[76] of the C-O stretch causes deviations from harmonic behavior. As the level of excitation in the system increases, v = 1 to 2 transitions become coupled to the cavity, in addition to the fundamental transition, thus influencing polariton formation and dispersion. Both the red-shift of ω_{12} compared to ω_{01} (nuclear anharmonicity) and the reduced oscillator strength μ_{12} compared to $\sqrt{2}\mu_{01}$ (electrical anharmonicity) lead to a red-shift of the UP (i.e., contraction of the vacuum Rabi splitting leading to derivative-like lineshape). Classical expressions for transmission through a cavity capture this effect well with respect

to coupled reservoir population, but here we develop a full quantum-mechanical treatment to provide a microscopic perspective and shed light on the conditions of validity of the classical approximation.

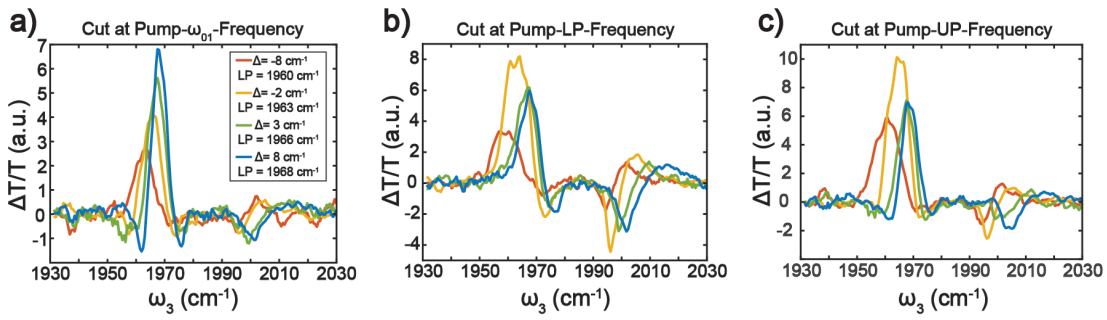

Figure 4.4: Scaled spectral cuts at pump frequency of (a) ω_{01}, (b) LP, and (c) UP with different detuning (Δ).

Ribeiro et. al.[1, 2] developed a QM model with us which utilizes a Hamiltonian including a single-cavity mode interacting weakly with external vacuum electromagnetic modes, and with the polarization generated by N independent anharmonic molecular vibrations, which are themselves weakly-coupled to low-energy bath modes. We utilize input-output theory to estimate the probe transmission in the presence and absence of a transient excited-state population of molecular vibrations. The Hamiltonian includes the effects of both nuclear and electrical anharmonicity, which may be understood to induce self- and cross-interactions between the LP and UP, as well as between polaritons and dark states. With either the classical expression or the QM model, we can estimate the degree of coupled reservoir excitation by comparing the modeled and experimentally determined shift of the UP. From the classical model, we estimate that 5% of the molecules are excited at t_2 = 25 ps, while the QM model suggests 5-7.5%.[1, 2] Both estimates are reasonable for the pulse energies used. The QM model captures the main features of the vibrational-polariton (Figure 4.5) pump-probe signal, including excited-state absorption, stimulated emission, and ground-state bleach, as well as the order of their corresponding intensities. We only present a comparison of experimental and theoretical pump-

probe signals because simulation of the complete 2D spectrum requires a detailed theory of nonlinear multi-polariton dynamics including many-body interactions between dark-states and polaritons, which we are currently developing.

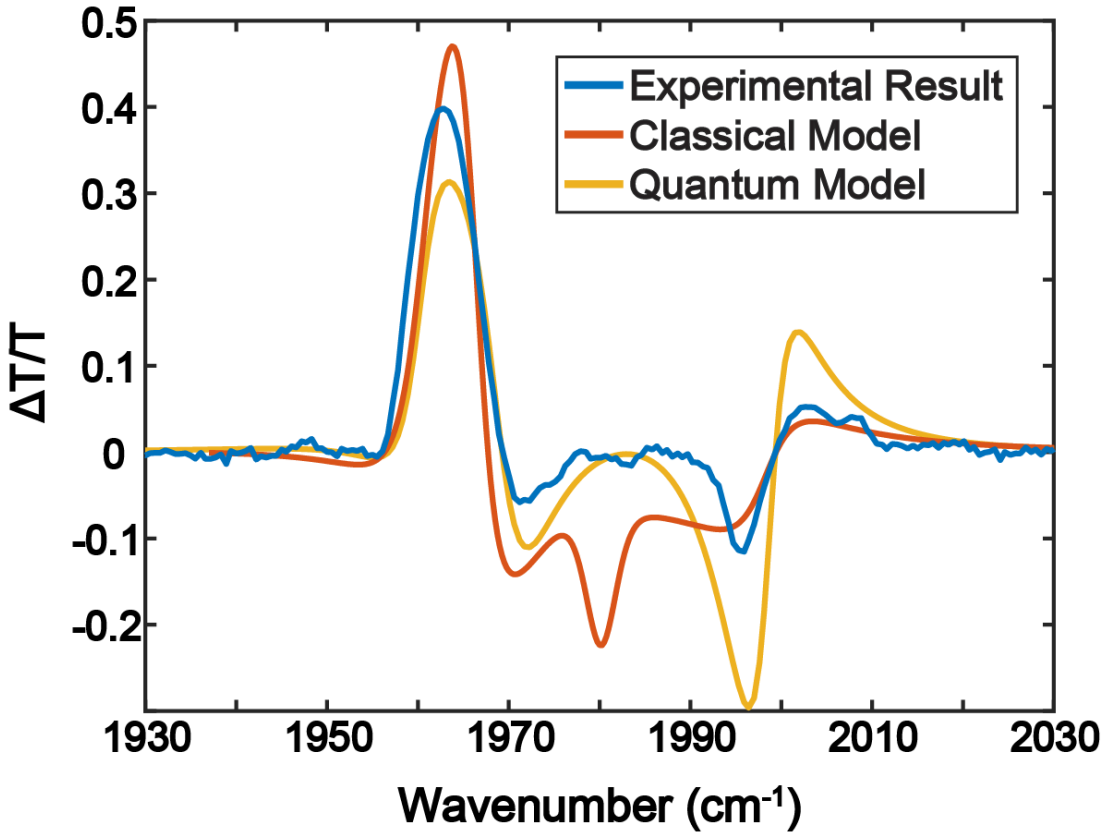

Figure 4.5: Comparison between the experimental pump-probe signal and the classical and quantum models. Reasonable qualitative agreement is achieved.

4.3 Discussion

While the assumption of transient reservoir state population seems sufficient to capture several of the described 2D IR features (e.g., the derivative lineshape at UP and large absorptive feature at LP), the differences of 2D IR signals taken at ω_1 = LP, UP relative to those at ω_1 =ω_{01} (Figure 4.4) indicate that the time-dependent population of reservoir modes from polariton

relaxation is surprisingly sensitive to cavity detuning. The quantum description presented here reproduces all the characteristic features of the transient response at longer times and a full treatment which includes the dynamic coherence and population transfer between polaritons and reservoir states is under development.

The multidimensional spectroscopy[77, 78] of the cavity-coupled C-O stretch of $W(CO)_6$ reveals direct excitation of reservoir states (despite their weak linear response) and unambiguous evidence of interactions between reservoir and polariton modes. The visibility of reservoir dark mode excitation in 2D IR signals arises from vibrational coherences are detected through free-induction-decay (FID) along t_1 of the emitted signal, instead of measuring the emitted optical responses, which can be weakened by reabsorption. The present work can be extended by performing polarization resolved measurements, quantum process tomography,[79] or even 3D spectroscopy[80–82] for tracking emergent two-point correlations between vibrational-polaritons and uncoupled vibrations. The integration between molecular vibrational transitions and quantized microcavity modes enables new possibilities to design photonic materials in the mid-IR regimes, taking advantages of the large selection of vibrational transitions. Many novel molecular systems deserve attention, including heterogeneous systems, intrinsically coupled,[76] and decoupled molecular vibrations, and molecular systems that undergo isomerization.[83] In addition, many novel nanoplasmonic optics can be designed and used to enhance local electric field and hence the coupling strength.[84]

Chapter 4, in full, is a reprint of the material as it appears in Proceedings of the National Academy of Sciences, 2018. Bo Xiang; Raphael F. Ribeiro; Adam D. Dunkelberger; Jiaxi Wang; Yingmin Li; Blake S. Simpkins; Jeffrey C. Owrutsky; Joel Yuen-Zhou; Wei Xiong., National Academy of Sciences, 2018. The dissertation author was the primary investigator and author of this paper.

Chapter 5

Manipulating Optical Nonlinearities of Molecular Polaritons by Delocalization

5.1 Introduction

Molecular polaritons are hybrid quasiparticles resulting from strong coupling between molecular excitations[56, 57] and confined electromagnetic degrees of freedom, e.g. Fabry-P*é*rot (FP) microcavity modes. Heuristically, polaritons arise when a cavity photon mode interconnects the microscopic molecular degrees of freedom, rendering their wavefunction coherently delocalized across a macroscopic length scale. This interplay between microscopic and macroscopic characteristics is at the heart of the versatility of polaritons. Much of the recent research on molecular polaritons has focused on the modification of molecular properties through the interaction with an optical cavity.[1, 2, 13, 14, 37, 40, 74] Conversely, control of polariton optical response via manipulation of the macroscopic parameters which define the electromagnetic modes (e.g., cavity length) has received far less attention[3] (Figure 5.1a) and, in fact, we are not aware of any investigations of these effects in the nonlinear photonic regime.

In this work, we first reveal that ultrafast molecular polariton nonlinearities can be conve-

niently manipulated by controlling the size of the optical cavity and the molecular concentration. The ease and adaptability of such operations make them applicable to in-situ control of optical nonlinearities for photonic circuitry and quantum information processing applications[43]. The microscopic origin of the distinctive polariton optical signals is subsequently investigated via analysis of the vibrational polariton 2D IR spectral dynamics. In contrast to generic molecular nonlinearities which tend to be modulated by excited-state population, we find that nonlinear dephasing is the main contributor to the coherent polariton optical response. We conclude by commenting on the potential implications of this research to the deployment of novel infrared devices.

5.2 Results

5.2.1 Polariton bleach dependence on cavity longitudinal length

To investigate the optical nonlinearities of vibrational polaritons, we measure their third-order nonlinear susceptibilities by femtosecond IR pump-probe spectroscopy. The hybrid light-matter system consists of a FP microcavity filled with an ensemble of asymmetric carbonyl stretch modes originating from $W(CO)_6$ molecules in a hexane solution.[2] At zero waiting time, when IR pump and probe pulses overlap, we see a significant reduction in the intensity of the polariton transmission (Figure 5.1b). This reduction gives rise to absorptive features in the differential transmission spectra (Figure 5.1c). Qualitatively, the observed behavior resembles the well-known "photon blockade effect" in the single-emitter quantum regime of the Jaynes-Cummings model[85]: when a photon excites the emitter-cavity system, the latter is blocked from further interactions with incoming photons of the same frequency. Here, we observe a similar effect, although it is in the ensemble regime and the mechanism for reduced transmission is quite different from the single oscillator case. We hereafter term this phenomenon "polariton bleach". Note this effect is not a trivial coherent artifact from the overlap between the pump and probe

pulses. The employed IR pulse duration is ∼100 fs, while the bleach lasts for less than 5 ps (which is also the approximate lifetime of the cavity photon), indicating the effect is intrinsic to the lifetime of the cavity polaritons. The polariton bleach concept provides a foundation for developing mid-IR photonic devices in the ensemble regime of light-matter strong coupling.

The polariton bleach shows peculiar dependence on the cavity thickness: it is dramatically stronger when the cavity longitudinal length is decreased. In fact, as shown in Figure 5.1c, when the cavity thickness decreases from 25 to 5 μm, the magnitude of the polariton bleach increases. This observation leads to the remarkable conclusion that substantially enhanced nonlinearities are induced on molecular vibrational polaritons by merely changing the longitudinal length of the optical microcavity. Importantly, the concentration of $W(CO)_6$ is kept constant so that polariton resonance frequencies detected with linear transmission measurements are independent of the cavity thickness (the Rabi splitting is fixed within 2 cm^{-1}. The change of Rabi splitting is due to the change of cavity lifetime of different cavity thickness.[86] From a molecular spectroscopy standpoint, this is an unexpected and important result given that a sample of independent emitters in the weak light-matter coupling regime features nonlinear optical signals (e.g., 3rd order to 1st order nonlinear transmission ratios, $\zeta = \Delta T^{(3)}/T^{(1)}$ that remain unchanged upon scaling of system size, i.e., molecular nonlinearities are typically intensive properties of the system.[87]

5.2.2 Polariton bleach dependence on molecular concentration

In addition to a cavity-length dependence, we also observed that the magnitude of the polariton bleach can be tuned by changing the concentration of the molecular oscillators in a fixed-thickness cavity. Here we show pump-probe spectra performed with the 25 μm cavity at zero waiting time as a function of molecular concentration (Figure 5.2). We focus on the transient signal at $\omega_{probe} = \omega_{UP}$ (Figure 5.2), to avoid complications of the spectral peak at $\omega_{probe} = \omega_{LP}$ stemming from overlap with the 1-2 dark mode transition.[1, 2, 37] The UP-peak intensities (faded green region in Figure 5.2) show an inverse dependence on the molecular absorber concentration.

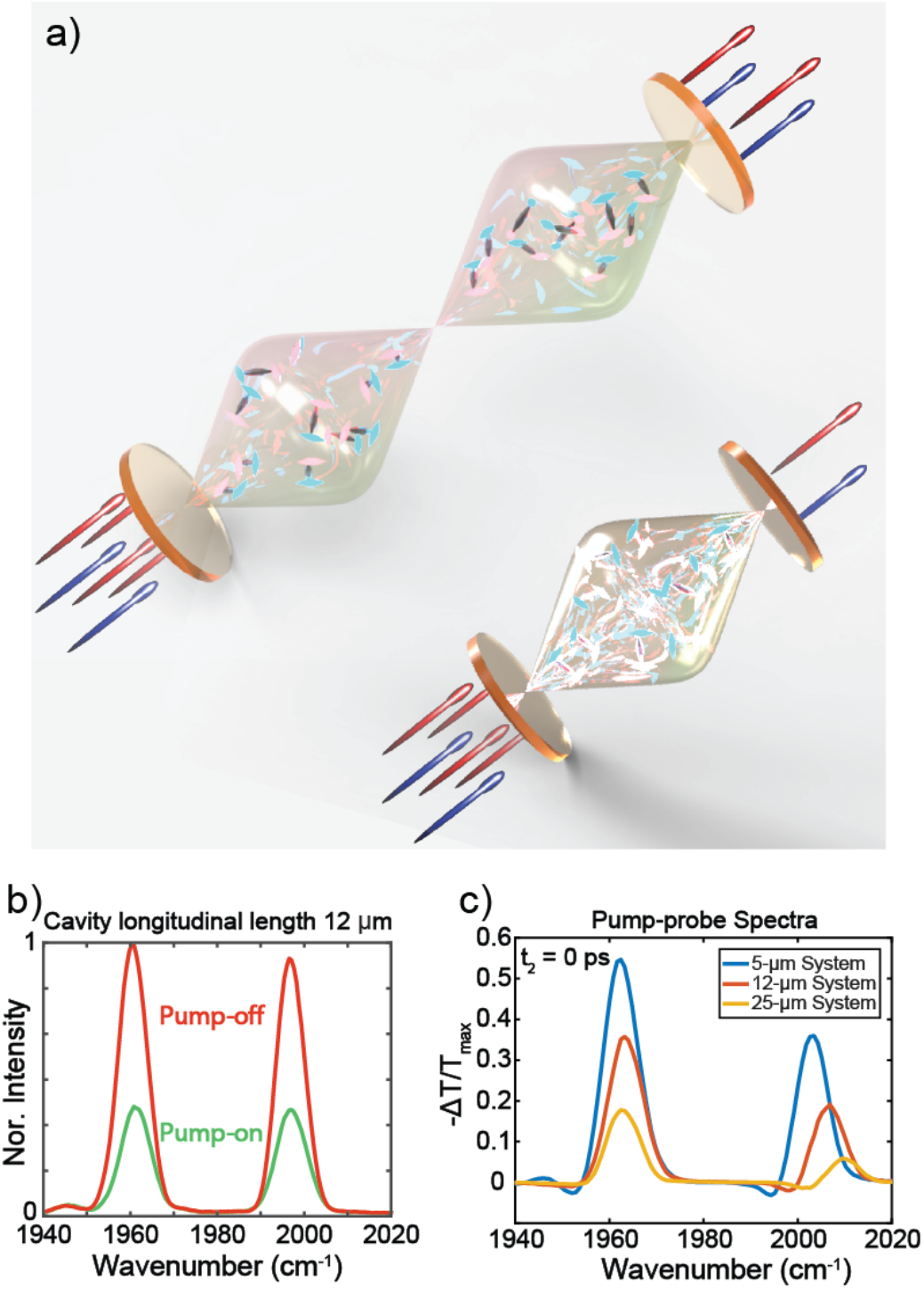

Figure 5.1: (a) The central concept for optical nonlinearity manipulation. (b) Polariton bleach: transmission reduction. (c) Pump-probe spectra with various cavity longitudinal lengths (5, 12.5 and 25 microns).

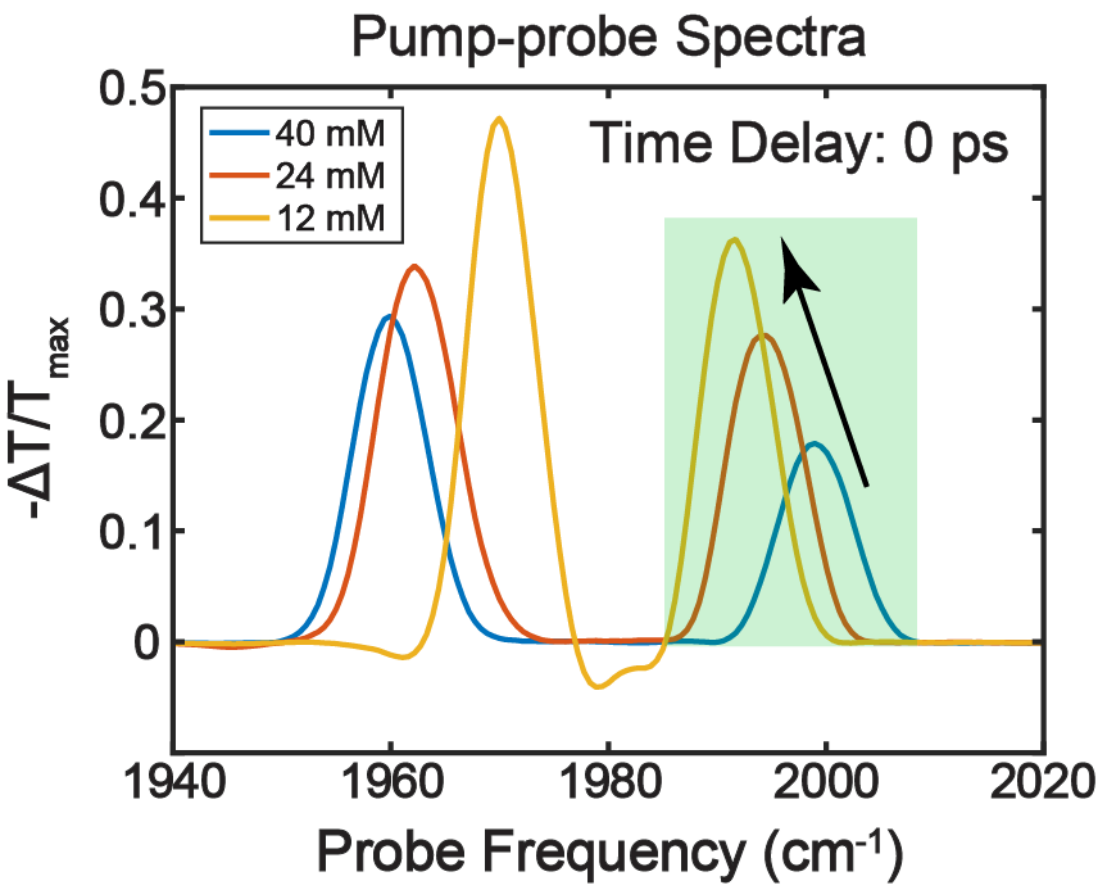

Figure 5.2: Polariton bleach effect at pump probe delay time (t_2) of 0 ps (optical nonlinearity) as a function of concentration.

Again, this is a striking effect from the perspective of conventional molecular spectroscopy in the weak light-matter coupling regime, where ζ typically remains constant with molecular concentration (i.e., the molecules act as independent quantum oscillators). Importantly, these results also suggest the macroscopic dependence of the nonlinear optical response on cavity length cannot be simply ascribed to the variations of intracavity electromagnetic energy density since it is not affected by molecular concentration. We note that the choices of concentration and cavity thickness are limited by the requirement of strong coupling. Assuming normal incidence, there is a discrete set of cavity lengths approximately equal to $(n\lambda)/2$ (where n is the order of the mode and λ is the molecular resonant wavelength) which makes 5, 12 and 25 μm the only readily available thicknesses for use in this experiment (due to practical spacer thickness options).

Similarly, the 40-mM solution is nearly saturated, and 12 mM is the lowest concentration we achieve before the onset of weak-coupling, so we have explored the entire available concentration range.

The nonlinear signal dependence on the cavity thickness (Figure 5.1c) and molecular concentration (Figure 5.2) show that an entirely new scaling of nonlinear interactions with size and concentration occurs in the molecular strong coupling regime. These properties can be qualitatively understood as consequences of the ratio between generated polaritonic excitations to the total number of molecular states composing the polariton wavefunctions. When either molecular concentration or cavity thickness is changed, the absolute number of polariton transitions accessed by the IR pulses is approximately unchanged (determined by the number of IR photons entering the cavity). However, the number of molecular states composing polariton wavefunctions is increased when the cavity thickness or molecular concentration increases, thus leading to a reduced probability for any given molecule to be detected in an excited-state in both cases, and therefore resulting in the weakening of all nonlinearities. Quantitatively, the observed inverse dependence of the polariton nonlinear response with respect to cavity thickness and molecular concentration is mediated by intra and intermolecular anharmonicity. These interactions lead to polariton nonlinear response proportional to the ratio of the pump-induced polariton density $\rho_{pol}(E_{pump})$ to the molecular density ρ. To see this, note that the nonlinear signal can be written in terms of a sum over all pump-driven polaritons, which scales with , $\sum_{\mathbf{k}} \frac{|E_{pump}(\mathbf{k})|^2}{N(\mathbf{k})} \propto \frac{\rho_{pol}(E_{pump})}{\rho}$, where the in-plane 2D cavity wave-vectors are labeled by $\mathbf{k}$, and the average number of molecules composing the corresponding polariton is N($\mathbf{k}$). The 1/N factor arises from the dilution of molecular anharmonicity by the polariton volume.

The preceding argument clarifies the observed scaling of polariton nonlinearity with system size and molecular concentration. However, it does not reveal the microscopic nonlinear dynamical process which gives rise to the distinctive polariton bleach lineshape. In the next section, we further explore the microscopic mechanism responsible for the polariton bleach effect.

5.2.3 Origin of Polariton Bleach and Rabi Oscillation Dynamics Revealed by 2D IR

Previous research on inorganic semiconductor exciton polaritons has shown that Coulomb scattering of charge carriers leads to similar phenomena to the polariton bleach described above.[88] The same mechanism is unlikely to apply for localized molecular vibrations (or Frenkel excitons which form organic exciton-polaritons under strong coupling), since local molecular modes typically only interact weakly with each other via dipole-dipole couplings. These considerations motivate our investigation of the physical mechanism corresponding to the molecular polariton bleach with two-dimensional infrared (2D IR, Figure 5.3a) spectroscopy. 2D IR measures the third-order nonlinear optical response function of a material, providing detailed spectral and dynamical features[2, 32, 33] hidden from pump-probe spectra. Specifically, 2D IR can state-selectively excite and probe particular transitions, a feature which is critical to discern the origin of nonlinearities in polaritons and dark modes. In Figure 5.3d, we show the 2D IR spectrum of vibrational polaritons (cavity thickness = 25 μm) at t_2 = 0 ps. Four absorptive peaks dominate the spectra: two lie along the diagonal while the remaining correspond to cross-peaks. The polariton 2D IR spectra obtained with the 12 μm-cavity display qualitatively similar features (Figure 5.4a). Spectral cuts of 2D IR that correspond to the nonlinear response obtained by pumping specific polaritons (UP or LP) explicitly show that all peaks have absorptive lineshapes. Furthermore, comparison of the 12 and 25 μm cavity-polariton spectral cuts (Figure 5.4e and 5.4f) demonstrates agreement with the pump-probe results – there are stronger nonlinearities in the thinner cavity. We note that, due to heterogeneity and polariton relaxation, dark modes may also be weakly excited, and induce similar absorptive features.[2] Overall, the observed 2D IR spectral features and the corresponding cavity longitudinal length dependence are consistent with the polariton bleach observed in the pump-probe data.

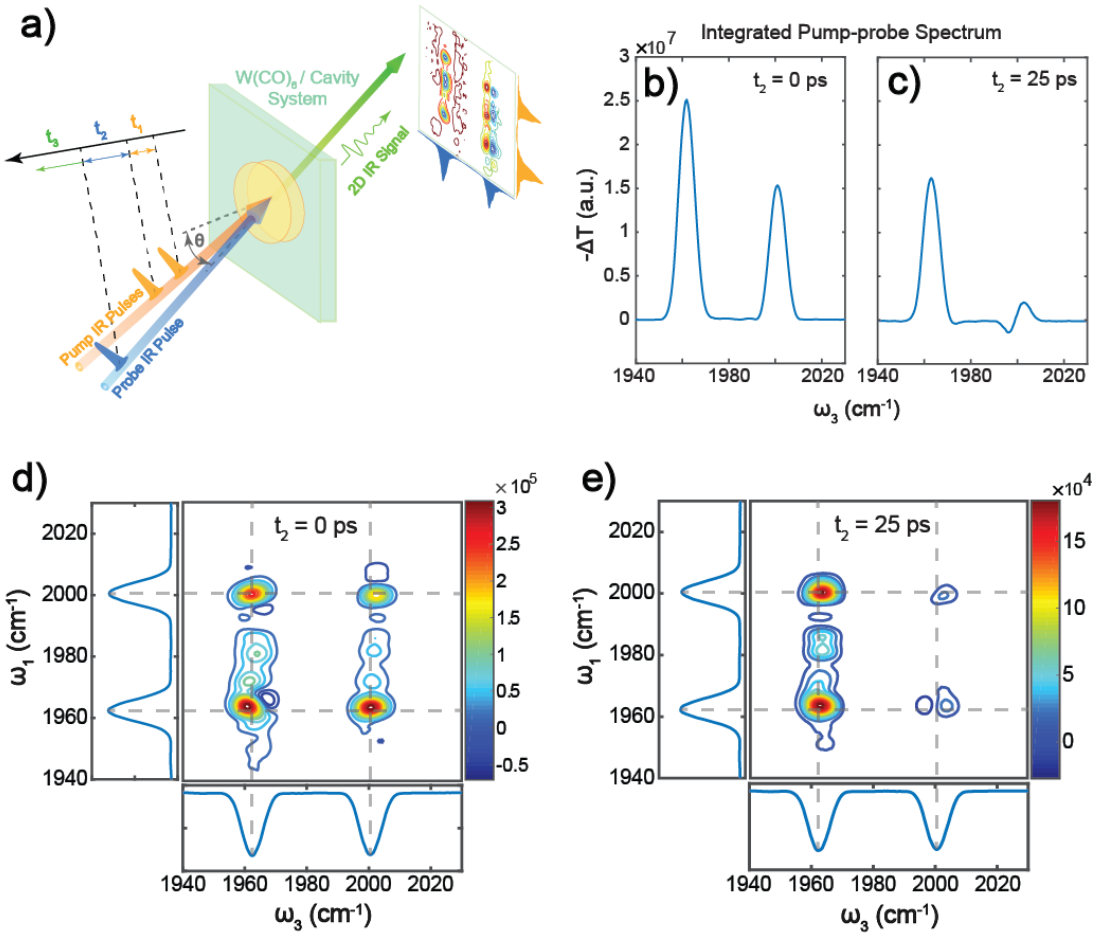

Figure 5.3: (a) 2D IR experimental setup. Pump-probe differential transmission at (b) early and (c) late time delays. 2D IR spectra of molecular vibrational polaritons at (d) early and (e) late time delays.

Additional insights on the nonlinear dynamics giving rise to polariton bleach can be obtained by examining the corresponding spectral lineshape evolution. Specifically, both the pump-probe and 2D IR signals at t_2 = 0 ps (Figure 5.3b and d) show different spectral lineshapes from those measured at t_2 = 25 ps (Figure 5.3c and e). At 25 ps, the peaks located at the probe frequency $\omega_3 = \omega_{LP}$ are much stronger than those at $\omega_3 = \omega_{UP}$, and the signal centered around $\omega_3 = \omega_{UP}$ evolves into a derivative shape. As explained in previous work,[1, 2] these features may be viewed to arise from ground-state population bleach, or equivalently, by the existence of transient excited reservoir population. The large absorptive peaks at $\omega_3 = \omega_{LP}$ arise

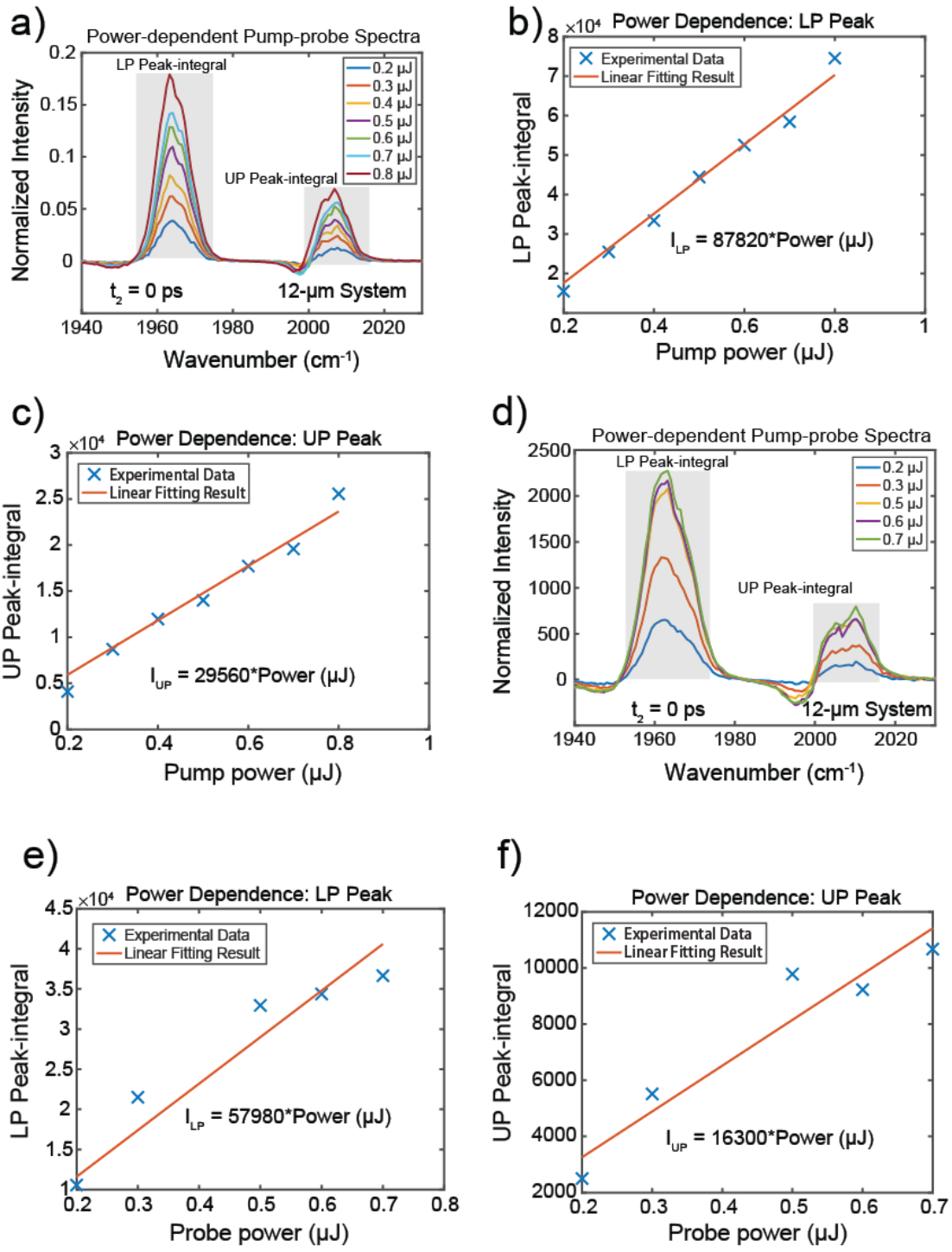

Figure 5.4: (a) Pump-probe spectra at t_2 = 0 ps for 12-μm polariton system; (b) LP peak integrated signal; (c) UP peak integrated signal. Probe power-dependence: (d) Pump-probe spectra; (e) LP peak integrated signal; (f) UP peak integrated signal.

primarily from the interference of the LP transition with the excited state absorption of dark reservoir population. The dispersive lineshape at $\omega_3 = \omega_{UP}$ is mainly a result of the Rabi splitting contraction induced by the bleaching of molecular absorbers. In contrast, the polariton bleach at t_2 = 0 ps has a qualitatively distinct lineshape with the feature at $\omega_3 = \omega_{UP}$ being stronger and purely absorptive (see Figure 5.3b and c). This indicates that vibrational-polariton dynamics is significantly different at ultrafast (shorter than the polariton lifetime ~5 ps) from the one at late times (e.g. 25 ps).

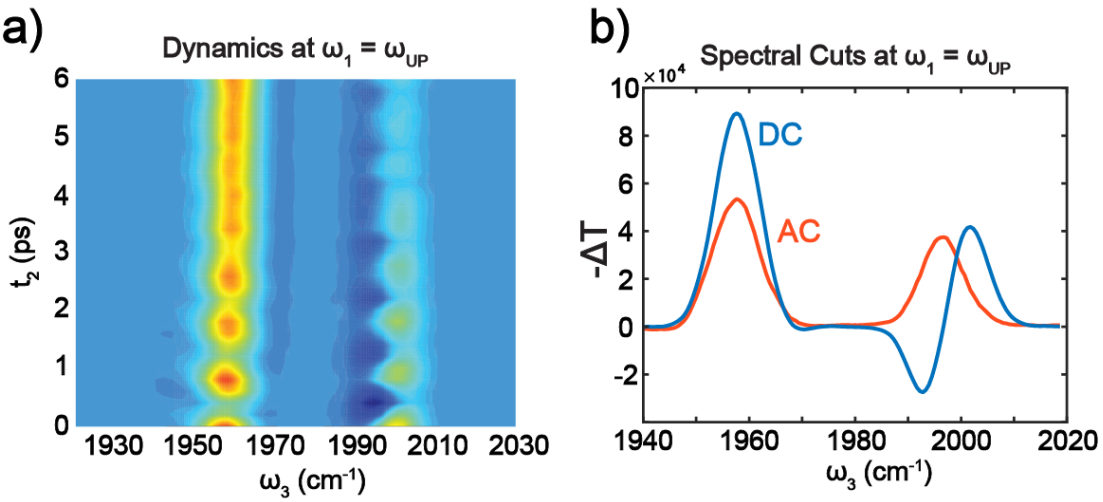

Figure 5.5: (a) Time-dependent nonlinear response at UP cut. (b) AC and DC spectral cuts of differential transmission at UP state, showing a purely absorptive lineshape in the AC spectrum and a dispersive lineshape in the DC spectrum.

The time-dependent dynamics extracted from 2D IR further confirms that the spectral signatures at early times and at 25 ps are dominated by distinct polariton nonlinearities rather than molecule, e.g., localized dark or reservoir states. The most notable difference between the early and late time dynamics is that at early times, the pump-probe and 2D IR spectral features are absorptive and the spectra oscillate as a function of t_2. These oscillations are revealed in the t_2 dynamics of the 2D IR spectral response when the pump is resonant with polariton frequencies, i.e., when $\omega_1 = \omega_{UP}$ (Figure 5.5a) or $\omega_1 = \omega_{LP}$. The oscillation period is c.a. 0.8 ps (41.7 cm^{-1} in frequency domain), which agrees well with the independently measured Rabi splitting

of 38 cm^{-1}. Therefore, we assign these periodic dynamics to Rabi oscillations, which may be understood to arise from the evolution of polariton coherences $|UP\rangle\langle LP|$ and $|LP\rangle\langle UP|$, or equivalently from the energy exchange between the cavity electromagnetic field and the collective vibrational polarization.

By applying a Fourier filter at the Rabi frequency to a series of t_2-dependent 2D IR spectra of the 25μm system, we extract a signal component which oscillates as a function of t_2 (referred to as AC) and isolate it from the non-oscillatory (DC) part. In Figure 5.5a, we provide the time-dependent evolution of the AC signal, while in Figure 5.5b we show examples of AC and DC spectral cuts obtained from 2D IR spectra at t_2 = 0.8 ps. The AC features at the LP and UP frequencies (Figure 5.5b) are absorptive and have almost equal intensity matching the lineshape of the polariton bleach (Figure 5.3b). Conversely, the DC spectra show a dispersive shape at the UP and much stronger nonlinear response at the LP (Figure 5.5b), agreeing with our previous model[2, 14] for late-time pump-probe response (Figure 5.3c). Because the AC signal requires the evolution of a coherent superposition of LP and UP (or equivalently, of $|UP\rangle\langle LP|$ and $|LP\rangle\langle UP|$ coherences) during t_2, the corresponding nonlinear resonances can be ascribed to a small subset of Feynman diagrams including coherence evolution. Interestingly, this implies that signal pathways containing polariton population (represented by $|LP\rangle\langle LP|$ and $|UP\rangle\langle UP|$) are inessential for the generation of polariton bleach. In summary, our experiments allow clear identification of two regimes of qualitatively distinct nonlinear polariton phenomena: at early times (<5 ps, which is roughly the polariton dephasing time), a nearly-symmetric bleaching of transmission is observed with a lineshape essentially indistinguishable from the AC signal (Figure 5.6a), while at late times, (>5 ps) the time-dependent nonlinear signal is dominated by DC dynamics arising from the existence of ground state population bleach and excited dark-state (Figure 5.6b)

Given that the Rabi splitting is nearly invariant when the polariton bleach regime dominates the nonlinear response and only coherent excitations lead to AC signals, pump-induced

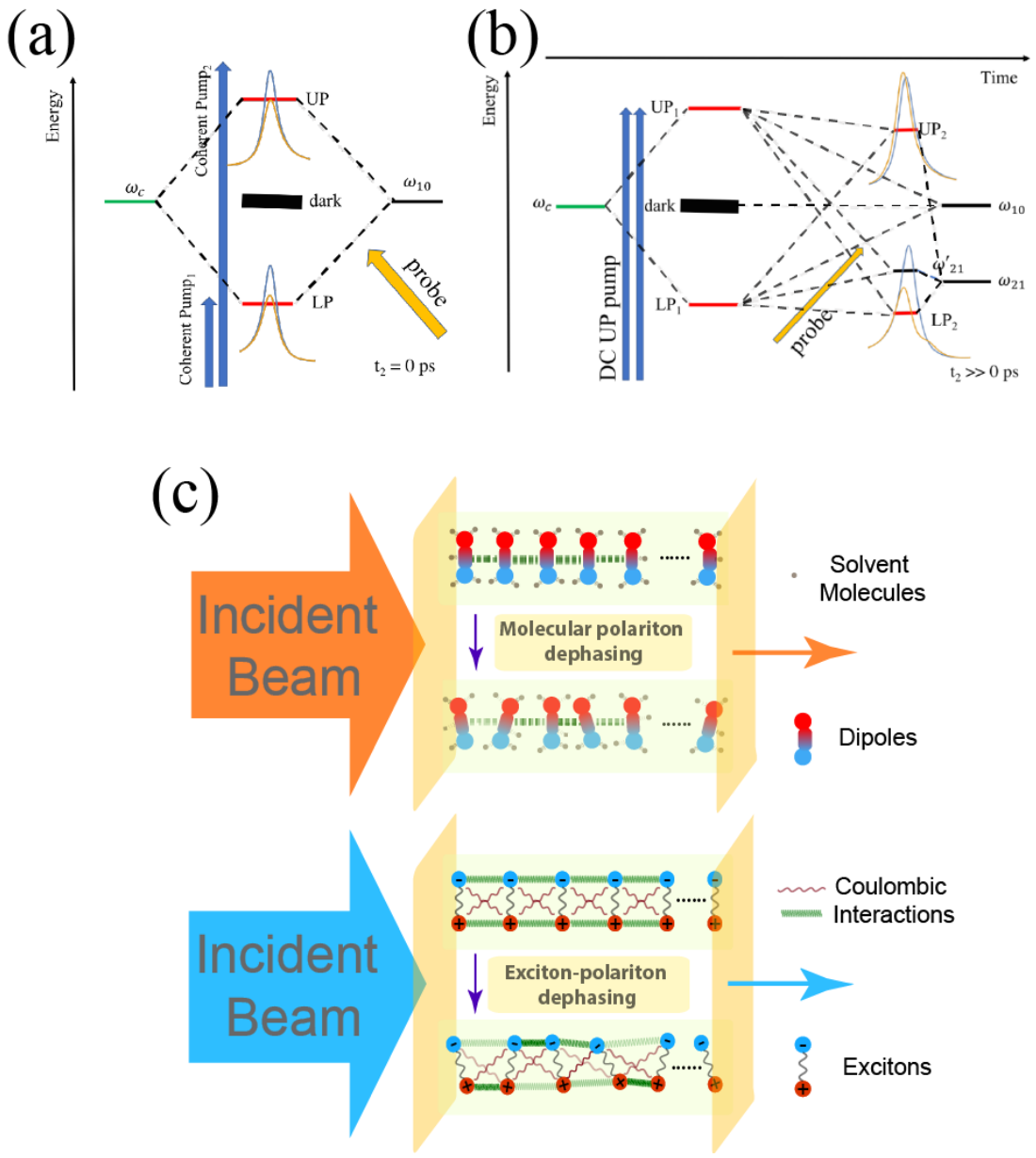

Figure 5.6: Energy diagrams of (a) the polariton bleach (AC signal) and (b) the DC signal. (c) Schematic representation of nonlinear dephasing mechanisms for dipole-active vibrational (top) and inorganic exciton-polaritons (bottom).

oscillator strength loss can be neglected at early times, and the polariton bleach can be modeled by a phenomenological semiclassical theory.[89] In this description, the bleaching is reproduced when the molecular homogeneous broadening linewidth (FWHM, Γ) is changed from 3 cm^{-1} to 4.5 cm^{-1} for the 25 μm and from 3 cm^{-1} to 7 cm^{-1} for the 12 μm microcavities, respectively

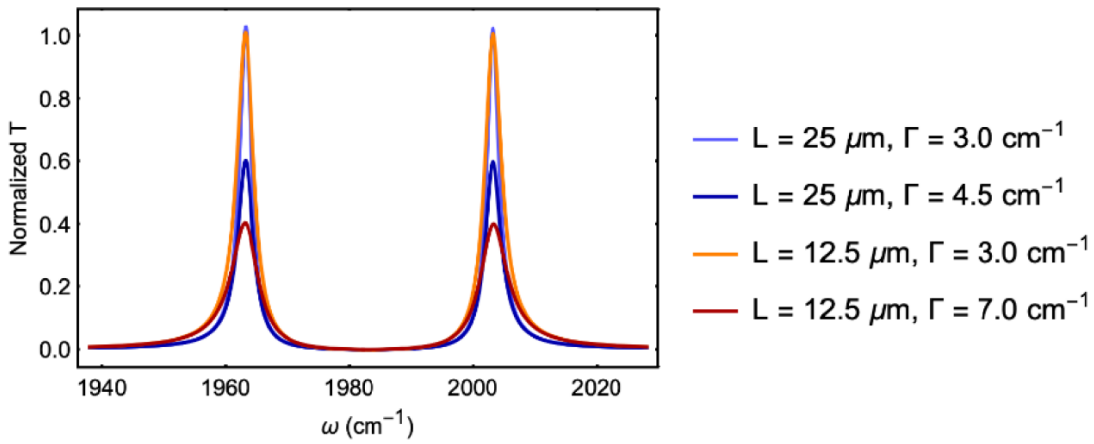

Figure 5.7: Simulated polariton transmission from a classical phenomenological model where the effect of the pump is to change the molecular homogeneous dephasing rate, here represented by the FWHM.

(Figure 5.7) (The fitting only considers the strong coupling between fundamental mode (1983 cm^{-1}) because the coupling between $1 \rightarrow 2$ asymmetric stretch transitions of $W(CO)_6$ (1968 cm^{-1}) and the cavity mode is small due to large detuning[2]). This result, together with the insights gained from the 2D IR studies described above, is in sharp contrast to the traditional view of molecular pump-probe spectroscopy, where the nonlinear optical response is essentially modulated by excited-state population. Here, the essential mechanism is dephasing which becomes exacerbated to generate broadened polariton linewidths and reduced probe transmission when the pump is resonant with polaritons.

The polariton bleach phenomenon may also be visualized via a quantum mechanical analysis using double-sided Feynman diagrams.[87] These diagrams represent the quantum pathways associated to the four peaks observed in the AC 2D IR spectra. Each AC peak has a stimulated emission (SE) and an excited-state absorption (ESA) pathway associated to the fundamental $|g\rangle \rightarrow |LP\rangle$ (or $|g\rangle \rightarrow |UP\rangle$) or combination band $|LP\rangle \rightarrow |UP,LP\rangle$ (or $|UP\rangle \rightarrow |UP,LP\rangle$) transitions. The phases corresponding to these pathways are opposite in sign. Therefore, if the fundamental and overtone transitions had equal oscillator strength, transition frequency, and linewidth (as is the case in harmonic systems), their amplitudes would interfere destructively

leading to a vanishing 2D IR signal. In the nonlinear spectroscopy of conventional molecular systems, the 2D response is generally dominated by features resulting from the anharmonic shift in frequency of the ESA which leads to incomplete cancellation of the SE and GSB amplitudes. This paradigm does not apply to the observed polariton bleach since no anharmonic energy shifts are visible in the recorded AC spectra; rather, the anharmonicity seems to be expressed in the linewidths, corresponding to nonlinear coupling to the environment. In particular, there is an incomplete cancellation of Feynman diagrams which is induced by a nonlinear dephasing mechanism that affects the $|LP,UP\rangle\langle LP|$ and $|UP,LP\rangle\langle UP|$ coherences but does not act on $|UP\rangle\langle g|$ or $|LP\rangle\langle g|$

5.3 Discussion

The observed nonlinear molecular polariton dephasing provides yet another instance where novel physical processes become relevant when light-matter interactions transition from the weak to the strong coupling regime. From a microscopic perspective, the polariton bleach arises from nonlinear dephasing activated by strong polariton excitation ($\sim$10 mJ/cm2). This effect has been observed before in inorganic semiconductor exciton-polaritons under intense pumping.[88] In these systems, the rapid dephasing is induced by Coulomb scattering (Figure 5.6c), which leads to enhanced broadening of the exciton homogeneous linewidth also detected in bare exciton pump-probe spectroscopy (32). For most chemical systems, the intermolecular Coulomb interactions can be well described by nonradiative dipole-dipole forces which decay with the inverse sixth-power of the distance. These interactions are likely too weak for the vibrational modes here studied due to large average distance between $W(CO)_6$ molecules (roughly 3 nm when $[W(CO)_6] \cong 40$ mM) and small effective dipole moments ($\cong$ 1D for the CO asymmetric stretch of $W(CO)_6$).[67]

We are led to conclude that alternative microscopic mechanisms induce the nonlinear

dephasing manifested in the molecular polariton pump-probe response (Figure 5.6c). Given that the bleach effect is clearest in the AC signal (Figure 5.5a and 4b), we can obtain insight into this phenomenon by analyzing the contributing Feynman diagrams. This indicates that the AC response is particularly sensitive to the nonlinear dynamics of the two-particle state $|LP,UP\rangle$. This many-body state undergoes efficient irreversible decay due to its resonance with a macroscopic collection of states containing two vibrational quanta in the same or different molecules. The dephasing could be accelerated by the triple degeneracy of the CO asymmetric stretch which gives an enhanced phase space for relaxation potentially mediated by the local fluctuations of the weak liquid-phase solute-solvent forces.[90] Nevertheless, any nonlinear intra or intermolecular interaction can contribute to the observed nonlinear dephasing by assisting the $|LP,UP\rangle$ decay.

The dependence of polariton optical nonlinearities on macroscopic properties (cavity longitudinal length and molecular concentration) is a result of the hybridization of a collection of molecular transitions with macroscopic cavity modes. The long polariton coherence length makes their optical nonlinearities particularly sensitive to macroscopic descriptors. At short pump-probe delay times, we consistently observed reduced polariton transmission due to nonlinear dephasing. As the cavity volume and the number of molecules in the polariton coherence volume decrease, polariton nonlinearities become stronger. This trend conforms with the notion that giant nonlinearities (e.g., photon blockade) emerge in the limit of single emitter strong coupling (unattainable in our experiment).

Multidimensional spectroscopy allowed us to tease out the mechanism that drives the oscillating polariton bleach and unambiguously show that it depends on polariton coherences. In contrast to exciton-polariton studies in the UV-visible range, where fluorescence measurements inform much of their excited state dynamics, 2D IR is a suitable method for the study of vibrational polaritons due to the weak fluorescence featured in this range of the electromagnetic spectrum.

The mid-IR nonlinear optical phenomena reported in this article rely on a delicate interplay between microscopic molecular anharmonicities and macroscopic electromagnetic parameters.

The ease with which the described samples can be fabricated and handled at room-temperature, together with their unique effects that interpolate between the molecular and the photonic realms, make vibrational polaritons ideal platforms to design novel mid-IR nonlinear optical switches, control chemical reactivity, or serve as building blocks for quantum information processing applications. As an example, from our previous work(13, 14), polariton nonlinear effects disappear within 200 ps. Thus, an all-optical modulator for mid-IR frequencies operating at repetition rate as high as 5 GHz can be developed based on polariton bleach. Our study has also evidenced that polariton nonlinearities can be straightforwardly tuned via macroscopic controls. This notion may prove particularly suitable in the context of microfluidic devices, where molecular concentrations, and therefore, optical nonlinearities can be changed on-the-fly. Alternatively, polariton nonlinear response could be actively modified by combining cavities with piezo, thermal, and optically responsive materials,[91] thus providing additional features to integrated photonic circuitry. Finally, the polariton anharmonicities underlying the respective nonlinearities may have nontrivial implications to vibrational dynamics and thermally-activated chemical reactions.[5, 92] In summary, we envision the exotic nonlinear phenomena explored in this work to play an important role in the emergent field of molecular polaritonics in the upcoming years.

Chapter 5, in full, is a reprint of the material as it appears in Science Advances, 2019. Bo Xiang; Raphael F. Ribeiro; Yingmin Li; Adam D. Dunkelberger; Blake S. Simpkins; Joel Yuen-Zhou; Wei Xiong., American Association for the Advancement of Science, 2019. The dissertation author was the primary investigator and author of this paper.

Chapter 6

State-Selective Polariton to Dark State Relaxation Dynamics

6.1 Introduction

Strong coupling between excitations of molecular vibrations and high-quality (Q) optical cavities leads to hybridized matter-photon states, known as molecular vibrational polaritons.[1–3, 11, 14, 40] In this interaction regime, the energy exchange rate between cavity-photon and vibrational modes is faster than the dephasing lifetimes of the isolated modes. Therefore, the eigenstates of the system can no longer be described as either bare cavity or vibrational states, but rather, as superpositions of both types of excitations. In the frequency domain, this criterion can be described as $g > \Gamma_{vib}$, Γ_{cav},[25] meaning the light-matter coupling strength, g, needs to be larger than the homogeneous full-width-at-half-maximum (FWHM) of both modes (Γ_{vib} and Γ_{cav}). When this condition is satisfied, two new bright hybrid eigenstates, known as polaritons, are formed with their own characteristic transition frequencies (Figure 6.1a). The mode with lower frequency is referred to as lower polariton (LP), and the one at higher frequency is called upper polariton (UP).

Because of the mixing between the vibrational and cavity-photon wavefunctions, molecular vibrational polaritons simultaneously feature properties of both photons and molecules, which leads to fascinating emergent phenomena. Notable examples include manipulation of rate and selectivity of organic deprotection reactions inside cavities.[5, 93] In addition, the optical nonlinearity of molecular polaritons can be controlled through macroscopic parameters such as cavity longitudinal length and molecular concentration,[9] whereas such effects are absent from the weak coupling regime or pure molecular systems.[94] Further developments of many of these new features hinge on a deep understanding of the polariton dynamics. However, molecular vibrational polariton dynamics are complicated by virtue of the dark states, e.g., excited polariton states only last a short duration and then either decay by photonic leakage or relaxation to dark states. Having relaxed to the latter, the system loses it photonic character, and most novel polaritonic features disappear. Thus, a sufficiently long timescale for the relaxation of polaritons into the dark reservoir is essential for certain strategies of cavity chemistry[4, 13] and polariton photonic applications.[89, 95] To understand the microscopic basis of dark states, we will briefly go through the quantum mechanical description of polaritons. For more detailed theoretical descriptions, we refer to the works in several review papers.[13, 25, 89]

The Hamiltonian of the polariton system can be written as[1, 2, 11]

$$\widehat{H}_{polariton} = E_{cav}\hat{a}^{\dagger}\hat{a} + \sum_{i=1}^{N} E_{vib}\hat{b}_i^{\dagger}\hat{b}_i + \sum_{i=1}^{N} g_i(\hat{a}^{\dagger}\hat{b}_i + \hat{b}_i^{\dagger}\hat{a}) \tag{6.1}$$

where E_{cav} (E_{vib}) is the energy of the cavity photon (vibrational dipole) modes, $\hat{a}^{\dagger}(\hat{a})$ is the creation (annihilation) operator of the photon, the creation (annihilation) operator of the ith vibrational dipole is $\hat{b}_i^{\dagger}(\hat{b}_i)$, and g_i is the strength of interaction between the electromagnetic resonance and the vibrational dipole of the ith molecule. Without loss of generality, we take the

light-matter interaction to be equal across the molecular ensemble, i.e., g_i=g_0.[25] Molecular inhomogeneous broadening is also neglected as its effect on polariton states is suppressed, especially in the resonant regime of our interest (when $E_{cav} \approx E_{vib}$).[25]

The eigenstates and eigenvalues of this Hamiltonian can be found by diagonalizing the (N+1)×(N+1) matrix which represents N vibrational modes, each equally coupled to the single cavity-mode; the corresponding secular determinant reads,

$$\begin{vmatrix} E_{cav} & g_0 & \cdots & g_0 \\ g_0 & E_{vib} & & \\ . & . & & \\ . & & . & \\ g_0 & & & E_{vib} \end{vmatrix} = 0 \tag{6.2}$$

At zero detuning, E_{cav}=E_{vib}=E_0, the eigenvalues of the Hamiltonian are

$$\begin{aligned} E_{LP} &= E_0 - \sqrt{N} g_0 = E_0 - g_c \\ E_{UP} &= E_0 + \sqrt{N} g_0 = E_0 + g_c \\ (E_{dark})_{i=1,2,\ldots,(N-1)} &= E_0 \end{aligned} \tag{6.3}$$

where g_c=$\sqrt{N} g_0$ is the collective coupling strength of an N - molecule system in the cavity electromagnetic volume. Notably, aside from the two optically bright states (LP and UP), there are N-1 dark states, which are non-totally symmetric superpositions of vibrational states, composed of products of N-1 molecular wavefunctions in the ground-state, a single molecular excited-state, and the cavity field is in its vacuum state (Figure 6.1d). Recent theoretical discussions[1, 2, 14]

indicate that - because of the large density of dark states compared to polariton states - the dark reservoir must play an essential role in polariton dynamics and novel polariton chemistry.

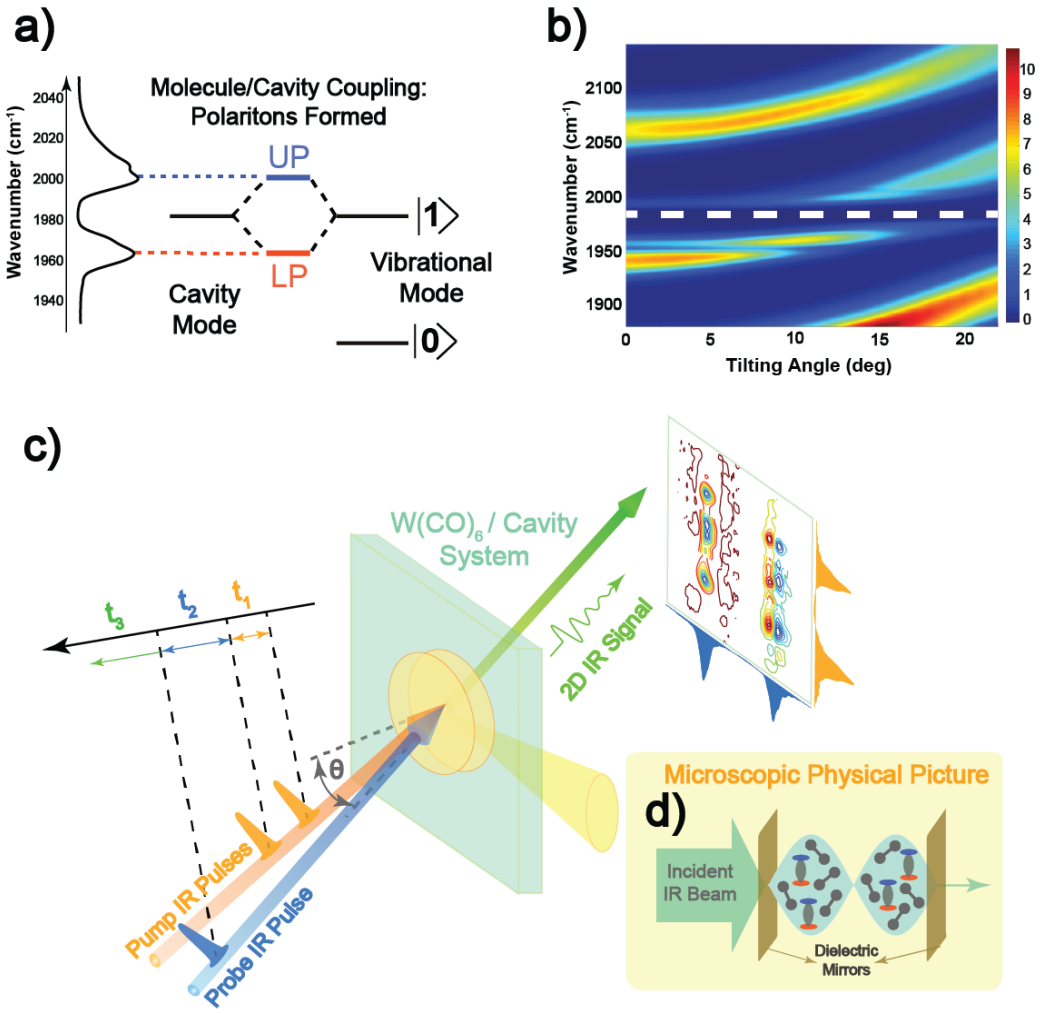

Figure 6.1: (a) The formation of vibrational. (b) Dispersive IR transmission curves. (c) 2D IR setup. (d) Microscopic physics of vibrational polariton formation.

Both polariton and dark modes have been studied, and their spectroscopic signatures have been reported by us and others.[1, 2, 14] In this work, building on our previous study, we describe the first state-resolved dynamics of molecular vibrational polaritons, using time-resolved pump-probe and two-dimensional infrared (2D IR) spectroscopy[32, 33] (experimental setup illustrated in Figure 6.1c). Both spectroscopies are critical to characterize molecular vibrational

polariton ultrafast physics, because unlike exciton-polaritons, vibrational-polaritons feature many more intramolecular vibrational relaxation pathways that can suppress their fluorescence, making techniques[25, 96, 97] developed for characterization of exciton-polaritons inapplicable here. 2D IR measures the third-order nonlinear optical response function of a material, providing detailed spectral and dynamical features hidden from pump-probe spectra.[1, 2, 14] Specifically, 2D IR can selectively excite and probe specific transitions, a feature which is critical to discerning the nonlinear optical response mediated by polariton or dark state excitations. We quantify relevant timescales for relaxation of LP and UP into the dark reservoir and propose a mechanism. We find that these relaxation times can be different depending on whether the initial state is LP or UP. This effect can be attributed to the stronger interactions between highly excited molecular states and the LP. More importantly, we have discovered that the relaxation from LP to the (single-excitation) dark states is highly dependent on the microscopic solvent environment, and that energy harvested by the polariton states can be channeled into highly excited vibrational modes with lifetimes longer than the polaritons, a feature which is likely relevant for the manipulation of cavity chemistry.[57]

6.2 Results and Discussion

6.2.1 Transient Pump-Probe and 2D IR Spectra of Molecular Vibrational Polariton Systems

Figure 6.2 shows representative transient pump-probe spectra under strong coupling conditions, along with 1D transmission polariton spectra (strongly coupled $W(CO)_6$ in hexane) under pump-on and pump-off conditions, at $t_2 > 3$ ps (Figure 6.2a).[1, 2, 14] When the pump is turned on, the UP resonance undergoes a shift towards a lower frequency (Figure 6.2b). Under the same condition, the LP lineshape acquires a small positive shoulder appears at higher frequency,

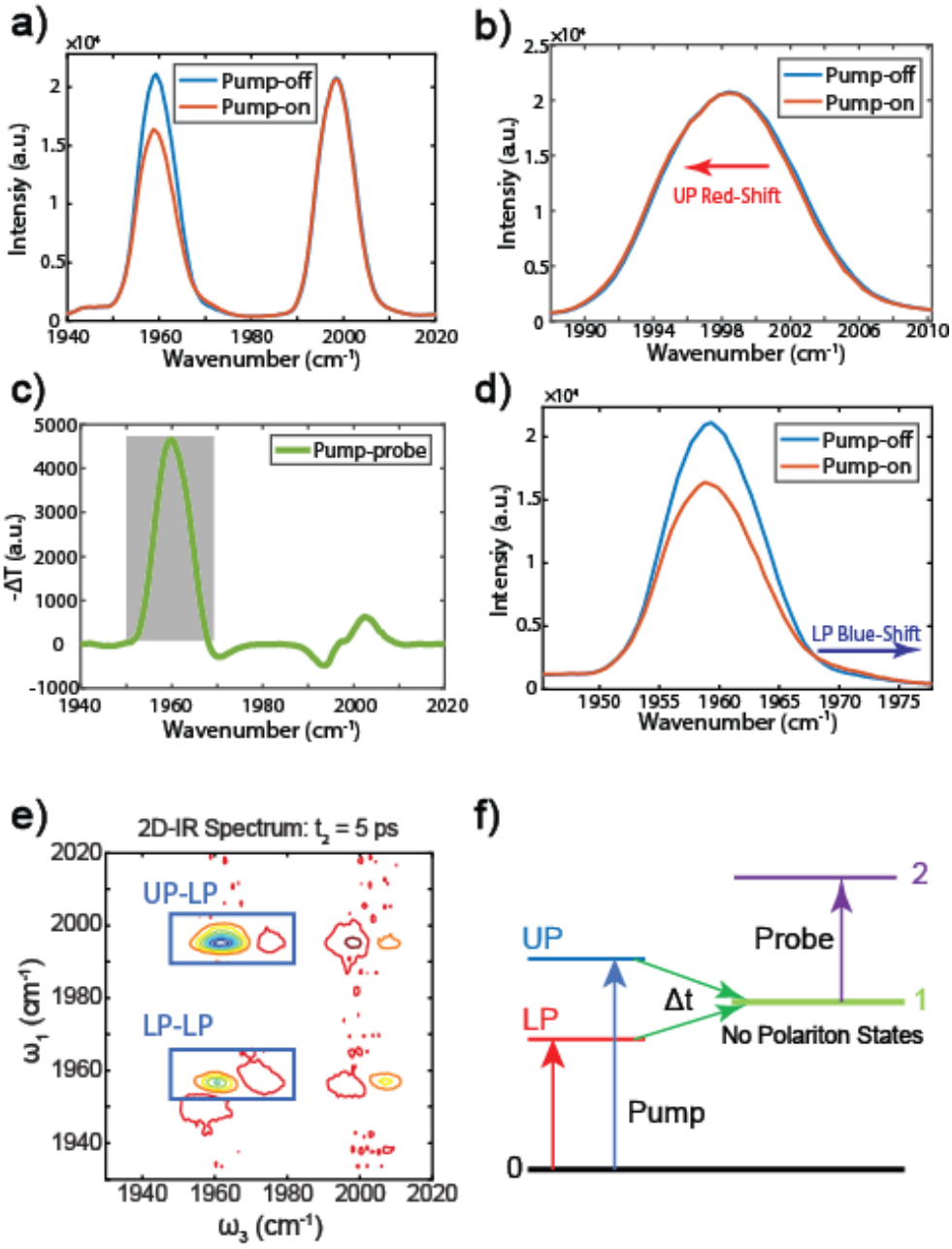

Figure 6.2: (a) Pump-on/pump-off spectra of strongly coupled $W(CO)_6$/hexane system; b) UP branch zoom-in; c) pump-probe spectrum; d) LP branch zoom-in; (e) 2D IR spectrum of strongly coupled system; (f) Schematic illustration of the population transfer process.

which corresponds to a blue shift (Figure 6.2d). These shifts are small but consistent and result in a derivative lineshape in the transient pump-probe spectrum (Figure 6.2c). The peak-shift is induced by the Rabi splitting contraction which arises due to the pump-induced reduction of

molecular ground-state population. The substantially reduced LP transmission upon pumping, and consequently the absorptive lineshape in the pump probe spectra, results from that the dark mode overtone ν_{12} transition (from first excited to second excited states, purple arrow in Figure 6.2f) is near resonance with LP transition. As a result, ν_{12} become visible through the LP transmission window. Thus, when LP and ν_{12} are near resonance, the appearance of strong absorptive transient signal at ω_{LP} is a signature of populating first excited state of dark modes.

While pump probe spectroscopy allows following polariton to dark state dynamics, state-selective 2D IR spectrum (Figure 6.2e) enables disentangle the dynamics: The UP-LP peak labeled in Figure 6.2e (left-top) represents the population transfer from UP state to dark mode while the LP-LP peak (Figure 6.2e, left-bottom) is mainly due to the LP to dark mode population transfer. As summarized in Figure 6.2f, it is believed that the UP/LP population transfer to dark modes in a fast timescale, which subsequently makes the dark mode ν_{12} appear in the pump probe or 2D spectra. However, the timescale and mechanisms of LP/UP transferring to dark modes remain largely unexplored and are the interests of this work. We learn the polariton dynamics by measuring dynamics of LP peak in pump probe spectra (integrating over the transient pump probe peak near LP position, e.g. shaded area in Fig.2c)), and dynamics of UP-LP and LP-LP peaks from 2D IR spectra (integrating 2D spectral peaks at UP-LP and LP-LP area, e.g, green boxes in Figure 6.2e). We note that the exact integrated areas depend on the peak positions of various polariton systems.

6.2.2 Polariton Dynamics in Acetone

The transmission spectrum of the strongly coupled $W(CO)_6$/acetone system exhibits LP and UP peaks with separation of ~ 48 cm^{-1}, with ω_{LP} = 1948 cm^{-1} and ω_{UP} = 1996 cm^{-1} (Figure 6.4a). When the probe is close to resonance with the LP (near 1948 cm^{-1}, see Figure 6.4c, grey area), The pump-probe spectral dynamics of LP peak reveals the relaxation dynamics of the dark molecular system (Figure 6.3a). The early-time spike is attributed to the polariton

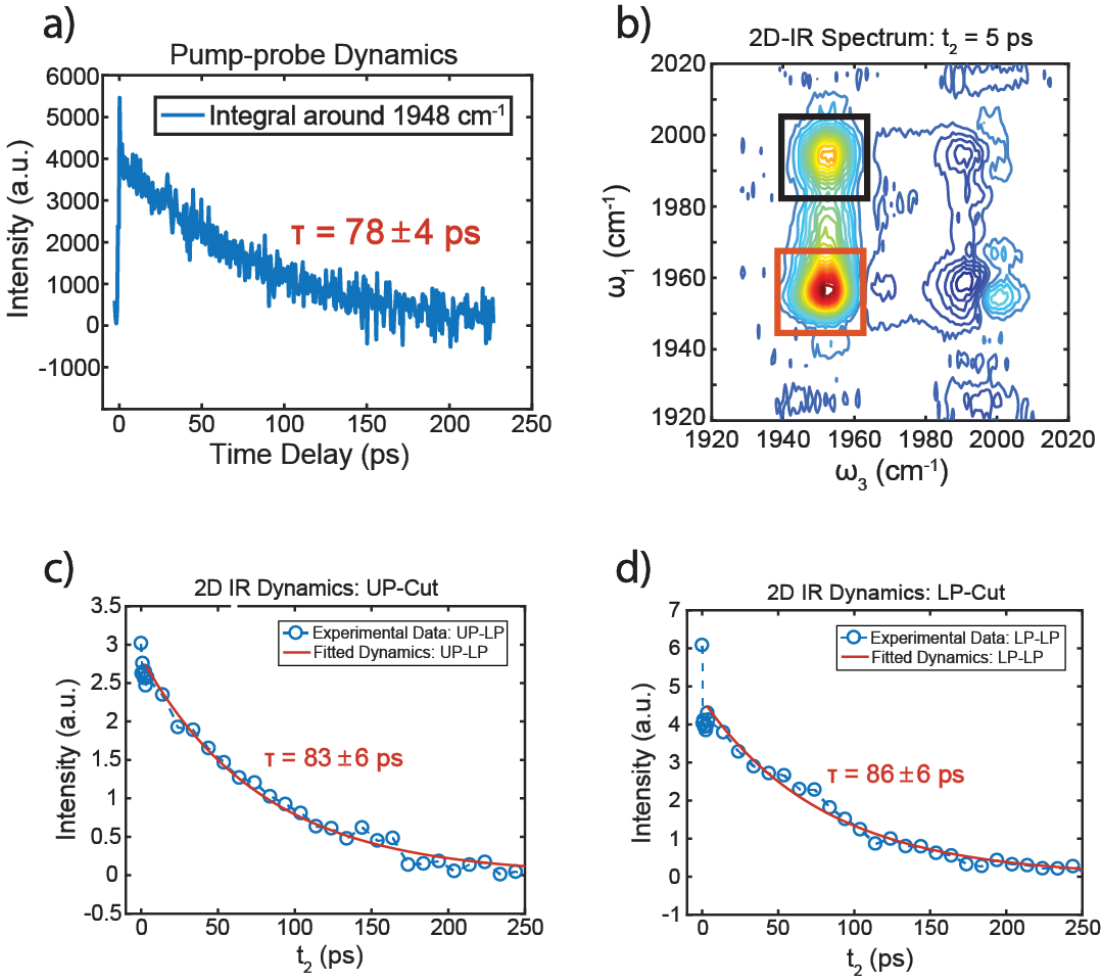

Figure 6.3: Dynamics of molecular polaritons in acetone at (a) LP state. (b) 2D-IR spectra of $W(CO)_6$/acetone in strong coupling regime. (c) 2D IR dynamic trace of UP-LP peak. (d) 2D IR dynamic trace of LP-LP peak.

bleach effect, which results from the interactions between polariton states created by pump and probe pulses.[9] Within the cavity lifetime (∼5 ps), the signal reflects rapid polariton decay by photon leakage or population transfer to the first excited-state of dark modes. After this timescale, the polariton to dark state population transfer has equilibrated, and the evolution of the signal reflects the relaxation dynamics of dark modes, which exhibit a lifetime of 78±4 ps (Figure 6.3a). As discussed in the previous section, these dynamics are detected by the probe pulse inducing excited-state absorption via the dark mode ν_{12} (1947 cm^{-1}) transitions.[98] The ensuing relaxation phenomena exhibits an exponential decay kinetics which is similar to that of

the fundamental peak of uncoupled $W(CO)_6$ in acetone (84±4 ps, Figure 6.5b). The similarity of the measured lifetimes is unsurprising, since the rate of change of the nonlinear signal in both cases is linearly proportional to the population of molecules in the first excited-state.

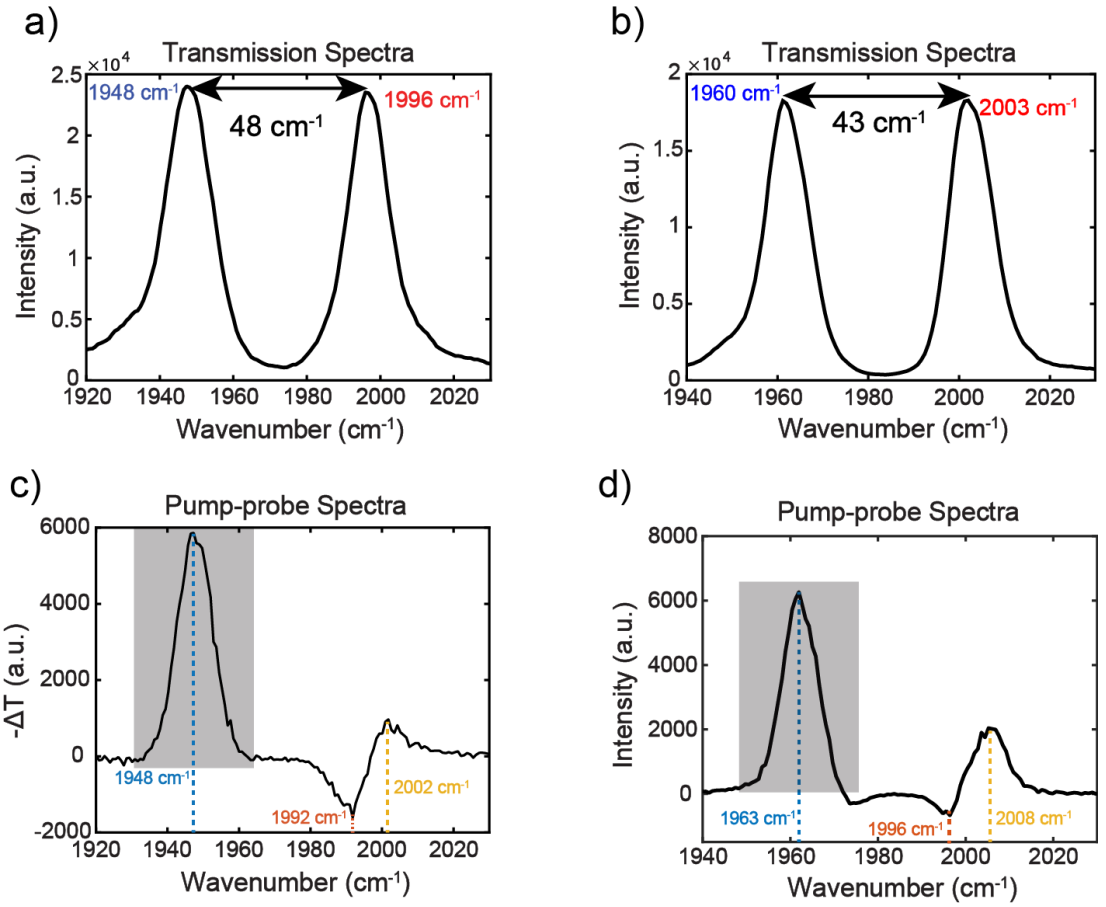

Figure 6.4: Transmission spectrum of vibrational polaritons in (a) acetone and (b) hexane. Transient pump-probe spectra at 25 ps with labeling of LP absorptive peak and UP derivative shape in (c) acetone and (d) hexane.

Because both LP and UP are bright but could have different dynamics, we need to track the relaxation dynamics of each type of polariton to gain the full picture. We applied 2D IR spectroscopy to follow state-resolved dynamics. The 2D IR spectra at t_2 = 5 ps is shown in Figure 6.3b. The relaxation dynamics is studied by plotting the integrated spectral region (indicated as black and red boxes in Figure 6.3b) as a function of t_2. As discussed in the previous section, the

black and red boxed regions in Figure 6.3b represent the population transfer from UP and LP to dark modes, respectively. The time traces indicate LP and UP both relax into the dark modes in a fast time scale (< 5 ps), independently of whether LP or UP are pumped, agreeing with the mechanism described in Figure 6.2f. It is reasonable that LP and UP relaxation to dark states occurs at similar time scales, because the energy difference LP and UP is only 48 cm^{-1}, and thermal fluctuations promoting upwards or downwards transitions within this energy range have similar likelihood at room temperature. The time traces (Figs. 3c and 3d) exhibit lifetimes of 83 ± 6 ps for the UP-dark(ν_{12}) relaxation and 86 ± 6 ps for LP-dark (ν_{12}) relaxation, validating our pump-probe data. As explained before, we ascribe these essentially identical late-time relaxation dynamics to the dark modes of strongly coupled $W(CO)_6$ in acetone. Importantly, within our fitting uncertainty, this exponential kinetics is same as that featured by the bare fundamental transition of $W(CO)_6$ in acetone (with fundamental transition ν_{01} lifetime of 84 ± 4 ps, see Figure 6.5b).

6.2.3 Polariton Dynamics in Hexane

For the $W(CO)_6$ vibrational polariton system in hexane, the Rabi splitting equals 43 cm^{-1} (see Figure 6.4b), which is close to that for the acetone system (48 cm^{-1}). Its pump-probe spectrum at $\sim$5 ps also shows an LP absorptive peak and a UP derivative lineshape (Figure 6.4d). Interestingly, the pump-probe signal for the polariton system in hexane is distinct when compared to its acetone counterpart, even though the bare system ν_{01} dynamic trace (Figure 6.5a) shows a pure decay trend which is similar to that for the acetone-system (Figure 6.5b). By performing spectral integration of the probe-LP peak area (around 1963 cm^{-1}, Figure 6.4d), we found the most notable difference in the pump-probe dynamics when compared to the acetone counterpart (Figure 6.6a): the rising time for the dark state overtone (or equivalently, for the absorptive LP) feature near 1963 cm^{-1} becomes significantly longer (it rises to a maximum at $\sim$ 20 ps), suggesting an intermediate state might exist in the pathway for polariton relaxation to

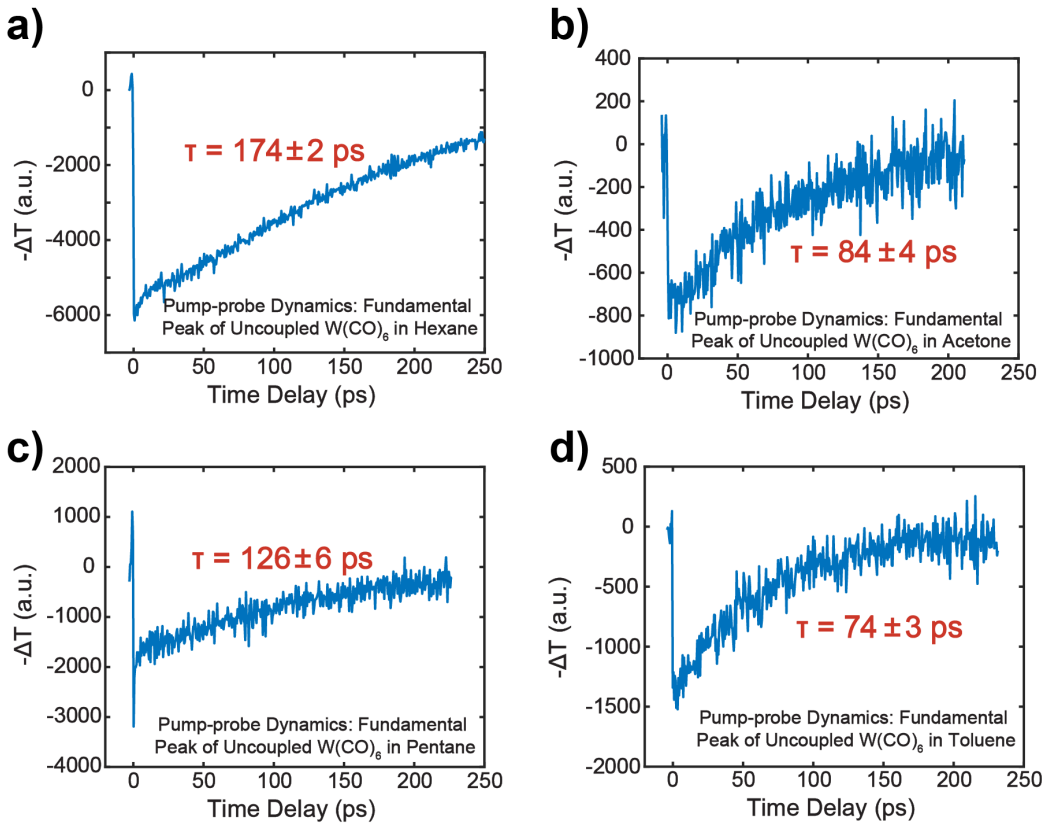

Figure 6.5: Pump-probe dynamics and fitted lifetimes of the CO asymmetric stretch mode of uncoupled $W(CO)_6$ in (a) hexane, (b) acetone, (c) pentane and (d) toluene.

the first excited states of dark modes. This dynamic feature has been first observed and reported by Dunkelberger and co-workers in their pump-probe dynamics of the same system, which was attributed to a transition from UP to second excited state of dark modes.[14] To further understand the change in dynamics, we applied 2D IR spectroscopy to the molecular vibrational polariton system in hexane.

The state-resolved dynamics from 2D IR can be obtained by doing spectral integration around pump-LP /UP and probe-LP frequencies (red and black boxes in Figure 6.6b). The results show distinct dynamics in hexane compared to acetone (compare Figs. 4c and 4d with 3c and 3d). Excitation of the UP results in fast polariton relaxation (< 5 ps) and similarly fast decay into the dark reservoir (Figure 6.6c), in analogy to the observation for polaritons in acetone. The dark mode relaxation lifetime is ca. 167 ± 6 ps from the single-exponential fitting shown in Figure

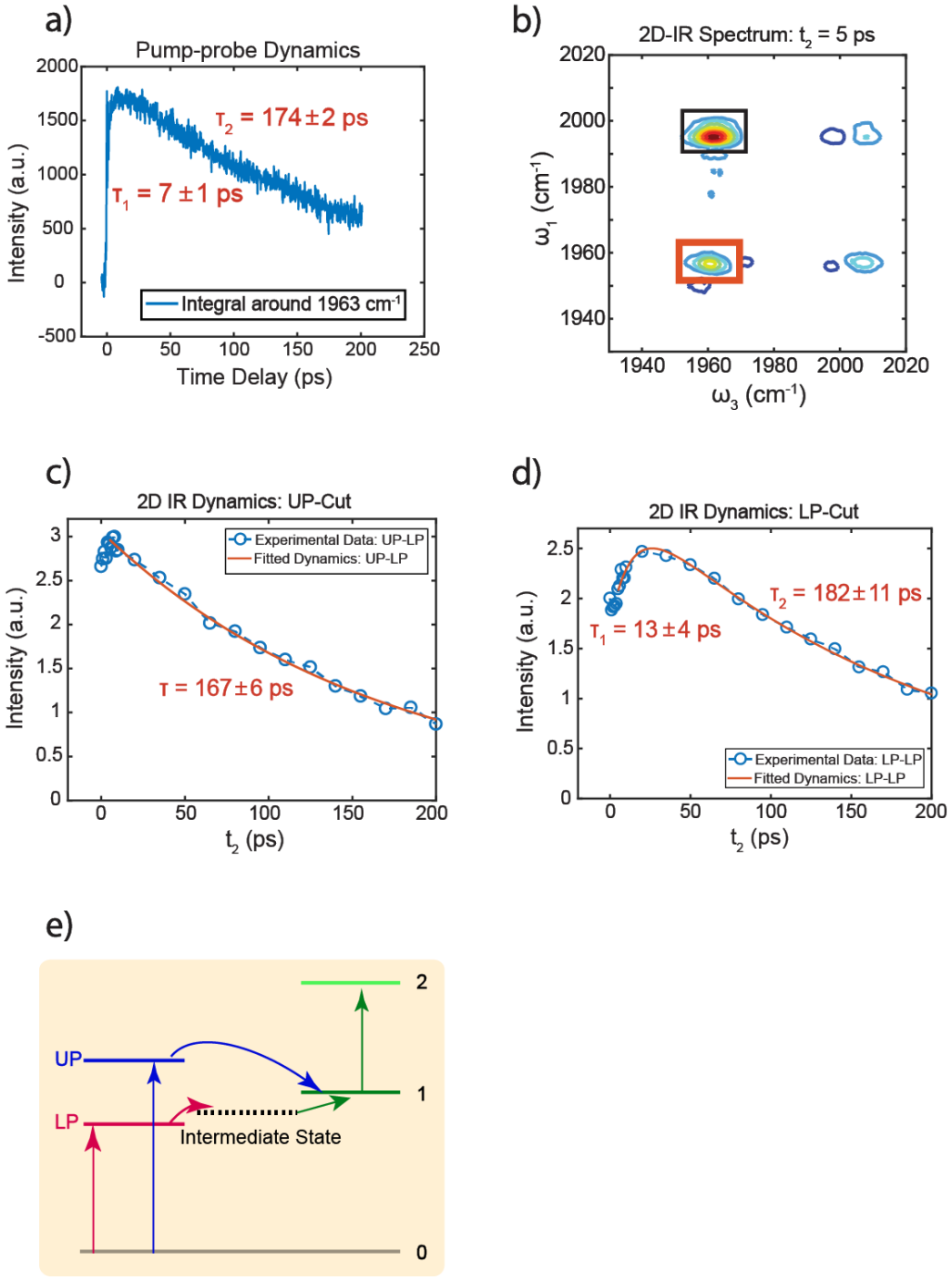

Figure 6.6: (a) Pump-probe dynamic trace at LP state for strongly coupled $W(CO)_6$ in hexane. (b) 2D-IR spectra of strongly coupled $W(CO)_6$/hexane. 2D IR dynamic trace of (c) UP-LP peak and (d) LP-LP peak. (e) Polariton-to-dark mode population transfer pathways.

6.6c. Clearly, distinct dynamics arise when the LP state is pumped (Figure 6.6d). When LP is excited, it first undergoes fast (<5 ps) polaritonic decay induced primarily by cavity leakage similar to the UP, and then it takes tens of picoseconds (13±4 ps) for the dark mode (absorptive) signature to maximize (Figure 6.6d). This observation indicates that the dynamics in hexane is different from described in Figure 6.2f: when the LP mode of molecular vibrational polaritons are excited in hexane, the resulting excited-state population is first trapped in an intermediate state, and only subsequently relaxes into the singly-excited dark modes (Figure 6.6e), which show a decay lifetime of 182±11 ps. The latter shows similar relaxation dynamics when compared to data obtained from experiments performed outside of cavity (174±2 ps, Figure 6.5a).

6.2.4 Origin of Solvent Dependent LP to Dark State Relaxation

Our experimental results indicate several interesting phenomena in the vibrational polariton dynamics. First, the time that polaritons take to fully relax into the dark modes depends on whether UP or LP is pumped. It seems that the relaxation of UP happens without intermediates and is independent of solvent. However, when the LP is excited, the relaxation dynamics of LP to dark modes as tracked by 2D IR seems highly dependent on the solvent environment and can be significantly delayed.

Given that the choice of solvent allows us to control the LP relaxation dynamics into dark modes, it is worth discussing the physical parameters that govern these phenomena. We rule out the possibility that the difference in dynamics is due to the cavity lifetime (or finesse factor) or Rabi splitting, because both factors are kept approximately constant in the above experiments. The only significant difference between the two systems is the solvent environment. From FT IR (see Figure 6.8c and d), it can be seen that aside from a small solvatochromic shift (of approximately 9 cm^{-1}), the lineshapes of the fundamental CO asymmetric stretch $T_{1\mu}$ are significantly different outside of the cavity: in hexane, the FHWM is 4.5 cm^{-1}, whereas in

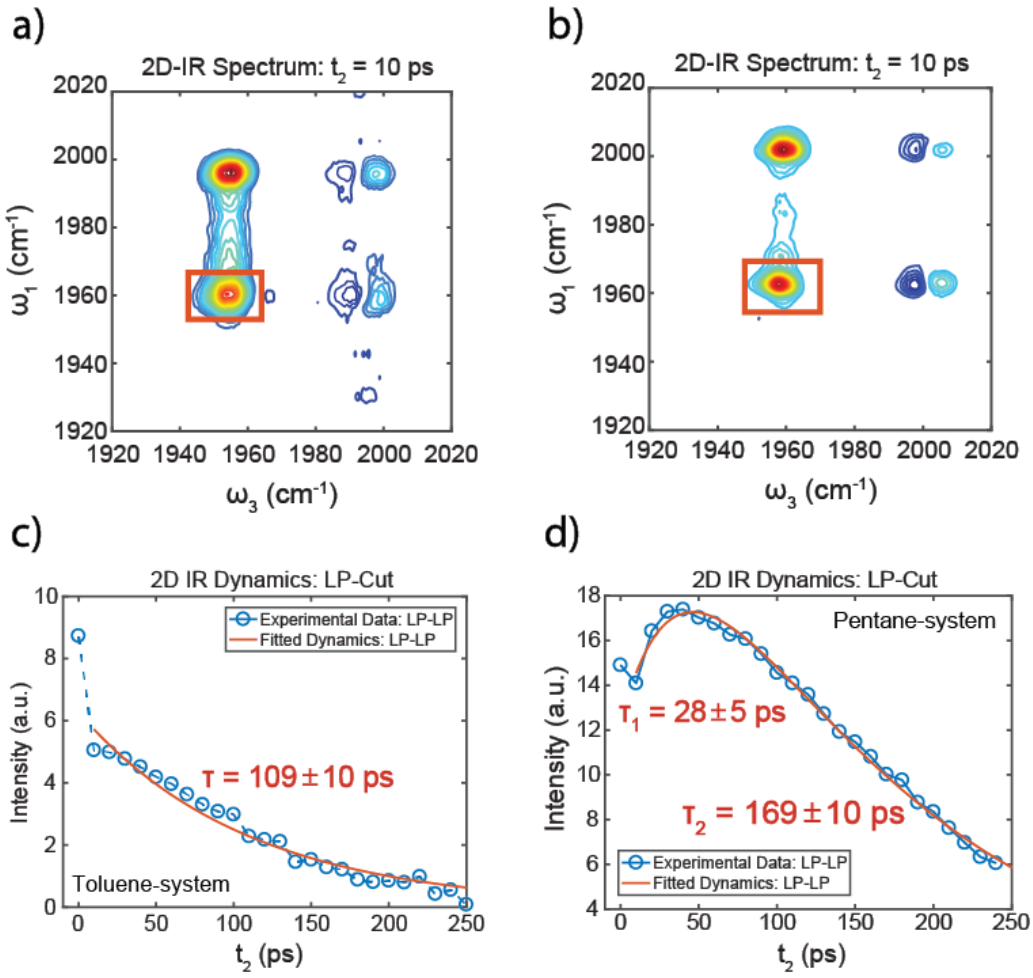

Figure 6.7: 2D-IR spectra of $W(CO)_6$ in strong coupling regime at 10 ps in (a) toluene and (b) pentane; the LP-LP peak is indicated by red boxes. 2D IR dynamic trace of LP-LP area (red boxes in a and b) in (c) toluene and (d) pentane.

acetone, it is 20.5 cm^{-1}. Based on corresponding polaritonic 2D IR spectra (Figure 6.3b and Figure 6.6b), it can be concluded that the dominant source of polariton lineshape broadening is homogeneous. In acetone, the asymmetric CO modes dephase much faster in comparison to hexane. The faster dephasing can be qualitatively explained by stronger system-bath interactions, as acetone is a much more polar solvent than hexane. It appears phenomenologically that the same system-bath interactions that cause faster dephasing also control the lifetime of the conjectured intermediate states.

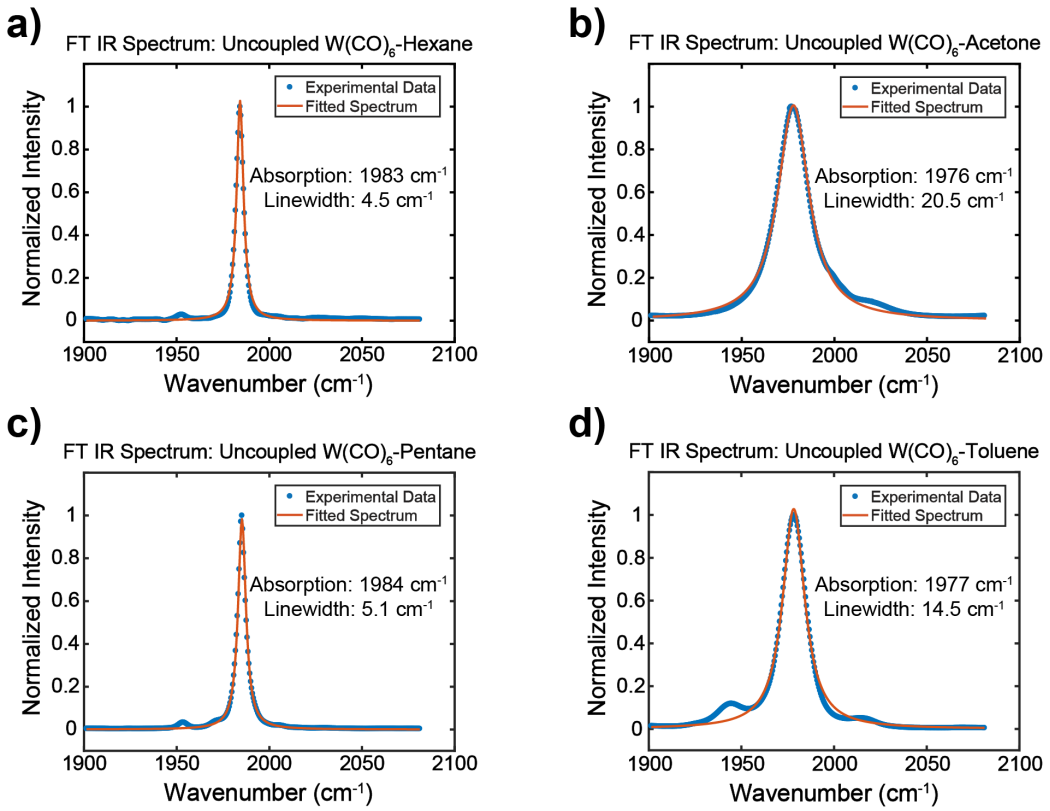

Figure 6.8: FT IR spectra and corresponding Lorentzian fits of uncoupled $W(CO)_6$ in (a) hexane, (b) acetone, (c) pentane and (d) toluene.

To further verify this phenomenological relationship, we performed dynamic measurements in two additional solvents, while keeping the Rabi splitting approximately constant in all experiments. The results are summarized in Figure 6.7. We find again that for pentane, a nonpolar solvent, the LP to dark mode dynamics exhibit a rise-to-decay trend (the rise lifetime is 28±5 ps and decay lifetime is 169±10 ps), whereas for toluene, a solvent that has strong interactions with $W(CO)_6$ (as evidenced e.g., by the corresponding broad linewidth), only decay is observed (the decay lifetime is 109±10 ps). We summarize the dynamics and vibrational linewidths as well as the solvent polarity in different solvent systems in Table 1. Our results show the rising dynamics is only resolvable for the dynamics of LP-to-dark mode transfer and they only occur in the low polarity solvents giving rise to vibrational FHWM significantly smaller than the cavity linewidth (see Table 1), further supporting the conclusion that that there is a direct connection between the

molecular homogeneous linewidth and the lifetime of the dark states: whenever the molecular linewidth exceeds that of the cavity (toluene or acetone systems), LP seems to relax directly to dark modes while, in the opposite case (pentane or hexane), LP appears to first relax into an intermediate state and only later into dark modes. We conjecture the threshold for the passage of population through intermediate states is given by the cavity mode linewidth (in our current experiment, $\sim$11 cm^{-1}). There is a competition between photon and vibrational decay: when vibrational relaxation to dark states is slower than photon leakage, the polariton population first transfers to intermediate states before relaxing to the first excited-states of dark modes. In this way, the decay time could also become longer in some cases. For instance, this could be due to a small number of delayed LP to dark mode relaxation pathways, i.e., not large enough to induce rising dynamics, but still significant to cause slower dark state decay, by gradually populating the latter from the intermediates.

Table 6.1: Correlation between the lifetimes of LP-dark mode and pure (i.e., outside the cavity) molecular linewidth.

Solvent Environment	Pure Molecular Mode Linewidth (cm^{-1})	Lifetimes(ps) of LP-LP Region		Lifetimes (ps) of UP-LP Region	0$\rightarrow$1 Lifetime (ps) of Uncoupled Molecules	Solvent Polarity Relative to Pure Water[99]
		τ(rise)	τ(decay)	τ(decay)		
Hexane	4.5$\pm$0.1	13$\pm$4	182$\pm$11	167$\pm$ 6	174$\pm$2	0.009
Pentane	5.1$\pm$0.1	28$\pm$5	169$\pm$10	175$\pm$5	126$\pm$6	0.009
Toluene	14.5$\pm$0.3	-	109$\pm$10	98$\pm$8	74$\pm$3	0.099
Acetone	20.5$\pm$0.2	-	86$\pm$6	83$\pm$6	84$\pm$4	0.355

6.2.5 Proposed Intermediate States and Polariton Relaxation Mechanism

While we have clarified the relationship between vibrational linewidths and LP to dark mode dynamics, the nature of the intermediate states is also worth our attention. In particular, the fact that UP and LP experience different dynamics indicates that the intermediate trap states are only involved in the pathway for relaxation between LP and dark modes. One of the major differences between LP and UP is that UP is isolated in energy space, e.g., there is no dipole-allowed transition which is nearly-resonant with UP, whereas near LP, in addition to the ν_{12} transition of the dark modes which directly couples to the LP transition, there are also the ν_{23} and ν_{34} transitions that are energetically close by. Previous narrow band pump-probe experiments on $W(CO)_6$ have shown that as the pump wavelength is redshifted from the fundamental transition, high-lying states can be preferentially excited over the first excited state.[67] Given the large density of high-lying ($n > 2$) dark states that is accessible near LP, this polariton can easily assist in the excitation of vibrational overtones in a ladder-climbing fashion. In contrast, UP is significantly blue-shifted from the fundamental, and even more so from overtone and all ladder-climbing transitions, and thus cannot couple effectively to the high-lying modes. Thus, our proposed mechanism (Figure 6.6e) illustrates that UP can directly decay into the first excited dark modes, whereas depending on solvent, LP first effectively performs ladder-climbing to high-lying vibrational dark modes, which slowly relax back to the first excited level of dark states. We note the measured lifetime of ν_{12} of pure vibrational modes without cavity, is about 70 ps,[14, 67] which is much longer than the relaxation time from the intermediate to the ν_1 of dark modes measured in our experiment. The difference in dynamic lifetimes could be due to cavity-enhanced high-lying excited state relaxation.

Further evidence supporting our assignment of the intermediate states to the high-lying dark states lies in the time-dependence of the probe-LP lineshape when pumping the LP state. Previous works assigned the broad and large absorptive lineshape of the LP-peak in the spectral cuts at $\omega_{pump} = \omega_{LP}$ to the population transfer from LP states to first excited states of dark modes,

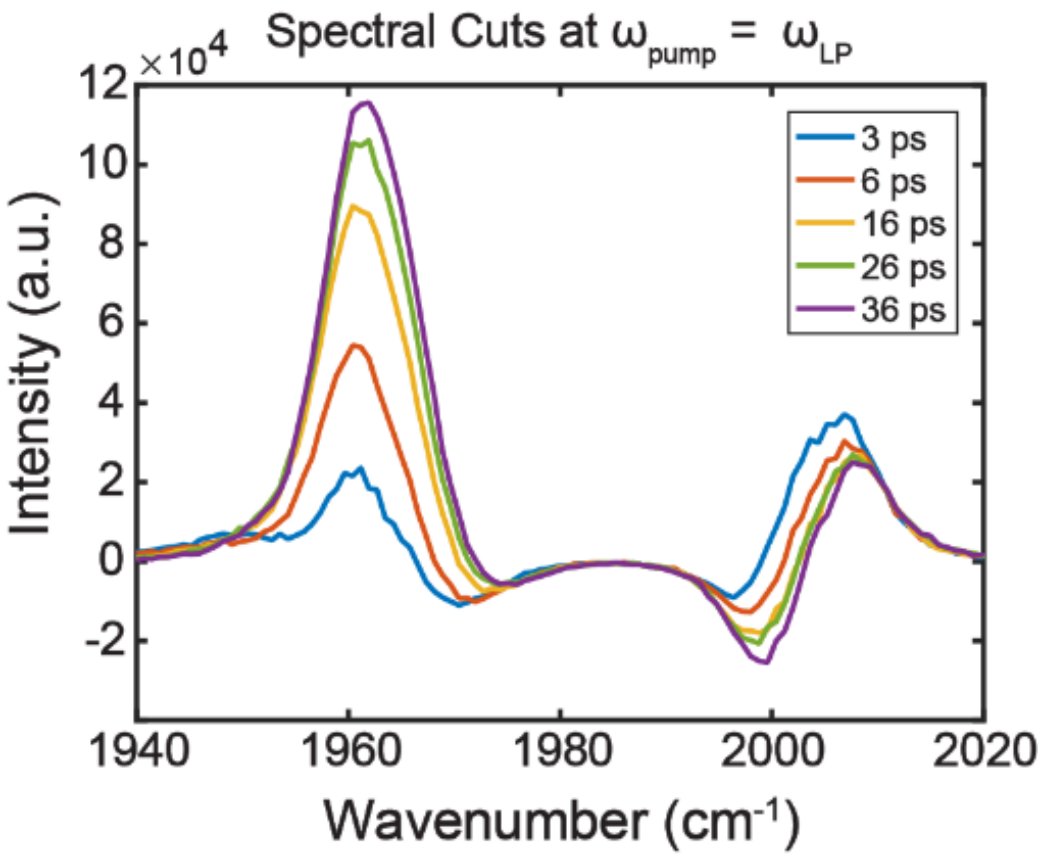

Figure 6.9: 2D-IR spectral cuts at pump-LP at various time-delays, showing the LP peak lineshape evolves from derivative shape (3 ps) to highly absorptive shape (6, 16 and 36 ps), while the UP-peak keeps derivative-shaped from early-time to later time-delay.

with subsequent ν_{12} absorption, while the UP has a derivative lineshape mostly because pumping depletes a sizable fraction of molecules in the ground-state. Here, however, we assign a fraction of the intermediate states to be higher-lying dark modes. Thus, when LP population first transfers to those states at early times, the probe-LP window would not be able to detect the relevant higher-order transitions, such as ν_{23} and ν_{34}. As a result, the absorptive feature of the LP peak should be largely suppressed, and hence, this peak would at early times have a similar derivative lineshape as the UP peak.

Indeed, our experimental results support this interpretation. In Figure 6.9, the LP lineshape evolves from derivative shape to absorptive feature as t_2 time-delay changes. At early-time (3$\sim$6 ps), the LP lineshape has significant derivative component, which indicates reduction in the

number of molecules in the ground-state, a significant fraction of which is not in the n=1 state, for if this was the case, then the strong absorptive feature generated by ν_{12} transitions would be clearly detected around the probe-LP frequency. After 16 ps, the LP lineshape is dominated by the absorptive feature. This spectral signature suggests that the population has relaxed back to first excited state of dark modes and subsequent ν_{12} transitions are detected by the probe pulse. The probe-UP region, however, preserves its derivative lineshape at all time-delays, meaning it does not experience such processes driven by efficient coupling to highly excited vibrational modes.

This mechanism also provides a hypothesis for the solvent dependence of the LP to dark state kinetics. Based on pump-probe measurements on $W(CO)_6$ outside of the cavity, it is found that it is harder to access the high-lying excited states via ladder climbing in high polarity media in comparison to the weakly. Stronger system-bath interactions enhance the anharmonicity of the CO mode, and thus inhibit ladder climbing, while accelerating energy relaxation. Therefore, in the cavity system, for solvent environments that strongly interact with the solutes, highly excited-states are unlikely to be efficiently excited by the LP, due to the larger anharmonicity of the former, and the dynamics will be dominated by the fast relaxation to first excited dark states within the polariton lifetime. On the contrary, the occupation of high-lying states could be preserved in nonpolar solvents, and this would provide a reason that they can act as intermediate states holding the energy obtained from LP, before transitioning into the singly-excited manifold of dark states.

6.3 Conclusions

By preparing polaritons in non-polar solvents, we found that the LP states relax into an intermediate state, before finally decaying into first excited dark states. The intermediate states are hypothesized to correspond to high-lying excited levels of dark modes. However, such

intermediate states cannot be observed in either solvent environments strongly interacting with solutes or when the UP is pumped. After the LP population transfers to high-lying levels of dark modes (the intermediate states), these high-lying states can last for as long as 30 ps. These dynamics are in sharp contrast to the vibrational dynamics outside cavities, where first excited-states carry most of the pumped energy. Thus, by coupling the delocalized collective vibrational polarization with the cavity electromagnetic field, vibrational dynamics can be substantially modified, and in particular, potentially effective vibrational ladder-climbing can be achieved.[100] This result could be helpful in the interpretation of recent cavity chemistry results, where reaction rates and selectivity are reported to be modified. We conclude by pointing out that the mechanism of molecular polaritons are excited as delocalized coherent oscillations, quickly decay into hot vibrational manifolds, and then evolving into equilibrated low vibration levels, resembles the two-temperature models in plasmonics[101] (e.g. collective plasmon motions decay into hot electron-hole pairs and then relax into equilibrated excited electron-hole populations). Yet, unlike plasmon, the potential of vibrational polaritons is nearly unexplored, which could be a fruitful ground for both fundamental chemical physics and applied chemistry, photonics and quantum information science.

Chapter 6, in full, is a reprint of the material as it appears in the Journal of Physical Chemistry A, 2019. Bo Xiang; Raphael F. Ribeiro; Liying Chen; Wang, Jiaxi; Matthew Du; Joel Yuen-Zhou; Wei Xiong., American Chemical Society, 2019. The dissertation author was the primary investigator and author of this paper.

Chapter 7

Ultrafast Nonlinear Infrared Polaritonic Interaction between Cavities Mediated by Molecular Vibrations

7.1 Introduction

Nonlinear interactions between molecular vibrational modes, referred as molecular vibrational nonlinearity hereafter, which are localized within angstroms due to the physical dimensions of molecular potential energy surfaces, e.g. Morse or double well potentials, are crucial to distribute energies among chemical groups during reactions. Even intermolecular nonlinear interactions through dipole-dipole interactions are limited to a few nanometers. Because the molecular vibrational nonlinearity are localized, the reactants have to be close to each other in liquid phase to react, which makes many reactions limited by diffusions. Being able to delocalize nonlinear interactions across micron-length thus has the potential to trigger reactions without the reactants to be close in spaces. Meanwhile, nonlinear interactions of photons are the crucial components for photonic circuitry,[102] and such interactions in the mid-IR regime can enable

chemical sensing at molecular fingerprints region. However, scaling up of these developments are prohibited, because nonlinear IR photonic interactions are also localized, which are mediated by molecules. Thus, delocalized nonlinear interactions in the IR regime could be critical for future photonic applications.

In this work, we report nonlinearity between polaritons in two adjacent cavities. By exciting polaritons in one cavity, we affect polaritons in the neighboring cavity, whose geometric center is tens of micron away from the first cavity, through strong coupling between the vibrational and cavity modes.[1–3, 14, 37] The strong coupling between molecular vibrational and cavity modes forms molecular vibrational polaritons, which enables novel phenomena such as vibrational energy transfer between molecules in the liquid phase,[8] and modified chemical reaction selectivity.[4] The local molecular vibrational anharmonicity provides sources of optical nonlinearity, while photon cavity modes are macroscopic and delocalized but linear. The strong light-matter coupling then combines photon delocalization with molecular nonlinearity, which otherwise would not exist in either mode alone. We note that the idea of combining material nonlinearity with hybridized cavities was first proposed in atomic-molecular-physics for quantum simulation,[103] and recently demonstrated in inorganic semiconductor exciton-polaritons[104]. To the best of our knowledge, this report is the first work to enable intercavity nonlinearity with liquid phase molecular systems, and to directly time-resolve the dynamics of the nonlinear interaction between polaritons in adjacent cavities. We refer to this nonlinearity as polaritonic intercavity nonlinear interactions.

7.2 Results

To realize polaritonic intercavity nonlinear interactions, we fabricate a coupled Fabry-Perot (FP) cavity and conduct linear and nonlinear IR spectroscopy on coupled-cavity polaritons. A checkerboard matrix is composed of individual FP cavities, where cavities with two thicknesses

(12.50 μm and 12.69 μm for cavity A and B respectively), and two distinct transition frequencies (1970 and 2000 cm^{-1}, Figure 7.1d), alternate (Figure 7.1b and c for SEM image). Here, neighboring cavities can overlap through evanescent waves along the transverse directions, and the molecular modes in the overlapping volumes should enable nonlinear interactions[1, 2, 14] between polaritons in adjacent cavities (Figure 7.1a). Experimentally, we found that the optimal cavity lateral dimension was 50 μm. We believe that at this size, it ensures a sufficient interaction between neighboring cavities while keeping the two cavity modes distinguishable. Furthermore, because the IR laser beam is c.a. 100 μm, cavity with this size avoid inhomogeneity introduced by pumping too many cavities together. We prepared the polaritons by encapsulating a saturated $W(CO)_6$/hexane solution ($\sim$40 mM) in the coupled-cavity). $W(CO)_6$ has a strong asymmetric stretch vibrational mode at 1983 cm^{-1}, which is ideal for forming polaritons in the IR regime.

The linear IR spectra of polaritons in the coupled-cavity show four spectral peaks (the right part of Figure 7.1e), which is surprising and makes the transfer matrix model[89] challenging to capture the results. From a naive perspective, if one molecular vibrational mode strongly couples to the two-cavity modes simultaneously, three IR peaks would be expected, which disagrees with the observed four-peak feature. An alternative model is that the molecular vibrations couple to the two cavities separately, each forming one pair of polaritons (upper polariton, UP, and lower polariton, LP), i.e., UP1 and LP1 in cavity A and UP2 and LP2 in cavity B, respectively, composing the total four peaks. To test this idea, we measure the IR spectra of two polariton systems prepared by regular FP cavities, e.g., UP1/LP1 and UP2/LP2, separately (Figure 7.1f and g), and then add them together numerically. The peak positions of the summed spectrum match well with the experimental spectrum, but the intensities do not (Figure 7.1h). Similarly, while the transfer matrix method (17) can simulate polariton spectra of each cavity perfectly (dashed line in Figure 7.1f and g), it cannot reproduce the spectral intensity of the polaritons in the coupled cavity (dashed line in Figure 7.1h).

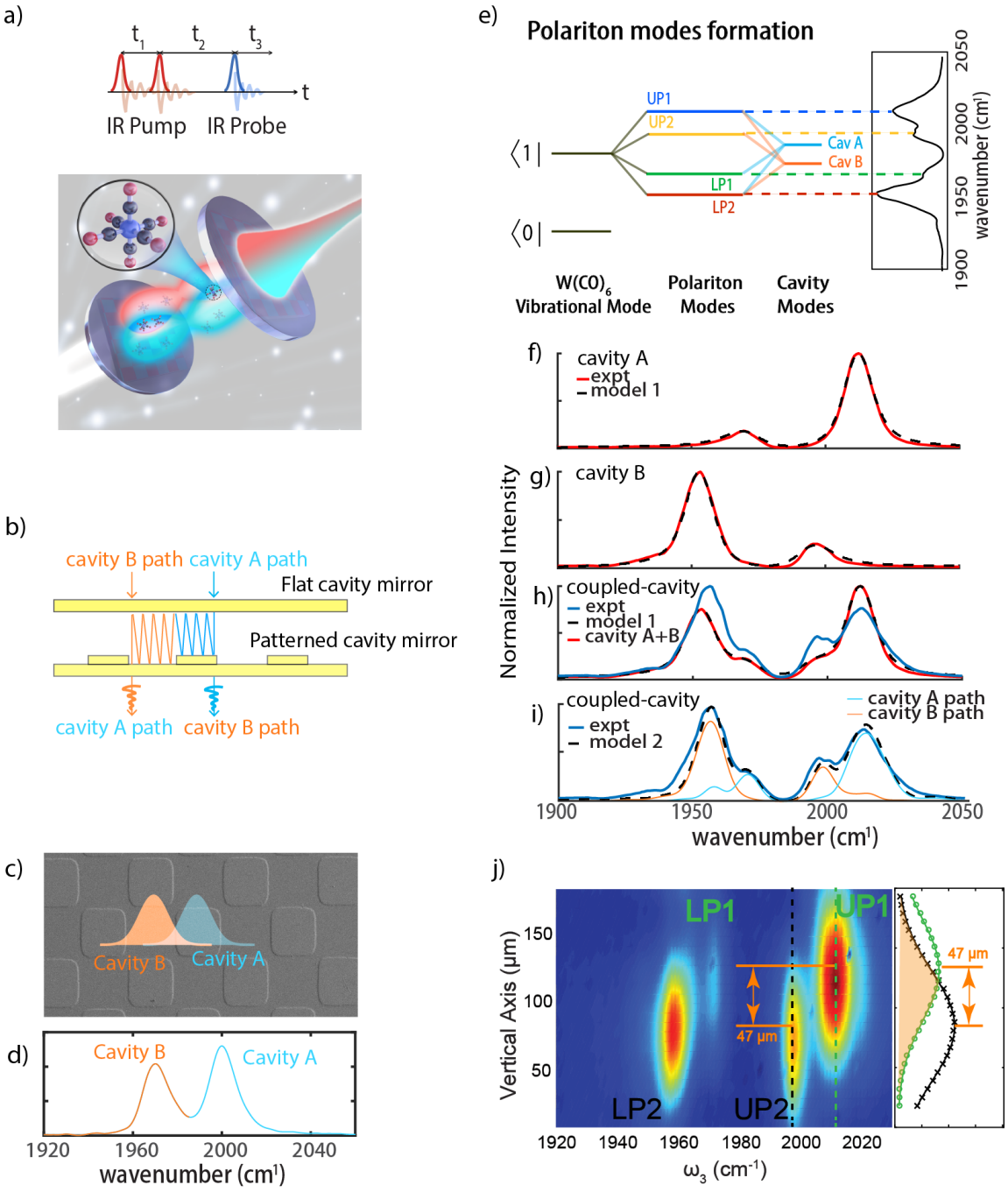

Figure 7.1: (a) Dual-cavity and 2D IR setup. (b) Photon hopping. (c) SEM of patterns. (d) FTIR of the dual cavity modes. (e) Energy diagram of polaritons. (f-i) Experimental and simulated linear IR of polaritons. (j) Transmission image of dual-cavity.

The intensity mismatch suggests a component is missing from the transfer matrix model to account for the intensity redistribution among spectral peaks. We extended the transfer matrix model by including photon hopping (model 2) and show that the missing component is the delocalization of cavity modes: Upon entering cavity A, photons can hop to cavity B and subsequently interact with molecular vibrations in cavity B, representing the delocalization between cavities (referred to as the cavity A path Figure 7.1b). An alternative path also exists (cavity B path in Figure 7.1b). The expression of transmission spectra based on model 2 is summarized in Eq.1.

$$T = [\frac{T_1 e^{(-\frac{1}{2}\alpha L_1)}}{1 - R_1 e^{i\Delta\varphi_1 - \alpha L_1}}(1 - R_1^n e^{-n\alpha L_1 + in\Delta\varphi_1}) + \frac{\sqrt{T_1 T_2} e^{-\frac{1}{2}\alpha L_1}}{1 - R_2 e^{i\Delta\varphi_2 - \alpha L_2}} (R_1^{n-1} e^{-(n-1)\alpha L_1 + i(n-1)\Delta\varphi_1} R_2 e^{-\alpha L_2 + i\Delta\varphi_2})]^2 \quad (7.1)$$

where T_m, R_m, L_m, and φ_n are transmission, reflection, cavity thickness, and phase shift of cavity m, respectively, α is the absorptive coefficient of molecules, and n represents the number of round trips before photon hopping to the adjacent cavity. Results from model 2 reproduced not only the spectral peak position but also the intensities from the experimental measurements. The new model result shows that the linear IR spectra are a combination of two sets of polaritons from the cavity A and B paths, respectively (orange and cyan traces in Figure 7.1i). Thus, molecular modes in each cavity strongly couple to the cavity mode that they reside in and weakly couple to the adjacent cavity mode (Figure 7.1e). We note the intermolecular interaction are negligible to contribute to the change of liner IR.

This theoretical picture is further supported by an IR hyperspectral image of the coupled-cavity polaritons. In this image (Figure 7.1j, detailed description of the IR hyperspectral imaging system in Figure 7.2), a vertical slice of the coupled-cavity image is spectral dispersed horizontally and imaged by an FPA MCT detector. Thus, the vertical axis of the image represents the location

of the polaritons and the horizontal axis corresponds to the frequency of the polariton features. We can identify the UP1 and LP1 from cavity A at 116 μm, and UP2 and LP2 from cavity B at 69 μm. All polaritons reside at their characteristic frequency on the horizontal axis, and they are spatially displaced along the vertical by 47 μm, agreeing with the SEM image. However, vertical cuts show polaritons in each cavity leak into their neighboring cavity, as the width of polaritons are c.a. 59 and 64 μm, larger than the 50 μm dimension of the cavity. Therefore, the IR hyperspectral image also agree with the theoretical picture that cavity mode delocalization exists, which is a critical component for polaritonic intercavity nonlinear interactions.[103] However, we have not yet demonstrated that polaritonic intercavity nonlinear interactions, in which excited polaritons influence those in an adjacent cavity, occurred.

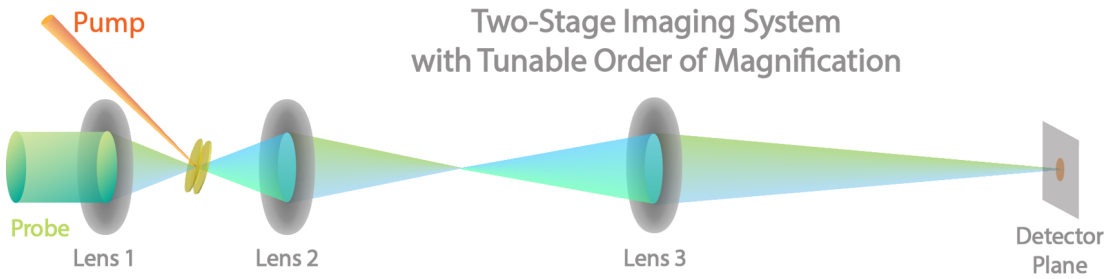

Figure 7.2: Schematic illustration of 2D IR-imaging setup.

To examine polaritonic intercavity nonlinear interactions, we conduct 2D IR spectroscopy.[2, 33] 2D IR measures the third-order nonlinear response of the systems. The pulse sequence described in Figure 7.1a excites two vibrational coherences at various time incidences and tracks the interaction and dynamics of quantum states. For example, when two modes interact with each other, e.g., exciting one mode can affect the other mode, cross-peaks appear at the corner defined by the resonance frequencies of the two coupled modes.

2D IR spectra of the coupled-cavity polaritons show clear cross-peaks (t_2 = 20 ps, shown in shaded green areas in Figure 7.3a). In the following, we perform detailed spectral analysis to show these cross-peaks are signatures of polaritonic intercavity nonlinear interactions. Based on

knowledge from previous publications,[1–3, 7, 14, 37] we focus on analyzing 2D IR signal at a t_2 that is longer than polariton lifetime, e.g., t_2 = 20 ps, where the physics is well understood: the source of nonlinear signals at is a non-equilibrium population of dark states of the $W(CO)_6$ asymmetric modes in the cavities. At the long-time limit, polaritons decay and excite dark modes, leading to the derivative signals near UP due to Rabi splitting contraction, and overtone absorptions for the strong absorptive feature at the LP side.[1, 2, 14]

To quantitively understand the spectra, we take cuts of the 2D spectra at several ω_{pump}, corresponding to pump-probe spectra by exciting specific polariton states, and simulate them using model 2 where α, the absorptive coefficient of molecules, will be influenced by the the pump-induced ground-state molecular population reduction in both cavity components. The simulated spectra match with the experimental results very well, capturing the derivative features on the UP side and the double absorptive features on the LP side (Figure 7.3c is a spectral cut at ω_{pump}= ω_{UP1}=2010 cm^{-1}). The only mismatch is a small positive feature near 1940 cm^{-1} due to lineshape changes appears in the simulated result but not the experimental data. This feature could be canceled in the experiment by higher order excited state absorptions of the reservoir mod2 - a term that was not included in the simulation.

Further physical insights of the intercavity nonlinear signal are obtained by decomposing the simulated spectra into contributions from cavities A and B. A representative result shows that both the cross-peaks of the spectral cut at UP1 of cavity A - a noticeable derivative feature near ω_{probe} = 1995 cm^{-1} and a large absorptive peak at ω_{probe} =1955 cm^{-1} - are derived from the nonlinear responses from cavity B (the green trace in Figure 7.3c). In contrast, the nonlinear signal of cavity A shows a tiny peak at ω_{probe} = 1995 cm^{-1} (the purple trace in Figure 7.3c). Because this spectral cut is obtained by pumping UP1 of cavity A, it confirms that exciting cavity A can affect polaritons in cavity B - a nonlinear interaction delocalized between cavities.

Because the simulation shows that it is necessary to change the reservoir ground and

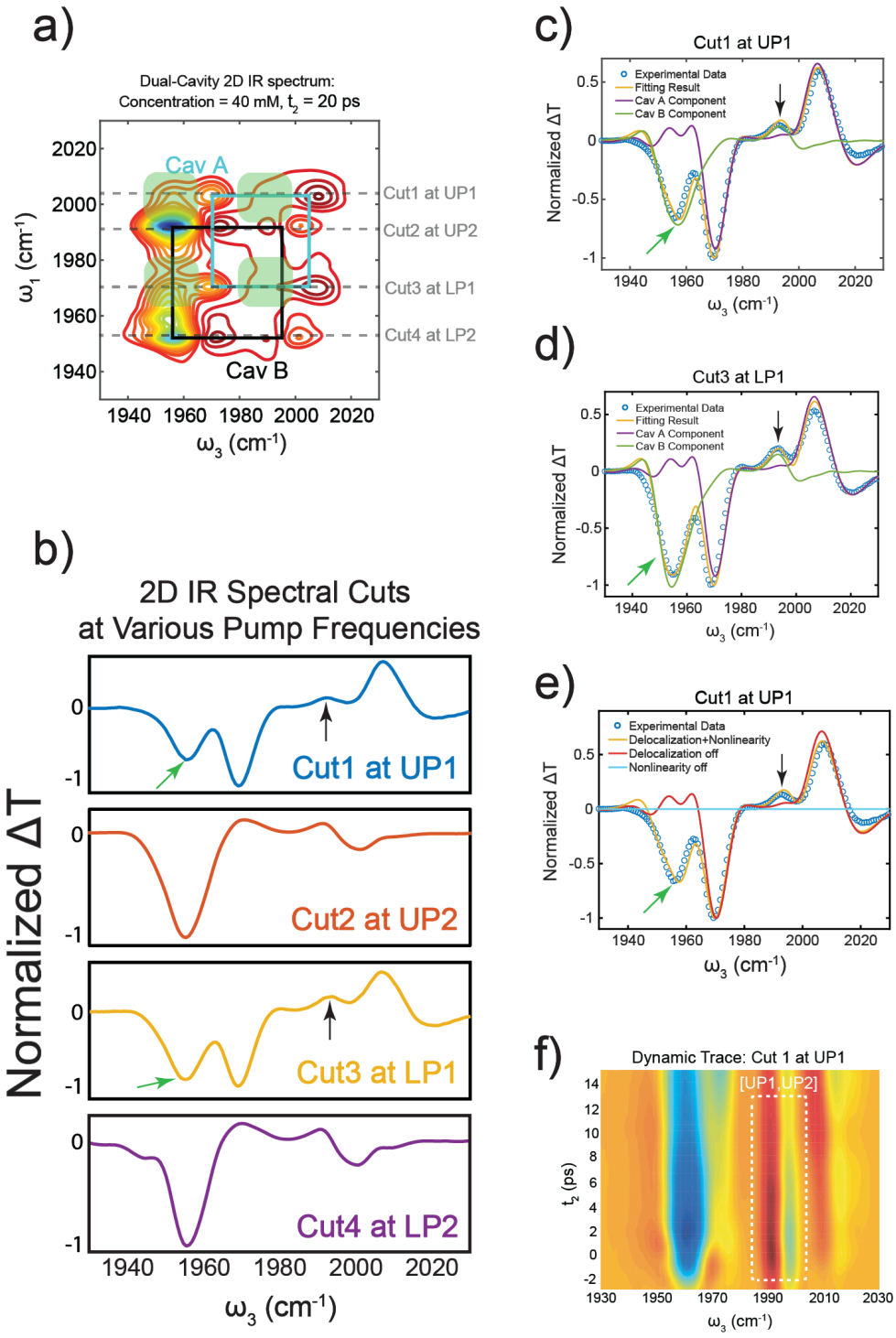

Figure 7.3: (a) 2D IR of $W(CO)_6$/hexane in dual-cavity. (b) 2D IR cuts at LP2, LP1, UP2 and UP1 states. (c)-(e) Experimental and simulated spectral cuts at UP1 and UP2. (f) 2D IR dynamics at UP1 state.

excited state population in both cavities (dc1, dc12, dc2, and dc22 determine the values of A_i which would be the amplitudes of Lorentzian terms that determine the absorptive constant, α), in order to reproduce the experimental results, it suggests that the changes of reservoir population lead to the observed nonlinear signals. Thus, the source of polaritonic intercavity nonlinear interaction is polariton-reservoir mode interactions (similar to those observed in exciton polaritons[105]), in which excited polaritons in cavity A transfer their population to dark reservoir modes, a portion of which is shared with cavity B. The shared excited dark modes reduced the Rabi splitting of polaritons in cavity B, thereby generating nonlinear signals.

We note that such a nonlinear interaction is not detected in spectral cuts of exciting UP2 (Figure 7.3d) or LP2 of cavity B, as the cavity B contribution can well simulate these spectral cuts. Further study on the 2D IR spectra suggest that the intercavity interaction cross peaks are highly sensitive to the incident angle: at certain angle the interactions are mutual between two cavities, i.e. cross peaks exist when either cavity is excited; whereas at other angles, interactions are optimized in one direction, i.e. only cross peaks due to exciting either cavity A or B exist. The angular sensitivity further demonstrates that the intercavity polariton-interaction are originated from photon hopping which highly depends on beam angles, instead of intermolecular interactions. The physical origin of this dependence is beyond our modified transfer matrix model (eq. 7.1), which warrants future momentum imaging experiments and more comprehensive theoretical studies in the future. Without further notification, all 2D IR study are done at angle = 11.3°, where the cavity A to B interactions are favorable.

Both cavity delocalization and molecular nonlinearity are critical for polaritonic intercavity nonlinear interactions, as shown by turning off either factor (Figure 7.3e). When delocalization is turned off, a simulated spectrum is similar to the ones of single cavity polaritons (the red trace in Figure 7.3e). When molecular nonlinearity is turned off by setting anharmonicity to zero, there are simply no signals (the light-blue trace in Figure 7.3e).

The crucial roles of cavity delocalization and molecular nonlinearity can be viewed from

the theoretical aspect. It is the strong light-matter coupling and photon hopping that render the local molecular mode a linear combination of polaritons in different cavities, and thereby delocalize the nonlinearity. The role of mixing Hopfield coefficient is verified by manipulating the polaritonic intercavity nonlinear interactions through changing molecular concentration, and thereby Rabi splitting. No apparent 2D IR signature of intercavity coupling appears for the polariton at lower concentrations (26 mM, Figure 7.4b). Spectral cuts at ω_1=ω_{UP1}, and ω_{LP1} further confirm this observation. This result also serves as a control experiment to show that the observed cross-peaks are not photonic artifacts (e.g., spectral filter effects). We further extract the relative population of excited dark modes in cavity B, when polaritons in A are excited from the 2D IR results, at various Rabi splitting. The relative population decreases from 24.0% to 3.5%, as the molecular concentration declines from 40 mM to 26 mM (Figure 7.4d). These results qualitatively agree with the result from the four-by-four Hamiltonian matrix model that describe the coupled-cavity polaritons. Lowering the concentration results in fewer shared vibrational modes between the two cavities. As summarized in Figure 7.4d, large Rabi-spliting leads to that a non-negligible amount of vibrational modes in cavity B (vib-B) participates in the formation of LP1 and UP1 states, and a portion of vib-A composes LP2 and UP2. Upon pumping LP1 and UP1, it excites the shared vib-A and -B populations, perturbing the energy levels of LP2 and UP2. With small concentration, such a state-mixing between cavities becomes negligible, causing polaritonic intercavity nonlinear interaction to disappear.

We lastly measure the dynamics of the cross-peaks (Figure 7.3f), by scanning the waiting time t_2 of the 2D IR spectra. The spectral cut dynamic around ω_1=ω_{UP1}=1995 cm^{-1} (Figure 7.3f, 2D IR cut at UP1 in the dashed white box) shows [ω_{UP1},ω_{UP2}] cross-peak appears within the polariton lifetime ($<$ 3 ps, a similar trend can be observed when cutting at ω_1=ω_{LP1}as well). This result agrees with the mechanism that the evanescent wave of cavity mode leads to the polaritonic intercavity nonlinear interactions, because the photon hopping can only happen before it leaks out of the cavity.

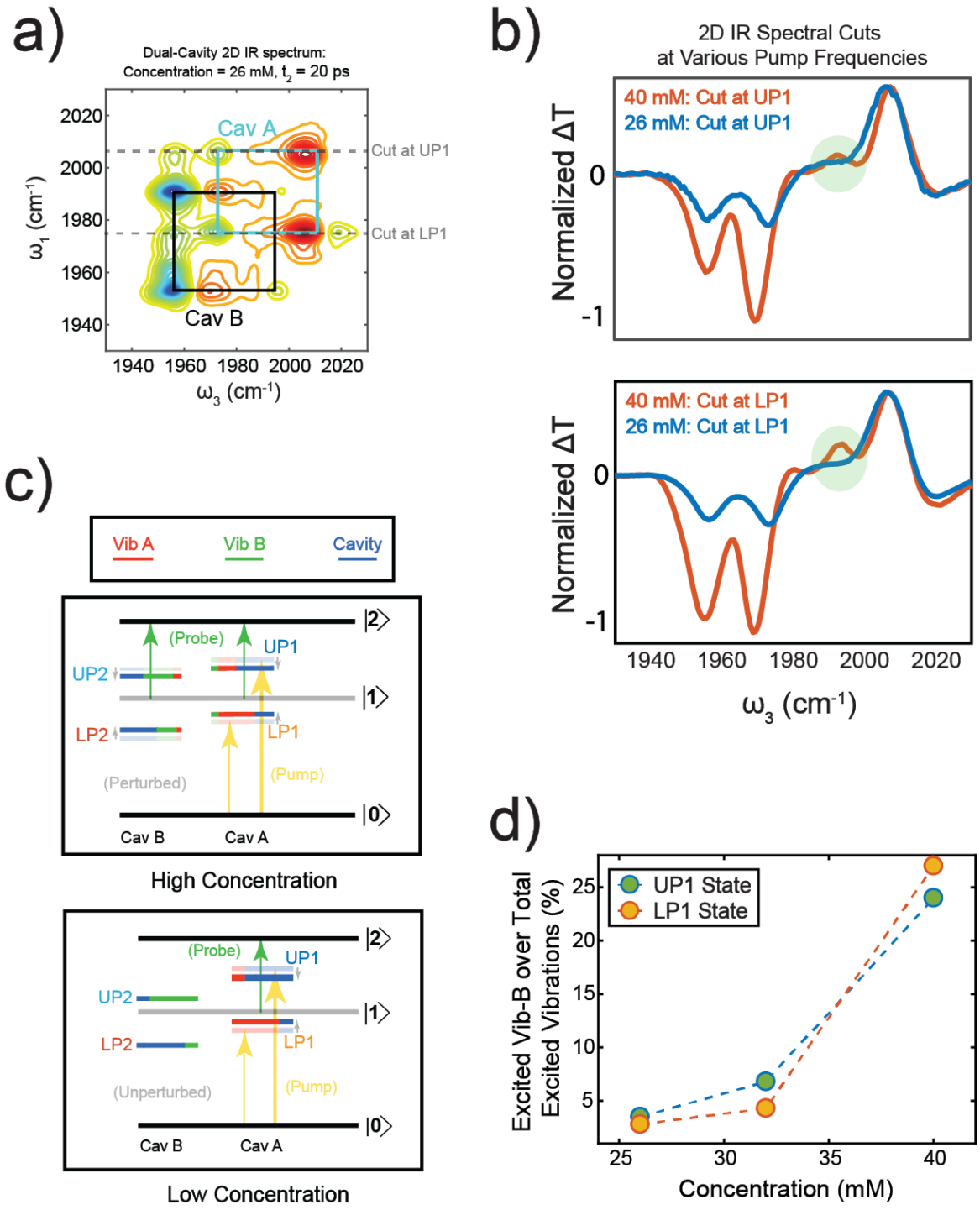

Figure 7.4: (a) 2D IR of $W(CO)_6$/hexane in dual cavity with 26 mM concentration. (b) 2D IR UP1/LP1 cuts with 26/40 mM. (c) The intercavity coupling enabled/disabled in dual cavity systems. (d) Vib-B composition in LP1/UP1 states.

7.3 Discussion

The photonic intercavity nonlinear interaction is exclusively a result of the joint merits of the evanescent wave of cavity modes and molecular nonlinearity. By combining them, a unique new property is created which does not exist in either mode. This demonstration could enable polaritonic photonic circuitry in the molecular fingerprint IR regime for low-concentration threshold, compact chemical sensing. The micron-range nonlinear interaction can be further extended to even longer distances when combined with polariton propagation. This experiment also lays a foundation for remote chemistry,[12] enabling chemistry in one cavity by manipulation of molecules (e.g., as catalysts) in the other cavity. By selectively pumping using a pulse shaper,[39] the coupled cavity can be a new platform for entangled polaritonic qubits.

Chapter 7, in full, is currently being prepared for submission for publication of the material. Bo Xiang; Jiaxi Wang; Zimo Yang; Wei Xiong. The dissertation author was the primary investigator and author of this paper.

Chapter 8

Intermolecular Vibrational Energy Transfer Enabled by Microcavity Strong Light-Matter Coupling

8.1 Introduction

Vibrational energy transfer (VET) is ubiquitous to many molecular processes in the condensed phase, ranging from chemical catalysis[106] to biological signal transduction and molecular recognition[94]. Due to through-bond anharmonic couplings, intramolecular and solute-solvent VET is widespread, leading to rapid intramolecular vibrational redistribution (IVR) that competes with other chemical events.[107] However, through-space, selective intermolecular (solute-solute) VET is relatively rare. The scarcity of intermolecular VET is a consequence of weak intermolecular forces. Compared to electronic transitions, which readily undergo intermolecular energy transfer (via e.g., the F*ö*rster and Dexter mechanisms[108, 109]), vibrational transition dipole moments are ten to hundred times smaller,[13] leading to uncompetitive intermolecular dipole-dipole couplings when compared to their electronic counterparts (Figure 8.1a,

top). As such, intermolecular VET is usually obfuscated by IVR.

Here, we report a state-of-the-art strategy to engineer intermolecular vibrational interactions via strong light-matter coupling. When a highly concentrated molecular sample is inserted into an optical microcavity (e.g., a F-P cavity) or placed onto a plasmonic nanostructure,[110] the confined electromagnetic modes interact reversibly with the collective macroscopic molecular vibrational polarization such that hybridized light-matter states, known as vibrational polaritons, are formed.[1, 2, 14] Due to the delocalized nature of polaritons, the relaxation kinetics of strongly-coupled systems is substantially changed from their weakly-coupled counterparts.[7] While pioneering studies have demonstrated such effects in the context of electronic energy transfer,[11, 16] intermolecular VET under strong light-matter coupling seems to operate by different mechanisms, as we describe below. Furthermore, given the scarcity of selective intermolecular VET in condensed phases, its polaritonic counterpart introduces a powerful concept to alter the course of ground state chemistry in solution.[4]

8.2 Results

To study cavity-assisted intermolecular VET, we designed a strongly coupled system composed of a microcavity and ensembles of two vibrational modes from different molecules. We encapsulated an equimolar solution of $W(CO)_6$ and $W(^{13}CO)_6$ in hexane/DCM solvent (total concentration 100 mM, 1:1 volumetric ratio) in a FP cavity. These molecules are ideal for achieving vibrational strong coupling, as they have degenerate asymmetric stretch modes with large oscillator strength and narrow linewidths. The cavity with thickness L has resonances at $\lambda = 2L/n$, where n= 1,2,3, ... is the cavity mode order. Because the carbonyl asymmetric stretches of $W(CO)_6$ and $W^{13}(CO)_6$ absorb at 1980 and 1938 cm^{-1}, respectively, a cavity with L = n$\times$2.5 micron has modes which are nearly resonant with both vibrational transitions. In our experiments, unless specifically noted, we kept L at 12.5 micron and strongly coupled the 5th order cavity

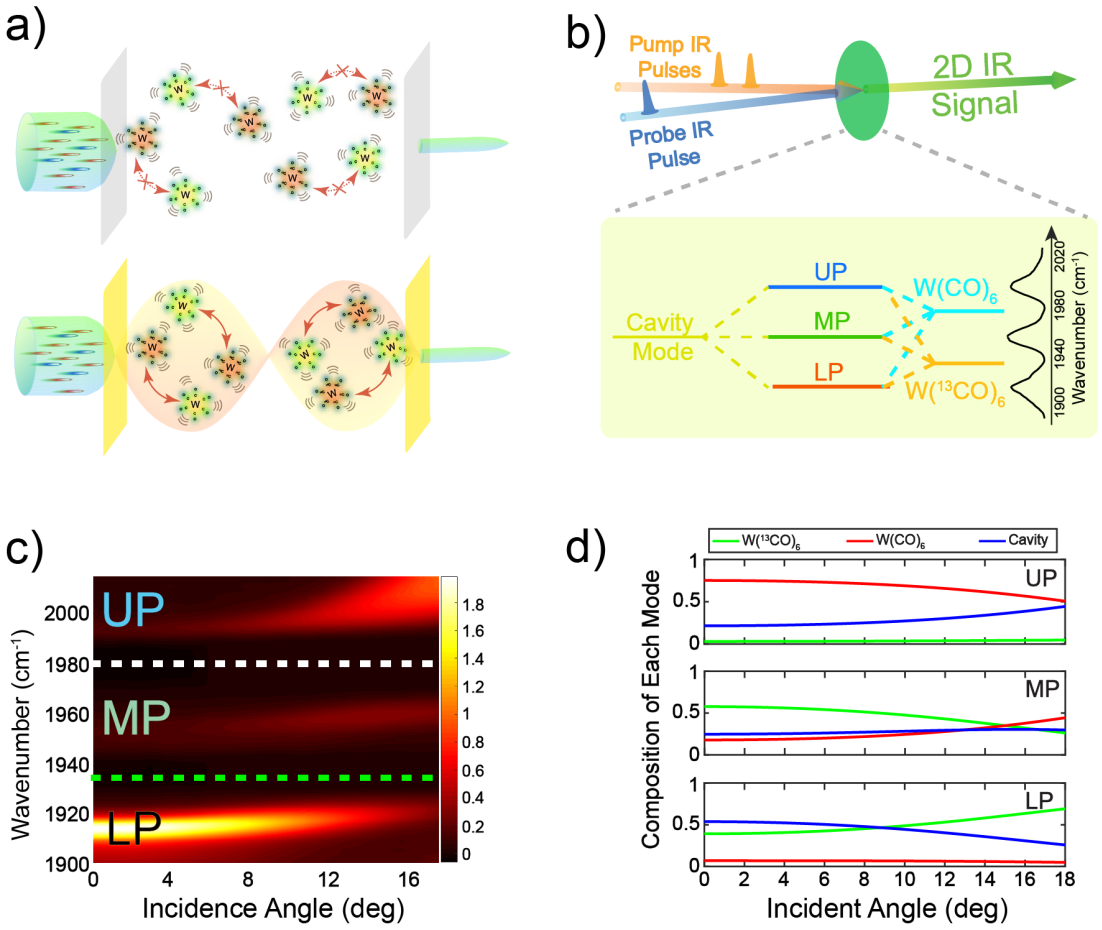

Figure 8.1: (a) Intermolecular VET processes of uncoupled system (top) and strongly coupled system (bottom). (b) 2D IR setup. (c) Dispersion curves. (d) Hopfield coefficients for LP, MP, and UP as a function of incidence angle.

modes to the vibrations.

For each molecular subsystem, the light-matter coupling g is proportional to $\sqrt{C}$, where C is the concentration of the absorbers. Given a large enough C, each molecular subsystem satisfies $g > \gamma_{vib}, \gamma_{cav}$, where γ_{vib} and γ_{cav} are the full-width at half-maximum (FWHM) of the vibrational and cavity modes, respectively. Therefore, the vibrational and the cavity modes (hereafter referred to as basis modes) hybridize and form new normal modes, denoted as upper, middle and lower polaritons (UP, MP and LP)[42] (Figure 8.1b, bottom). Each polariton consists of a superposition of the basis modes. The polariton resonant frequency and composition, characterized by Hopfield coefficients, can be controlled by changing the incidence angle (Figure 8.1c and 8.1d). For

example, at 15° incidence angle, the UP consists of 59.4% $W(CO)_6$ carbonyl asymmetric stretch, 4.3% analogous vibration in $W(^{13}CO)_6$, and 36.3% cavity photon, while the LP is composed of 5.8%, 60.8%, and 33.4% of the respective basis modes. As discussed later, this information is essential to investigate the ability of strong coupling to mediate intermolecular VET.

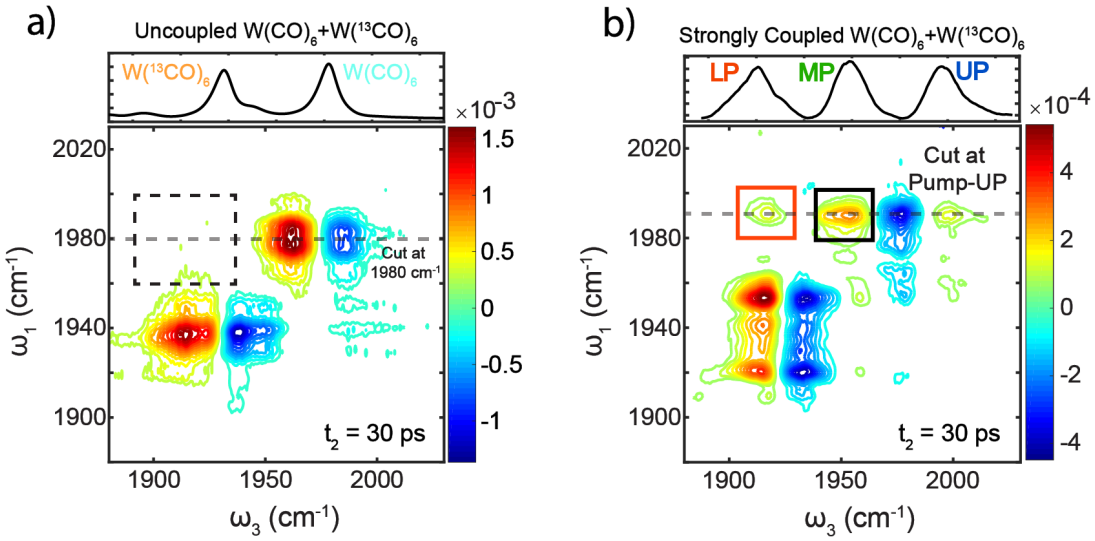

Figure 8.2: 2D IR spectra of (a) uncoupled and (b) strongly coupled $W(CO)_6/W(^{13}CO)_6$ with a total of 105 mM concentrations in binary solvent, along with the linear spectra (top panel).

8.2.1 2D IR Spectra of Uncoupled and Strongly Coupled Two-Molecular Systems

We used two-dimensional infrared spectroscopy (2D IR)[2] to show VET from $W(CO)_6$ into $W(^{13}CO)_6$. In 2D IR, if the UP was pumped and VET occurred, a substantial population of $W(^{13}CO)_6$ excited states would be generated and the intensity of the corresponding cross peak would rise. In Figure 8.2, we compare 2D IR spectra of the $W(CO)_6/W(^{13}CO)_6$ mixture inside and outside the microcavity. The 2D IR spectrum of the bare $W(CO)_6/W(^{13}CO)_6$ mixture (Figure 8.2a) confirms the absence of energy transfer between vibrational modes. It shows two pairs of diagonal peaks, corresponding to excitations of asymmetric carbonyl modes of $W(CO)_6$ and

$W(^{13}CO)_6$, respectively, whose vibrational lifetimes are c.a. 200 ps. There are no cross-peaks (dashed black box in Figure 8.2a), indicating absence of intermolecular VET.

The strongly coupled $W(CO)_6$/$W(^{13}CO)_6$ system provided a strikingly different picture. The 2D IR spectrum (Figure 8.2b) shows several cross-peaks at t_2 = 30 ps, indicating cavity-induced intermolecular correlations. From previous studies,[2, 14] at t_2 = 30 ps (greater than the polariton lifetime), the remaining pumped energy equilibrates into the first excited state of dark modes. Furthermore, the $W(^{13}CO)_6$ dark modes have $\nu = 1 \rightarrow \nu$=2 transitions at 1917 cm^{-1}, while those of $W(CO)_6$ are at 1961 cm^{-1}. Thus, the transient absorption at $\omega_3 = \omega_{LP}$ ($\sim$1920 cm^{-1}) and ω_{MP} ($\sim$1959 cm^{-1}) provide an optical window into population dynamics of the $W(^{13}CO)_6$ and $W(CO)_6$ reservoir modes, respectively. In particular, the cross peak at $\omega_1 = \omega_{UP}$ and $\omega_3 = \omega_{LP}$ (denoted as [ω_{UP} , ω_{LP}] hereafter; see red box in Figure 8.2b) suggested that a larger fraction of the energy in UP (dominated by $W(CO)_6$) was transferred into the dark $W(^{13}CO)_6$ modes after 30 ps, a signature of intermolecular VET. We have also conducted 2D IR experiments with pump tailored to selectively excite $|UP\rangle\langle UP|$ population states and a similarly strong cross peak appeared at $\omega_3 = \omega_{LP}$. Thus, the [ω_{UP} , ω_{LP}] and [ω_{UP} , ω_{MP}] cross-peaks (Figure 8.2b) arise from UP population, whereas pump-driven coherences such as $|UP\rangle\langle LP|$ and $|UP\rangle\langle MP|$ provide no contribution to the observed spectral features.

8.2.2 Pump-Probe Dynamics of Intermolecular VET

We compared the cross-peak intensities at [ω_{UP} , ω_{LP}] ($I_{UP,LP}$, red box in Figure 8.2b) and [ω_{UP} , ω_{MP}] ($I_{UP,LP}$, black box in Figure 8.2b) to determine the equilibrated excited-state populations of $W(^{13}CO)_6$ and $W(CO)_6$ arising from UP relaxation. Based on the Hopfield coefficients (for incidence angle of 15°), only 4.3% of the UP energy would be stored in $W(^{13}CO)_6$ reservoir modes, whereas 59.4% would be allocated to $W(CO)_6$ dark states. Therefore, in the absence of VET, the average population ratio between these reservoir modes ($I_{UP,MP}$/$I_{UP,LP}$) must be approximately equal to the ratio of the corresponding Hopfield coefficients, or 59.4%:4.3% $\approx$

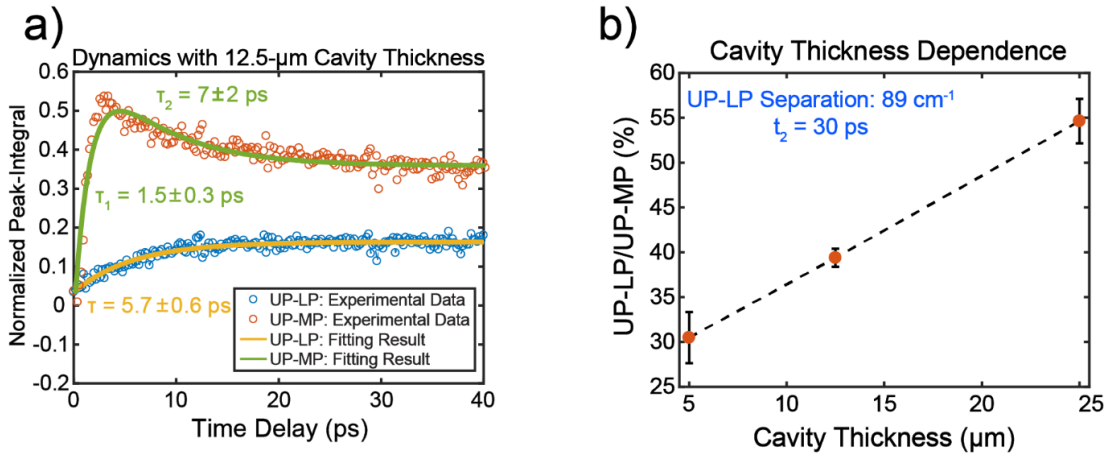

Figure 8.3: (a) Dynamics of [ω_{UP} , ω_{LP}] and [ω_{UP} , ω_{UP}] peak integrals and the fitting results. (b) A plot of $I_{UP,MP}/I_{UP,LP}$ as a function of cavity thickness at t_2 = 30 ps. The error bars are obtained from the standard deviation of three independent scans.

14:1. However, experimentally, $I_{UP,MP}/I_{UP,LP}$ is 2.5:1. This observation suggested that after the UP population was optically generated, its energy was preferentially channeled into $W(^{13}CO)_6$, increasing the relative peak intensity of [ω_{UP} , ω_{LP}]. To further examine this argument, we conducted similar measurements with the cavity blue-detuned so that UP had a greater fraction of $W(CO)_6$. Even at a Hopfield coefficient ratio of 25:1, there is still a significant amount of energy transfer ($I_{UP,MP}/I_{UP,LP}$ = 2.6±0.1). Additional evidence supporting intermolecular VET is the anisotropy decay of [ω_{UP} , ω_{MP}] and [ω_{UP} , ω_{LP}] peaks.

In Figure 8.3a, we monitored the VET dynamics via pump-probe spectroscopy, when only $|UP\rangle\langle UP|$ was excited, e.g. neither $|LP\rangle\langle LP|$ nor any coherence states were pumped. The intensity of [ω_{UP} , ω_{LP}] peak increased with a time constant of 5.7±0.6 ps. This value represents the timescale for energy transfer from UP into $W(^{13}CO)_6$ reservoir modes. In contrast, the direct relaxation of UP into $W(CO)_6$ happened much faster than VET with a lifetime of 1.5±0.3 ps, as indicated by the rising dynamics of $I_{UP,MP}$. The decay of $I_{UP,MP}$ is composed of a fast and a slow component. The fast dynamics has a lifetime of 7±2 ps, similar to the rising time of $I_{UP,LP}$. Thus, it implies energym 'leakage' from the $W(CO)_6$ mode into the $W(^{13}CO)_6$ mode. The slow component, whose decay extends beyond the time range of our scan, should correspond to the

population relaxation of reservoir $W(CO)_6$.[2, 14]

8.2.3 Cavity-Thickness Dependence of Intermolecular VET

To confirm the importance of cavity modes in facilitating polariton VET, we attempted to enhance VET by increasing the cavity thickness L. In Figure 8.3b, we present the $I_{UP,MP}/I_{UP,LP}$ ratio, for the same molecular mixture in cavities with L = 5, 12.5 and 25 μm, corresponding to 1.12, 2.80 and 5.60 ps cavity lifetimes, respectively. This ratio, which reflects the efficiency of VET at 30 ps, increased with L. Because thicker cavities have longer lifetimes, this dependence suggested a larger fraction of UP energy was collected into $W(^{13}CO)_6$ modes as polariton decay by photon leakage became slower. This property substantiates that intermolecular VET involved polaritonic intermediate states. The nature of the ultrafast energy redistribution process here requires further study, suggesting that, in contrast to measurements performed on organic microcavities,[16, 111] previously unexplored mechanisms should dominate the relaxation kinetics reported here. Possible mechanisms include polariton-mediated scattering and interaction of polaritons with other dark modes.

8.2.4 Discussion

The reported concept of polariton-enabled intermolecular VET could be expanded into the selective promotion or suppression of vibrational energy transport channels. The preferential relaxation into lower energy states is a key process for IR polariton condensation, remote energy transfer,[11] and cavity chemistry.[12]

Chapter 8, in full, is a reprint of the material as it appears in the Science, 2020. Bo Xiang; Raphael F. Ribeiro; Matthew Du; Liying Chen; Zimo Yang; Jiaxi Wang; Joel Yuen-Zhou; Wei Xiong., American Association for the Advancement of Science, 2020. The dissertation author was the primary investigator and author of this paper.

Chapter 9

Conclusions and Outlook

In this dissertation, the recent spectroscopic research on molecular vibrational polaritons (MVPs) has been discussed. The employment of ultrafast spectroscopy, such as multi-dimension and pump-probe spectroscopic technique, reveals the optical nonlinearity of MVPs and their ultrafast dynamics, including the early-time ($<$ 5 ps) Rabi oscillation and long-term (10$\sim$100 ps) polariton-to-dark state relaxation. Exotic phenomena and applications in the fields of chemistry, photonics and quantum technology have been proposed or reported. Many of these phenomena could be a result of photon-molecule duality of MVPs, as MVPs adopts the nonlinearity and reactivity of molecules, where photons are light and delocalized.

By providing the newly revealed knowledge of MVPs, we hope to stimulate more interest in this emerging field. The field is still at the infancy stage in both chemical reaction and its corresponding chemical physics and mechanism aspects. From the second and third chapters, the energetic behaviors of polaritonic states and dark modes and their coherent or incoherent interactions build the foundation of MVPs knowledge system. From chapter second and third, the whole life of MVPs has been studied, providing an basis to more inspiring developments. Current chemical physics studies have been limited to model systems, and relevant research in more complex systems is necessary. Lastly, early studies mentioned in chapter five and six have shown

molecular vibrational polariton's potential for new chemistry, ultrafast photonics and quantum information research. Thus, it is a fertile ground for physical chemistry and material chemistry research.

Bibliography

[1] Ribeiro, R. F.; Dunkelberger, A. D.; Xiang, B.; Xiong, W.; Simpkins, B. S.; Owrutsky, J. C.; Yuen-Zhou, J. Theory for Nonlinear Spectroscopy of Vibrational Polaritons. *The Journal of Physical Chemistry Letters* **2018**, *9*, 3766–3771.

[2] Xiang, B.; Ribeiro, R. F.; Dunkelberger, A. D.; Wang, J.; Li, Y.; Simpkins, B. S.; Owrutsky, J. C.; Yuen-Zhou, J.; Xiong, W. Two-dimensional infrared spectroscopy of vibrational polaritons. *Proceedings of the National Academy of Sciences* **2018**, *115*, 4845.

[3] Simpkins, B. S.; Fears, K. P.; Dressick, W. J.; Spann, B. T.; Dunkelberger, A. D.; Owrutsky, J. C. Spanning Strong to Weak Normal Mode Coupling between Vibrational and Fabry–Perot Cavity Modes through Tuning of Vibrational Absorption Strength. *ACS Photonics* **2015**, *2*, 1460–1467.

[4] Thomas, A.; Lethuillier-Karl, L.; Nagarajan, K.; Vergauwe, R. M. A.; George, J.; Chervy, T.; Shalabney, A.; Devaux, E.; Genet, C.; Moran, J.; Ebbesen, T. W. Tilting a ground-state reactivity landscape by vibrational strong coupling. *Science* **2019**, *363*, 615.

[5] Thomas, A.; George, J.; Shalabney, A.; Dryzhakov, M.; Varma, S. J.; Moran, J.; Chervy, T.; Zhong, X.; Devaux, E.; Genet, C.; Hutchison, J. A.; Ebbesen, T. W. Ground-State Chemical Reactivity under Vibrational Coupling to the Vacuum Electromagnetic Field. *Angewandte Chemie International Edition* **2016**, *55*, 11462–11466.

[6] Canaguier-Durand, A.; Devaux, E.; George, J.; Pang, Y.; Hutchison, J. A.; Schwartz, T.; Genet, C.; Wilhelms, N.; Lehn, J.-M.; Ebbesen, T. W. Thermodynamics of Molecules Strongly Coupled to the Vacuum Field. *Angewandte Chemie International Edition* **2013**, *52*, 10533–10536.

[7] Xiang, B.; Ribeiro, R. F.; Chen, L.; Wang, J.; Du, M.; Yuen-Zhou, J.; Xiong, W. State-Selective Polariton to Dark State Relaxation Dynamics. *The Journal of Physical Chemistry A* **2019**, *123*, 5918–5927.

[8] Xiang, B.; Ribeiro, R. F.; Du, M.; Chen, L.; Yang, Z.; Wang, J.; Yuen-Zhou, J.; Xiong, W. Intermolecular vibrational energy transfer enabled by microcavity strong light-matter coupling. *Science* **2020**, *368*, 665.

[9] Xiang, B.; Ribeiro, R. F.; Li, Y.; Dunkelberger, A. D.; Simpkins, B. B.; Yuen-Zhou, J.; Xiong, W. Manipulating optical nonlinearities of molecular polaritons by delocalization. *Science Advances* **2019**, *5*, eaax5196.

[10] Yuen-Zhou, J.; Menon, V. M. Polariton chemistry: Thinking inside the (photon) box. *Proceedings of the National Academy of Sciences* **2019**, *116*, 5214.

[11] Du, M.; Martínez-Martínez, L. A.; Ribeiro, R. F.; Hu, Z.; Menon, V. M.; Yuen-Zhou, J. Theory for polariton-assisted remote energy transfer. *Chemical Science* **2018**, *9*, 6659–6669.

[12] Du, M.; Ribeiro, R. F.; Yuen-Zhou, J. Remote Control of Chemistry in Optical Cavities. *Chem* **2019**, *5*, 1167–1181.

[13] Ribeiro, R. F.; Martínez-Martínez, L. A.; Du, M.; Campos-Gonzalez-Angulo, J.; Yuen-Zhou, J. Polariton chemistry: controlling molecular dynamics with optical cavities. *Chemical Science* **2018**, *9*, 6325–6339.

[14] Dunkelberger, A. D.; Spann, B. T.; Fears, K. P.; Simpkins, B. S.; Owrutsky, J. C. Modified relaxation dynamics and coherent energy exchange in coupled vibration-cavity polaritons. *Nature Communications* **2016**, *7*, 13504.

[15] Hutchison, J. A.; Schwartz, T.; Genet, C.; Devaux, E.; Ebbesen, T. W. Modifying Chemical Landscapes by Coupling to Vacuum Fields. *Angewandte Chemie International Edition* **2012**, *51*, 1592–1596.

[16] Zhong, X.; Chervy, T.; Zhang, L.; Thomas, A.; George, J.; Genet, C.; Hutchison, J. A.; Ebbesen, T. W. Energy Transfer between Spatially Separated Entangled Molecules. *Angewandte Chemie International Edition* **2017**, *56*, 9034–9038.

[17] Sekretenko, A. V.; Gavrilov, S. S.; Kulakovskii, V. D. Polariton-polariton interactions in microcavities under a resonant 10 to 100 picosecond pulse excitation. *Physical Review B* **2013**, *88*, 195302.

[18] Vladimirova, M.; Cronenberger, S.; Scalbert, D.; Kavokin, K. V.; Miard, A.; Lemaître, A.; Bloch, J.; Solnyshkov, D.; Malpuech, G.; Kavokin, A. V. Polariton-polariton interaction constants in microcavities. *Physical Review B* **2010**, *82*, 075301–.

[19] Sun, Y.; Yoon, Y.; Steger, M.; Liu, G.; Pfeiffer, L. N.; West, K.; Snoke, D. W.; Nelson, K. A. Direct measurement of polariton–polariton interaction strength. *Nature Physics* **2017**, *13*, 870–875.

[20] Werner, M. J.; Imamo̧glu, A. Photon-photon interactions in cavity electromagnetically induced transparency. *Physical Review A* **1999**, *61*, 011801–.

[21] Englund, D.; Majumdar, A.; Bajcsy, M.; Faraon, A.; Petroff, P.; Vučković, J. Ultrafast Photon-Photon Interaction in a Strongly Coupled Quantum Dot-Cavity System. *Physical Review Letters* **2012**, *108*, 093604–.

[22] Wang, J.; Xiang, B.; Xiong, W. Ultrafast Intercavity Nonlinear Couplings between Polaritons. *arXiv preprint arXiv:1912.05725* **2019**,

[23] Birnbaum, K. M.; Boca, A.; Miller, R.; Boozer, A. D.; Northup, T. E.; Kimble, H. J. Photon blockade in an optical cavity with one trapped atom. *Nature* **2005**, *436*, 87–90.

[24] Wang, H.; Gu, X.; Liu, Y.-x.; Miranowicz, A.; Nori, F. Tunable photon blockade in a hybrid system consisting of an optomechanical device coupled to a two-level system. *Physical Review A* **2015**, *92*, 033806–.

[25] Deng, H.; Haug, H.; Yamamoto, Y. Exciton-polariton Bose-Einstein condensation. *Reviews of Modern Physics* **2010**, *82*, 1489–1537.

[26] Wang, S.; Chervy, T.; George, J.; Hutchison, J. A.; Genet, C.; Ebbesen, T. W. Quantum Yield of Polariton Emission from Hybrid Light-Matter States. *The Journal of Physical Chemistry Letters* **2014**, *5*, 1433–1439.

[27] Zhang, L.; Gogna, R.; Burg, W.; Tutuc, E.; Deng, H. Photonic-crystal exciton-polaritons in monolayer semiconductors. *Nature Communications* **2018**, *9*, 713.

[28] Lather, J.; Bhatt, P.; Thomas, A.; Ebbesen, T. W.; George, J. Cavity Catalysis by Cooperative Vibrational Strong Coupling of Reactant and Solvent Molecules. *Angewandte Chemie International Edition* **2019**, *58*, 10635–10638.

[29] Vergauwe, R. M. A.; Thomas, A.; Nagarajan, K.; Shalabney, A.; George, J.; Chervy, T.; Seidel, M.; Devaux, E.; Torbeev, V.; Ebbesen, T. W. Modification of Enzyme Activity by Vibrational Strong Coupling of Water. *Angewandte Chemie International Edition* **2019**, *58*, 15324–15328.

[30] Li, T. E.; Subotnik, J. E.; Nitzan, A. Cavity molecular dynamics simulations of liquid water under vibrational ultrastrong coupling. *Proceedings of the National Academy of Sciences* **2020**, *117*, 18324.

[31] Saurabh, P.; Mukamel, S. Two-dimensional infrared spectroscopy of vibrational polaritons of molecules in an optical cavity. *The Journal of Chemical Physics* **2016**, *144*, 124115.

[32] Buchanan, L. E.; Xiong, W. Two-Dimensional Infrared (2D IR) Spectroscopy. *Encyclopedia of Modern Optics 2nd, ed.* **2018**, *2*, 164–183.

[33] Hamm, P.; Zanni, M. *Concepts and methods of 2D infrared spectroscopy*; Cambridge University Press, 2011.

[34] Campos-Gonzalez-Angulo, J. A.; Ribeiro, R. F.; Yuen-Zhou, J. Resonant catalysis of thermally activated chemical reactions with vibrational polaritons. *Nature Communications* **2019**, *10*, 4685.

[35] Vurgaftman, I.; Simpkins, B. S.; Dunkelberger, A. D.; Owrutsky, J. C. Negligible Effect of Vibrational Polaritons on Chemical Reaction Rates via the Density of States Pathway. *The Journal of Physical Chemistry Letters* **2020**, *11*, 3557–3562.

[36] Li, T. E.; Nitzan, A.; Subotnik, J. E. On the origin of ground-state vacuum-field catalysis: Equilibrium consideration. *The Journal of Chemical Physics* **2020**, *152*, 234107.

[37] Dunkelberger, A. D.; Davidson, R. B.; Ahn, W.; Simpkins, B. S.; Owrutsky, J. C. Ultrafast Transmission Modulation and Recovery via Vibrational Strong Coupling. *The Journal of Physical Chemistry A* **2018**, *122*, 965–971.

[38] Norris, T. B.; Rhee, J. K.; Sung, C. Y.; Arakawa, Y.; Nishioka, M.; Weisbuch, C. Time-resolved vacuum Rabi oscillations in a semiconductor quantum microcavity. *Physical Review B* **1994**, *50*, 14663–14666.

[39] Yang, Z.; Xiang, B.; Xiong, W. Controlling Quantum Pathways in Molecular Vibrational Polaritons. *ACS Photonics* **2020**, *7*, 919–924.

[40] Yuen-Zhou, J.; Saikin, S. K.; Menon, V. M. Molecular Emission near Metal Interfaces: The Polaritonic Regime. *The Journal of Physical Chemistry Letters* **2018**, *9*, 6511–6516.

[41] Kassal, I.; Yuen-Zhou, J.; Rahimi-Keshari, S. Does Coherence Enhance Transport in Photosynthesis? *The Journal of Physical Chemistry Letters* **2013**, *4*, 362–367.

[42] Muallem, M.; Palatnik, A.; Nessim, G. D.; Tischler, Y. R. Strong Light-Matter Coupling and Hybridization of Molecular Vibrations in a Low-Loss Infrared Microcavity. *The Journal of Physical Chemistry Letters* **2016**, *7*, 2002–2008.

[43] Ladd, T. D.; Jelezko, F.; Laflamme, R.; Nakamura, Y.; Monroe, C.; O'Brien, J. L. Quantum computers. *Nature* **2010**, *464*, 45–53.

[44] Wendin, G. Quantum information processing with superconducting circuits: a review. **2017**, *80*, 106001.

[45] Boyd, R. W. *Nonlinear Optics (Third Edition)*; Academic Press: Burlington, 2008.

[46] Kraack, J. P.; Hamm, P. Surface-Sensitive and Surface-Specific Ultrafast Two-Dimensional Vibrational Spectroscopy. *Chemical Reviews* **2017**, *117*, 10623–10664.

[47] Ulness, D. J.; Albrecht, A. C. Theory of time-resolved coherent Raman scattering with spectrally tailored noisy light. *Journal of Raman Spectroscopy* **1997**, *28*, 571–578.

[48] Kirkwood, J. C.; Ulness, D. J.; Albrecht, On the Classification of the Electric Field Spectroscopies: Application to Raman Scattering. *The Journal of Physical Chemistry A* **2000**, *104*, 4167–4173.

[49] Kuhs, C. T.; Luther, B. M.; Krummel, A. T. Recent Advances in 2D IR Spectroscopy Driven by Advances in Ultrafast Technology. *IEEE Journal of Selected Topics in Quantum Electronics* **2019**, *25*, 1–13.

[50] Shim, S.-H.; Strasfeld, D. B.; Fulmer, E. C.; Zanni, M. T. Femtosecond pulse shaping directly in the mid-IR using acousto-optic modulation. *Opt. Lett.* **2006**, *31*, 838–840.

[51] Shim, S.-H.; Zanni, M. T. How to turn your pump–probe instrument into a multidimensional spectrometer: 2D IR and Vis spectroscopiesvia pulse shaping. *Physical Chemistry Chemical Physics* **2009**, *11*, 748–761.

[52] Nee, M. J.; McCanne, R.; Kubarych, K. J.; Joffre, M. Two-dimensional infrared spectroscopy detected by chirped pulse upconversion. *Optics Letters* **2007**, *32*, 713–715.

[53] Rock, W.; Li, Y.-L.; Pagano, P.; Cheatum, C. M. 2D IR Spectroscopy using Four-Wave Mixing, Pulse Shaping, and IR Upconversion: A Quantitative Comparison. *The Journal of Physical Chemistry A* **2013**, *117*, 6073–6083.

[54] HOMMEL, E. L.; ALLEN, H. C. Broadband Sum Frequency Generation with Two Regenerative Amplifiers: Temporal Overlap of Femtosecond and Picosecond Light Pulses. *Analytical Sciences* **2001**, *17*, 137–139.

[55] Laaser, J. E.; Xiong, W.; Zanni, M. T. Time-Domain SFG Spectroscopy Using Mid-IR Pulse Shaping: Practical and Intrinsic Advantages. *The Journal of Physical Chemistry B* **2011**, *115*, 2536–2546.

[56] Long, J. P.; Simpkins, B. S. Coherent Coupling between a Molecular Vibration and Fabry–Perot Optical Cavity to Give Hybridized States in the Strong Coupling Limit. *ACS Photonics* **2015**, *2*, 130–136.

[57] Ebbesen, T. W. Hybrid Light–Matter States in a Molecular and Material Science Perspective. *Accounts of Chemical Research* **2016**, *49*, 2403–2412.

[58] Amo, A.; Lefrère, J.; Pigeon, S.; Adrados, C.; Ciuti, C.; Carusotto, I.; Houdré, R.; Giacobino, E.; Bramati, A. Superfluidity of polaritons in semiconductor microcavities. *Nature Physics* **2009**, *5*, 805–810.

[59] Kéna-Cohen, S.; Forrest, S. R. Room-temperature polariton lasing in an organic single-crystal microcavity. *Nature Photonics* **2010**, *4*, 371–375.

[60] Deng, H.; Weihs, G.; Santori, C.; Bloch, J.; Yamamoto, Y. Condensation of Semiconductor Microcavity Exciton Polaritons. *Science* **2002**, *298*, 199.

[61] Shalabney, A.; George, J.; Hiura, H.; Hutchison, J. A.; Genet, C.; Hellwig, P.; Ebbesen, T. W. Enhanced Raman Scattering from Vibro-Polariton Hybrid States. *Angewandte Chemie International Edition* **2015**, *54*, 7971–7975.

[62] Houdré, R.; Stanley, R. P.; Ilegems, M. Vacuum-field Rabi splitting in the presence of inhomogeneous broadening: Resolution of a homogeneous linewidth in an inhomogeneously broadened system. *Physical Review A* **1996**, *53*, 2711–2715.

[63] Lindberg, M.; Binder, R. Dark States in Coherent Semiconductor Spectroscopy. *Physical Review Letters* **1995**, *75*, 1403–1406.

[64] Cho, M. Coherent Two-Dimensional Optical Spectroscopy. *Chemical Reviews* **2008**, *108*, 1331–1418.

[65] Vasa, P.; Wang, W.; Pomraenke, R.; Lammers, M.; Maiuri, M.; Manzoni, C.; Cerullo, G.; Lienau, C. Real-time observation of ultrafast Rabi oscillations between excitons and plasmons in metal nanostructures with J-aggregates. *Nature Photonics* **2013**, *7*, 128–132.

[66] Takemura, N.; Trebaol, S.; Anderson, M. D.; Kohnle, V.; Léger, Y.; Oberli, D. Y.; Portella-Oberli, M. T.; Deveaud, B. Two-dimensional Fourier transform spectroscopy of exciton-polaritons and their interactions. *Physical Review B* **2015**, *92*, 125415–.

[67] Arrivo, S. M.; Dougherty, T. P.; Grubbs, W. T.; Heilweil, E. J. Ultrafast infrared spectroscopy of vibrational CO-stretch up-pumping and relaxation dynamics of W(CO)6. *Chemical Physics Letters* **1995**, *235*, 247–254.

[68] Tokmakoff, A.; Sauter, B.; Kwok, A. S.; Fayer, M. D. Phonon-induced scattering between vibrations and multiphoton vibrational up-pumping in liquid solution. *Chemical Physics Letters* **1994**, *221*, 412–418.

[69] Wen, P.; Christmann, G.; Baumberg, J. J.; Nelson, K. A. Influence of multi-exciton correlations on nonlinear polariton dynamics in semiconductor microcavities. **2013**, *15*, 025005.

[70] Gonzalez-Ballestero, C.; Feist, J.; Gonzalo Badía, E.; Moreno, E.; Garcia-Vidal, F. J. Uncoupled Dark States Can Inherit Polaritonic Properties. *Physical Review Letters* **2016**, *117*, 156402–.

[71] Pino, J. d.; Feist, J.; Garcia-Vidal, F. J. Quantum theory of collective strong coupling of molecular vibrations with a microcavity mode. **2015**, *17*, 053040.

[72] Scherer, J. J.; Paul, J. B.; O'Keefe, A.; Saykally, R. J. Cavity Ringdown Laser Absorption Spectroscopy: History, Development, and Application to Pulsed Molecular Beams. *Chemical Reviews* **1997**, *97*, 25–52.

[73] Koch, S. W.; Kira, M.; Khitrova, G.; Gibbs, H. M. Semiconductor excitons in new light. *Nature Materials* **2006**, *5*, 523–531.

[74] Mukamel, S.; Nagata, Y. Quantum field, interference, and entanglement effects in nonlinear optical spectroscopy. *Procedia Chemistry* **2011**, *3*, 132–151.

[75] Jin, G.-R.; Liu, W.-M. Collapses and revivals of exciton emission in a semiconductor microcavity: Detuning and phase-space filling effects. *Physical Review A* **2004**, *70*, 013803–.

[76] Khalil, M.; Demirdöven, N.; Tokmakoff, A. Coherent 2D IR Spectroscopy: Molecular Structure and Dynamics in Solution. *The Journal of Physical Chemistry A* **2003**, *107*, 5258–5279.

[77] Middleton, C. T.; Marek, P.; Cao, P.; Chiu, C.-c.; Singh, S.; Woys, A. M.; de Pablo, J. J.; Raleigh, D. P.; Zanni, M. T. Two-dimensional infrared spectroscopy reveals the complex behaviour of an amyloid fibril inhibitor. *Nature Chemistry* **2012**, *4*, 355–360.

[78] Xiong, W.; Laaser, J. E.; Paoprasert, P.; Franking, R. A.; Hamers, R. J.; Gopalan, P.; Zanni, M. T. Transient 2D IR Spectroscopy of Charge Injection in Dye-Sensitized Nanocrystalline Thin Films. *Journal of the American Chemical Society* **2009**, *131*, 18040–18041.

[79] Yuen-Zhou, J.; Arias, D. H.; Eisele, D. M.; Steiner, C. P.; Krich, J. J.; Bawendi, M. G.; Nelson, K. A.; Aspuru-Guzik, A. Coherent Exciton Dynamics in Supramolecular Light-Harvesting Nanotubes Revealed by Ultrafast Quantum Process Tomography. *ACS Nano* **2014**, *8*, 5527–5534.

[80] Garrett-Roe, S.; Hamm, P. Purely absorptive three-dimensional infrared spectroscopy. *The Journal of Chemical Physics* **2009**, *130*, 164510.

[81] Li, H.; Bristow, A. D.; Siemens, M. E.; Moody, G.; Cundiff, S. T. Unraveling quantum pathways using optical 3D Fourier-transform spectroscopy. *Nature Communications* **2013**, *4*, 1390.

[82] Turner, D. B.; Stone, K. W.; Gundogdu, K.; Nelson, K. A. Three-dimensional electronic spectroscopy of excitons in GaAs quantum wells. *The Journal of Chemical Physics* **2009**, *131*, 144510.

[83] Anna, J. M.; Ross, M. R.; Kubarych, K. J. Dissecting Enthalpic and Entropic Barriers to Ultrafast Equilibrium Isomerization of a Flexible Molecule Using 2DIR Chemical Exchange Spectroscopy. *The Journal of Physical Chemistry A* **2009**, *113*, 6544–6547.

[84] Gandman, A.; Mackin, R.; Cohn, B.; Rubtsov, I. V.; Chuntonov, L. Two-Dimensional Fano Lineshapes in Ultrafast Vibrational Spectroscopy of Thin Molecular Layers on Plasmonic Arrays. *The Journal of Physical Chemistry Letters* **2017**, *8*, 3341–3346.

[85] Rabl, P. Photon Blockade Effect in Optomechanical Systems. *Physical Review Letters* **2011**, *107*, 063601–.

[86] Vuckovic, J. *Quantum optics and cavity QED with quantum dots in photonic crystals*; 2014.

[87] Mukamel, S. *Principles of nonlinear optical spectroscopy*; Oxford university press New York, 1995; Vol. 6.

[88] Fehrenbach, G. W.; Schäfer, W.; Treusch, J.; Ulbrich, R. G. Transient Optical Spectra of a Dense Exciton Gas in a Direct-Gap Semiconductor. *Physical Review Letters* **1982**, *49*, 1281–1284.

[89] Khitrova, G.; Gibbs, H. M.; Jahnke, F.; Kira, M.; Koch, S. W. Nonlinear optics of normal-mode-coupling semiconductor microcavities. *Reviews of Modern Physics* **1999**, *71*, 1591–1639.

[90] Tokmakoff, A.; Urdahl, R. S.; Zimdars, D.; Francis, R. S.; Kwok, A. S.; Fayer, M. D. Vibrational spectral diffusion and population dynamics in a glass-forming liquid: Variable bandwidth picosecond infrared spectroscopy. *The Journal of Chemical Physics* **1995**, *102*, 3919–3931.

[91] Zhu, D.; Li, C.; Zeng, X.; Jiang, H. Tunable-focus microlens arrays on curved surfaces. *Applied Physics Letters* **2010**, *96*, 081111.

[92] Su, R.; Wang, J.; Zhao, J.; Xing, J.; Zhao, W.; Diederichs, C.; Liew, T. C. H.; Xiong, Q. Room temperature long-range coherent exciton polariton condensate flow in lead halide perovskites. *Science Advances* **2018**, *4*, eaau0244.

[93] Schwartz, T.; Hutchison, J. A.; Léonard, J.; Genet, C.; Haacke, S.; Ebbesen, T. W. Polariton Dynamics under Strong Light–Molecule Coupling. *ChemPhysChem* **2013**, *14*, 125–131.

[94] Baumann, T.; Hauf, M.; Schildhauer, F.; Eberl, K. B.; Durkin, P. M.; Deniz, E.; Löffler, J. G.; Acevedo-Rocha, C. G.; Jaric, J.; Martins, B. M.; Dobbek, H.; Bredenbeck, J.; Budisa, N. Site-Resolved Observation of Vibrational Energy Transfer Using a Genetically Encoded Ultrafast Heater. *Angewandte Chemie International Edition* **2019**, *58*, 2899–2903.

[95] Carusotto, I.; Ciuti, C. Quantum fluids of light. *Reviews of Modern Physics* **2013**, *85*, 299–366.

[96] Plumhof, J. D.; Stöferle, T.; Mai, L.; Scherf, U.; Mahrt, R. F. Room-temperature Bose–Einstein condensation of cavity exciton–polaritons in a polymer. *Nature Materials* **2014**, *13*, 247–252.

[97] Khitrova, G.; Gibbs, H. M.; Kira, M.; Koch, S. W.; Scherer, A. Vacuum Rabi splitting in semiconductors. *Nature Physics* **2006**, *2*, 81–90.

[98] Smith, J. M.; Jones, L. H. Anharmonic corrections for fundamental vibrations of the metal hexacarbonyls. *Journal of Molecular Spectroscopy* **1966**, *20*, 248–257.

[99] Reichardt, C.; Welton, T. *Solvents and solvent effects in organic chemistry*; John Wiley & Sons, 2011.

[100] Fink, J. M.; Göppl, M.; Baur, M.; Bianchetti, R.; Leek, P. J.; Blais, A.; Wallraff, A. Climbing the Jaynes–Cummings ladder and observing its nonlinearity in a cavity QED system. *Nature* **2008**, *454*, 315–318.

[101] Link, S.; El-Sayed, M. A. Size and Temperature Dependence of the Plasmon Absorption of Colloidal Gold Nanoparticles. *The Journal of Physical Chemistry B* **1999**, *103*, 4212–4217.

[102] Wada, O. Femtosecond all-optical devices for ultrafast communication and signal processing. **2004**, *6*, 183–183.

[103] Hartmann, M. J.; Brandão, F. G. S. L.; Plenio, M. B. Strongly interacting polaritons in coupled arrays of cavities. *Nature Physics* **2006**, *2*, 849–855.

[104] Rodriguez, S. R. K.; Amo, A.; Sagnes, I.; Le Gratiet, L.; Galopin, E.; Lemaître, A.; Bloch, J. Interaction-induced hopping phase in driven-dissipative coupled photonic microcavities. *Nature Communications* **2016**, *7*, 11887.

[105] Yagafarov, T.; Sannikov, D.; Zasedatelev, A.; Georgiou, K.; Baranikov, A.; Kyriienko, O.; Shelykh, I.; Gai, L.; Shen, Z.; Lidzey, D.; Lagoudakis, P. Mechanisms of blueshifts in organic polariton condensates. *Communications Physics* **2020**, *3*, 18.

[106] Tardy, D. C.; Rabinovitch, B. S. Intermolecular vibrational energy transfer in thermal unimolecular systems. *Chemical Reviews* **1977**, *77*, 369–408.

[107] Nesbitt, D. J.; Field, R. W. Vibrational Energy Flow in Highly Excited Molecules: Role of Intramolecular Vibrational Redistribution. *The Journal of Physical Chemistry* **1996**, *100*, 12735–12756.

[108] Foster, T. Intermolecular energy transfer and fluorescence. *Ann. Phys. (N. Y).* **1948**, *437*, 55–75.

[109] Dexter, D. L. A Theory of Sensitized Luminescence in Solids. *The Journal of Chemical Physics* **1953**, *21*, 836–850.

[110] Memmi, H.; Benson, O.; Sadofev, S.; Kalusniak, S. Strong Coupling between Surface Plasmon Polaritons and Molecular Vibrations. *Physical Review Letters* **2017**, *118*, 126802–.

[111] Coles, D. M.; Somaschi, N.; Michetti, P.; Clark, C.; Lagoudakis, P. G.; Savvidis, P. G.; Lidzey, D. G. Polariton-mediated energy transfer between organic dyes in a strongly coupled optical microcavity. *Nature Materials* **2014**, *13*, 712–719.